DYNAMICS OF SINGLE-SUBSTRATE CONTINUOUS CULTURES

By

SHAKTI GUPTA

A DISSERTATION PRESENTED TO THE GRADUATE SCHOOL
OF THE UNIVERSITY OF FLORIDA IN PARTIAL FULFILLMENT
OF THE REQUIREMENTS FOR THE DEGREE OF
DOCTOR OF PHILOSOPHY

UNIVERSITY OF FLORIDA

2005

I dedicate this work to my father Pawan Kumar Gupta and my mother Swatantra Gupta, who has always stood by me.

ACKNOWLEDGMENTS

I take this opportunity to state my deep sense of gratitude to my mentor, Dr. Atul Narang, for introducing me to the exciting field of modeling of biological systems. I am deeply indebted to his guidance and constant encouragement. I would like to thank my co-advisor, Dr. Sergei S. Pilyugin, for his guidance and encouragement. I would also like to thank the members of my committee, Dr. Ranganathan Narayanan, Dr. Lewis E. Johns, Dr. Spyros Svoronos and Dr. Ben Koopman, for their advice and availability.

I am very grateful to Jason Noel and Brent Cox for their valuable help and laboratory assistance. I would like to thank Dr. Karthik Subramanian, Eric May, Ved Sharma for their constant support and friendship in and outside the lab. This acknowledgement cannot be completed without these names: Saurabh, Rishabh, Krishna, Neeli, Gunjan, Ashish, Priyank, Himanshu, Dushyant, Samir, Arvind and all my other friends for making me feel comfortable and making my stay at Gainesville a blissful experience.

I would also like to thank Shirley, Nancy and Debbie for their tireless assistance throughout my graduate studies.

Last but not the least, I want to express the deep sense of my emotion for my parents, wife, brother, sister and my other family members, who always stood beside me, through thick and thin.

TABLE OF CONTENTS

LIST OF TABLES

LIST OF FIGURES

Abstract of Dissertation Presented to the Graduate School
of the University of Florida in Partial Fulfillment of the
Requirements for the Degree of Doctor of Philosophy

DYNAMICS OF SINGLE-SUBSTRATE
CONTINUOUS CULTURES

By

Shakti Gupta

August 2005

Chair: Atul Narang
Major Department: Chemical Engineering

When a chemostat is perturbed from its steady state, it displays complex dynamics. For instance, if the identity of the growth-limiting substrate is switched abruptly, the substrate concentration and cell density undergo a pronounced excursion from the steady state that can last several days. These dynamics occur because certain physiological variables respond slowly. In the literature, several physiological variables have been postulated as potential sources of the slow response. These include transport enzymes and ribosomes.

We studied the role of transport enzymes by considering experiments in which low levels of the transport enzyme limits the growth. It was shown that the long lags could occur because transport enzyme synthesis is autocatalytic. A model was developed to account for transport enzyme synthesis, which captured these transients quantitatively. We then extended the model to account for experiments in which the lags persisted even if the transport enzyme level was high. In this case, the growth rates appear to be limited by the protein synthetic machinery (ribosomes). We showed that an extended model taking due account of ribosomes synthesis could capture these transients qualitatively.

Further, we attempted to understand the behavior in which the cell allocates the metabolites to respiration, growth, and excretion. Since the cell frequently consumes excess substrate, it is unable to convert all the metabolites to proteins. The excess substrate in the cell is then discharged as partially oxidized metabolites. To understand this phenomenon, we have again extended our model by including adenine nucleotides as energy molecules. We showed that the resultant energy balance then imposes constraints which determine the relative rates of protein synthesis, metabolite excretion, and respiration.

CHAPTER 1
INTRODUCTION

1.1 General Objectives

The chemostats (CSTR) are commonly used in industry to grow the cell at the expense of nutrient consumption. The importance of the chemostat lies in various applications. The environmental industries use the chemostat to remove the toxic compounds from the waste. In this case, the cell consumes the toxic materials and produces benign cells. In pharmaceutical industries, the cells are grown at the expense of low value food and excrete high value products (e.g., penicillin). When a chemostat is exposed to abrupt disturbances, i.e., change in the flow rate, feed concentrations etc., the cells take time to adapt to the environment and display complex transient response involving overshoot in the substrate concentration, undershoot in cell density and excretion of partially oxidized metabolites in the reactor. These dynamics often cause regulatory violations in wastewater treatment plants and loss or deterioration of product in industrial fermenters. A better understanding of these processes is essential for developing rational operating protocols and model-based control strategies.

The complex dynamics of a chemostat can be attributed to the adaptive nature of cells. When environmental conditions are changed, the cell alters the intracellular machinery in order to adjust to the new environment. The slow response of the cell occurs because of the slow synthesis of certain intracellular components. *The general objective of this work is to analyze the various experimental data, identify the slow physiological variables responsible for complex transients and understand the kinetics of these slow physiological variable evolutions in terms of fundamental biochemistry and molecular biology.*

1.2 Specific Aims

The specific aim of this work is to develop an integrated model of bacterial cell on the basis of vast experimental data observed in the literature using only few key variables and to verify the model via experimentation. The hypothesis behind this approach is that despite the complexity of the metabolic pathways, only a few slow physiological variables play an important role in the dynamics of the chemostat. An extensive review of the literature indicates that we can describe most transients observed in experiments in two categories:

- The slow response of the cell due to its inability to pick up the growth limiting substrate. This implies that substrate uptake limits the growth.
- The slow response of the cell when it picks up the growth limiting substrate but unable to process toward the growth. This indicates that biomass (e.g., protein) synthesis restricts the growth.

We have attributed the above responses to two slow variables, (1) the ribosomes which are responsible for protein synthesis (2) and the peripheral enzymes that mediate transport of the growth-limiting substrate from the environment to inside the cell. When the environment is changed abruptly, the slow variables generally respond in a biphasic manner. Initially, their synthesis rates accelerate rapidly in time scale of seconds. This rapid response is triggered by two fast variables, free amino acids or/and nucleotide phosphates. And subsequently slow responses on a time scale of hours because of the autocatalytic synthesis of the slow variables.

After developing the model containing transport enzyme and ribosomes, the distribution of the incoming substrate in different metabolic pathways raised another question. When the cell picks up the substrate, it can distribute the incoming substrate in the different pathways (Figure 1–1), i.e., growth, respiration, storage or excretion. Then how does the cell makes the decision about the distribution of the incoming substrate? In order to overcome this obstacle, we have added an artificial intelligence feature to the model cell. Thus, the model was further extended to

account for the metabolic flux distribution during growth and starvation by adding adenine nucleotides as energy molecules.

The goal of the modeling is not merely to fit the data, but to gain further insights into the dynamics of the cell by analyzing the model with the help of theoretical and numerical tools drawn from dynamical systems and bifurcation theory.

In Section 1.3, we summarize the literature and formulate a conceptual model (Figure 1–1) that provides a qualitative explanation of all these observations.

1.3 Literature Review

The exhaustive literature review shows that the key processes that determine the dynamic response of microbial cells are substrate uptake, protein synthesis, storage, and excretion. To account for these processes, we propose the schematic model as shown in Figure 1–1. The goal of this section is to show that the literature provides strong experimental justification for this scheme. In Section 1.3.1, we define the key processes and summarize the literature on their regulations. In Section 1.3.2, we review the experimental literature on the steady states and dynamics of the variables.

1.3.1 Regulation of Key Processes

The goal of this brief overview is to show that the model scheme captures the essential features of the mechanisms that control the growth.

Substrate uptake [1]. The specific substrate uptake rate is determined by the concentration of the growth-limiting substrate and the activity of the *peripheral* enzymes that catalyze the substrate uptake and peripheral catabolism. The key mechanisms controlling peripheral enzyme synthesis are *induction* and *catabolite repression*. The molecular mechanism for induction of peripheral enzymes is universal. The Jacob-Monod model, or some variant of it, applies to most systems.

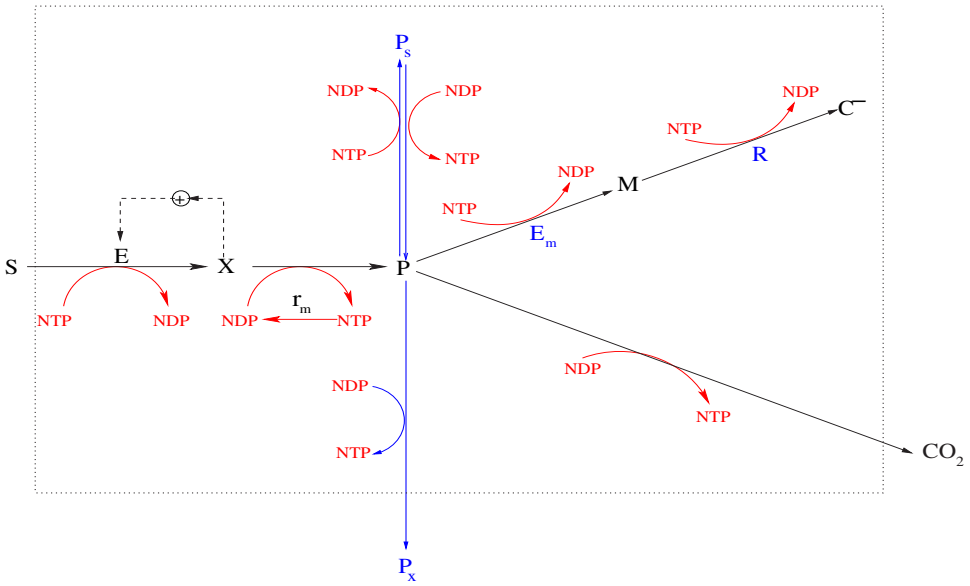

Figure 1–1: The proposed model of microbial growth. Here, S denotes the growth limiting carbon and energy source, E denotes the transport enzyme, X denotes the internalized substrate which induces the synthesis of E, P denotes the precursors produced by catabolism of X, P_s denotes stored compounds, P_x denotes excreted metabolites, E_m denotes biosynthetic enzyme(s), M denotes amino acid monomers, R denotes ribosomes, C^- denotes proteins, and NTP/NDP denote nucleotide tri and diphosphates.

However, there is considerable variation in the mechanisms of catabolite repression [1]. The best known is the classical *cAMP system* in which the uptake of glucose by the phosphotransferase system lowers the pool of cAMP, which inhibits the transcription of the mRNA for enzymes that transport and metabolize other carbon sources.

Protein synthesis [2]. The specific protein synthesis rate is determined by the concentration of free amino acids and ribosomes (Figure 1–2a). Ribosomes are assembled from ribosomal RNA (rRNA) and ribosomal proteins (r-proteins). A negative feedback mechanism ensures that the rate of r-protein synthesis is in synchrony with the prevailing rate of rRNA synthesis [3]. The excess r-proteins bind to the mRNAs that code for them. This inactivates the mRNA and stops

further synthesis of r-proteins. The rate of ribosomal synthesis is, therefore, completely determined by the rate of rRNA synthesis.

It is widely believed that the rRNA synthesis rate is controlled by the concentrations of free nucleotide phosphates (NTPs), amino acids and RNA polymerase (RNAP), but there is considerable disagreement on the molecular mechanism of their action [4]. Jensen and Pedersen proposed a model based on the following hypotheses [5]:

- RNA synthesis is limited by the *elongation* rate of RNA, i.e., the speed with which RNAP moves along the DNA. Consequently, most of the RNAP is bound to DNA, and the concentration of free (unbound) RNAP is relatively small.
- When the concentration of NTPs or/and amino acids increases, the elongation rate of RNAP increases. This increases the concentration of free RNAP, and hence the initiation rate of all genes. The mechanism by which free NTPs stimulate the elongation rate is straightforward, since free NTPs are substrates for RNAP. The mechanism by which amino acids influence the elongation rate is more involved. The ribosomes contain enzymes (*rel*A and *spo*T) that can sense the availability of amino acids. When the concentration of amino acids falls, these enzymes produce a compound called ppGpp which inhibits the elongation rate of RNAP; conversely, when the concentration of amino acids increases, the concentration of ppGpp decreases, and the elongation rate of RNAP increases.
- Genes coding for biosynthetic enzymes and rRNA (called *stringently-controlled* genes) are much more responsive to changes in free RNAP concentration than other genes. Consequently, the rRNA synthesis rate increases much more than the protein synthesis rate.

Recent experiments provide strong evidence supporting all three hypotheses of the Jensen and Petersen model [4].

Storage [6, 7]. Microbial cells store carbon as carbohydrates (glycogen) or lipids (polyhydroxyalkanoates). Although distinct pathways are involved in the synthesis of glycogen and polyhydroxyalkanoates, their regulatory circuits suggest a common principle. In both cases, storage is activated only if *both* precursors and energy are at high concentrations. Glycogen, for instance, is produced by the

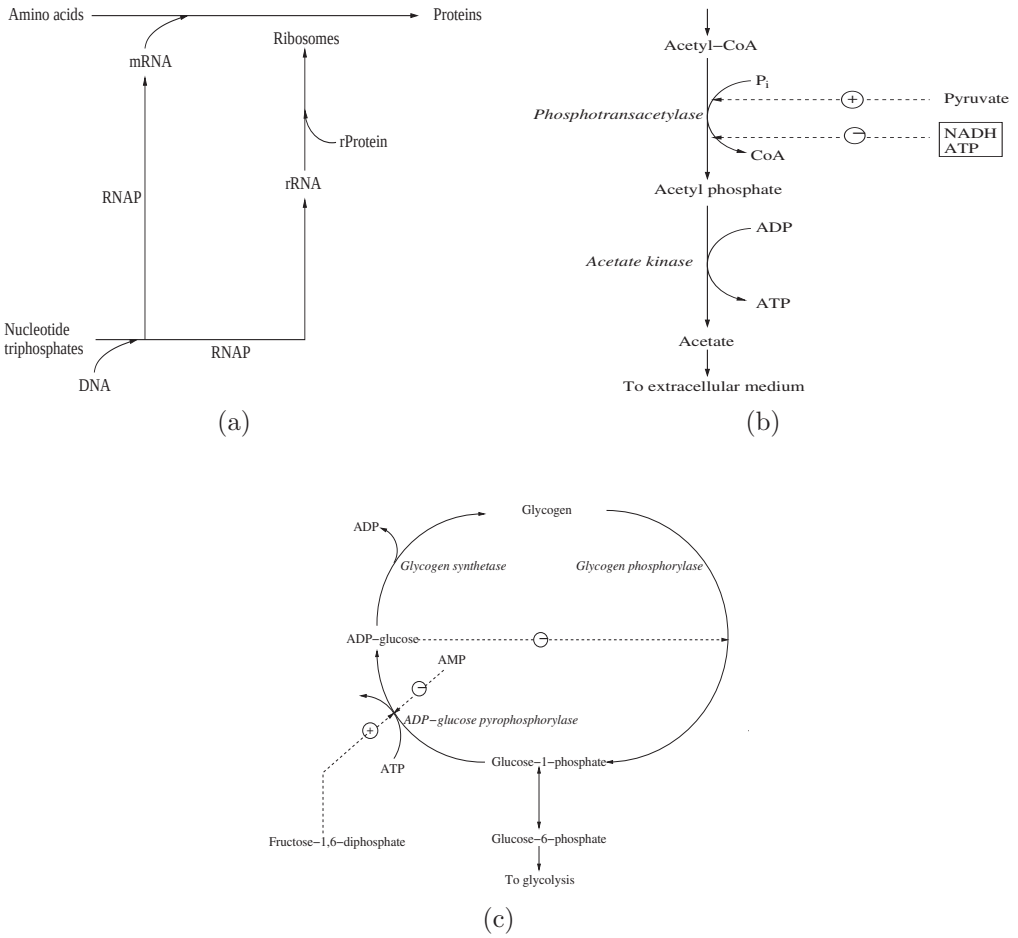

Figure 1–2: Control of protein synthesis, glycogen storage and acetate excretion: (a) Protein synthesis is activated by amino acids (b) Acetate excretion is activated by precursors (pyruvate) but inhibited by energy (NADH, ATP) (c) Acetate excretion is activated by precursors (pyruvate) but inhibited by energy (NADH, ATP) Glycogen storage is activated by precursors (fructose-1,6-diphosphate) and energy (ATP) .

consecutive action of ADP-glucose pyrophosphorylase and glycogen synthetase (Figure 1–2b). In prokaryote, ADP-glucose pyrophosphorylase is the regulated enzyme. It is activated by fructose-1,6-diphosphate and ATP, and inhibited by AMP [6].

Excretion [8]. Cells excrete a wide variety of compounds, depending on the growth-limiting substrate [9]. In carbon-limited growth, acetate is the predominant excreted compound [8]. It is produced by the consecutive action of two enzymes,

phosphotransacetylase and acetate kinase (Figure 1–2c). The regulated enzyme of this pathway is phosphotransacetylase. Its regulation is consistent with the fact that acetate excretion results in the net generation of energy (one mole of ATP for every mole of acetate excreted). It is activated by pyruvate, which signals an abundant supply of precursors, but inhibited by NADH and ATP, which signal an energy surplus [10].

1.3.2 Experimental Data

In this section, we have collated the data on the steady states and dynamics of continuous cultures.

1.3.2.1 Steady states

In single-substrate growth, the experimentalist can vary only two control parameters — the flow rate and the feed concentration. If the feed concentration is increased at a fixed dilution rate, the cell density increases such that the steady state values of all other variables are restored to their previous values [11]. As shown below, the steady state variations are considerably more complex if the dilution rate is changed at a fixed feed concentration.

Cell density and substrate concentration. The cells wash out at *both* small and large dilution rates. The washout at large dilution rates is universally accepted and has been extensively studied beginning with the classical work of Herbert *et al.* [18]. The washout at low dilution rates, often called the *minimum growth rate*, is widely accepted, but there are few systematic studies [19]. Schulze and Lipe showed that glucose-limited cultures of *E. coli* were washed out at dilution rates below 0.02 1/hr [20]. They argued that this washout occurred because at such low dilution rates, the specific uptake rate of the growth-limiting carbon source (glucose) became less than the maintenance coefficient (0.055 g/(gdw-hr)). Tempest *et al.* determined the steady states of glycerol-limited cultures of *K. aerogenes* at dilution rates down to 0.004 1/hr [12]. Under these conditions, the

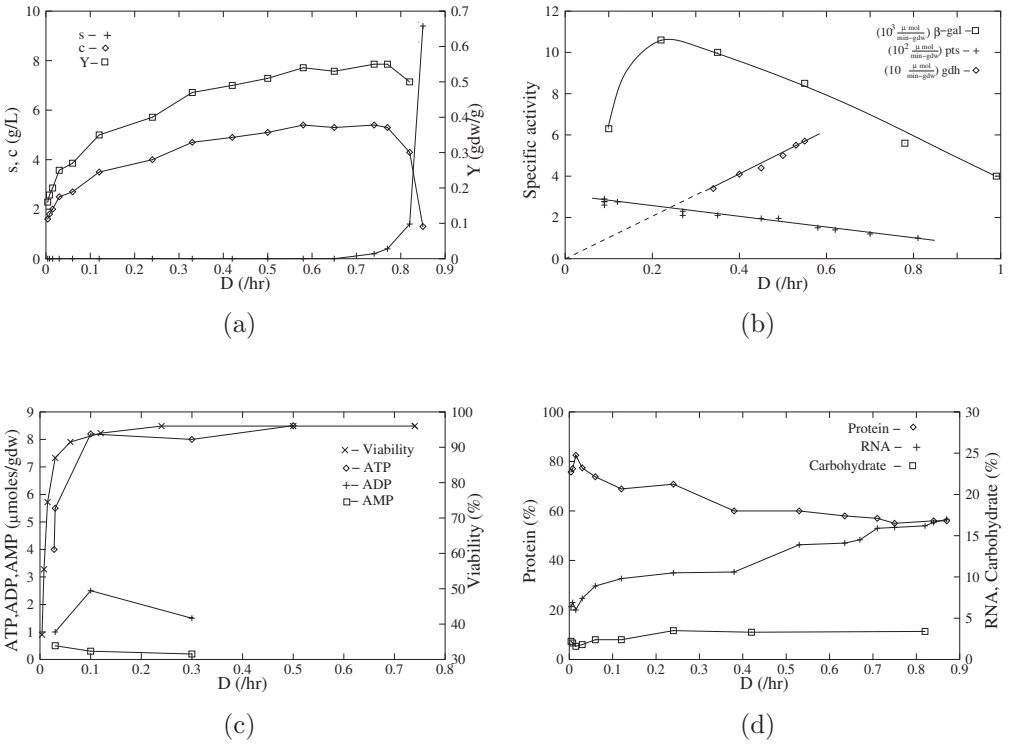

Figure 1–3: Variation of steady state concentrations with respect to dilution rate in carbon-limited cultures of *K. aerogenes*: (a) Cell density, substrate (glycerol) concentration and yield of biomass [12, 13] (b) Peripheral and biosynthetic enzyme levels [14–16] (c) Adenine nucleotides [17] and viability [12] (d) RNA, protein and carbohydrate contents [12, 13].

viability of the cultures dropped to 40% (Figure 1–3c), and the specific growth rate of the viable organisms asymptotically approached a minimum value of 0.009 1/hr.

Between the two washout dilution rates, the cell density passes through a maximum (Figure 1–3a). Since the substrate concentration equals the feed concentration at dilution rates above and below the two washout dilution rates, it should pass through a minimum between these dilution rates. Unfortunately, no data are available except at relatively large dilution rates near the upper washout dilution rate. At such large dilution rates, the substrate concentration is an increasing function of the dilution rate (Figure 1–3a).

Peripheral and biosynthetic enzyme levels [21–23]. Based on a comprehensive review of the literature, we concluded (see Figure 1–3b) that (1) the activity of

inducible peripheral enzymes (e.g., β-galactosidase) passes through a maximum at some intermediate dilution rate (2), the activity of *constitutive* peripheral enzymes [e.g., glucose phosphotransferase system (PTS)] decreases monotonically with the dilution rate (3) and the activity of biosynthetic enzymes [e.g., glutamate dehydrogenase] increases monotonically with the dilution rate [22].

The existence of a maximum in the steady state profile of inducible peripheral enzymes is an outcome of a competition between the opposing effects of enzyme induction and catabolite repression [15]. At low dilution rates, enzyme induction dominates, so that the enzyme level is an increasing function of the dilution rate. Conversely, at high dilution rates, enzyme induction saturates so that catabolite repression dominates, and the enzyme level is a decreasing function of the dilution rate. This argument also explains the decreasing trend of constitutive peripheral enzymes. In such cases, catabolite repression is the only mechanism influencing the enzyme activity, since induction of constitutive enzymes occurs at a constant rate.

Adenine nucleotides. The concentrations of adenine nucleotides are constant at dilution rates above 0.1 1/hr [17]. At lower dilution rates, the concentration of ATP decreases, the concentration of AMP increases, and the concentration of ADP passes through a maximum (Figure 1–3c).

To explain these trends, it suffices to understand the concentration profile of ATP — the concentrations of ADP and AMP are completely determined by the concentration of ATP. This is because ATP, ADP and AMP are in a quasi-equilibrium determined by adenylate kinase; i.e., $[\mathrm{ATP}]\,[\mathrm{AMP}]\,/\,[\mathrm{ADP}]^2 = K$ and the energy charge, defined as the ratio $[\mathrm{ATP}]+0.5\,[\mathrm{ADP}]\,/\,([\mathrm{ATP}]+[\mathrm{ADP}]+[\mathrm{ADP}])$, is ~ 0.9 at all but the smallest dilution rates [24].

Free amino acid pool. Although the data for free amino acid pools are sparse, they show that their total concentration increases with respect to the dilution rate. In ammonia-limited cultures of *A. aerogenes*, the free amino acid pool

concentrations were 5.5, 8.0 and 14.7 mM at dilution rates of 0.1, 0.3 and 0.7 1/hr, respectively [25]. In glucose-limited cultures of *S. cerevisiae*, the concentrations were 380 and 529 mM at dilution rates of 0.1 and 0.25 1/hr, respectively [26]. Glutamate is by far the most abundant amino acid (60–70% of the pool), which is consistent with the fact that glutamate supplies 85% of the amino groups required for protein synthesis.

RNA and protein. RNA and protein are the most predominant cellular constituents (Figure 1–3d). They constitute roughly 80-85% of the dry weight of the cell at all dilution rates between 0.004 and 0.85 1/hr [12, 13]. As the dilution rate increases, the RNA content increases three-fold from 6% at 0.004 1/hr to 18% at 0.85 1/hr. The protein content undergoes a corresponding decrease from roughly 80% to 70% of the dry weight. Thus, as the dilution rate increases, the RNA content grows at the expense of proteins.

At high dilution rates, the ribosome-to-protein ratio is proportional to the dilution rate, which implies that the specific rate of protein synthesis per ribosome or the *ribosomal efficiency* is constant [27]. This suggests that at high dilution rates, the speed with which ribosomes add amino acids to a peptide chain is constant. It follows that at high dilution rates, further improvements in the specific protein synthesis rate, and hence the specific growth rate, can be obtained only by increasing the concentration of the ribosomes. A similar conclusion is reached based on transient experiments described in Section 1.3.2.2.

Carbohydrates and excreted metabolites. The carbohydrate content varies dramatically with respect to the identity of the microbial species and the carbon source. However, for a given microbial species and carbon source, the carbohydrate content is almost independent of the dilution rate (Figure 1–3d). In glycerol-limited cultures of *K. aerogenes*, the carbohydrate content is 1.6–3.4% at all dilution rates

between 0.004 and 0.85 1/hr [12, 13]. In glucose-limited cultures of *T. utilis*, the carbohydrate content is 20% at all dilution rates between 0.04 and 0.5 1/hr [28].

The extracellular acetate concentration also varies significantly depending on the identity of the microbial species and the carbon source. In glycerol-limited cultures of *K. aerogenes*, there is no measurable excretion at all dilution rates between 0.004 and 0.85 1/hr [12]. In glucose- and pyruvate-limited cultures of *E. coli*, there is pronounced excretion of acetate (see dashed line in Figure 1–6d), but only at sufficiently high dilution rates [29–32].

1.3.2.2 Transients

Chemostats have been subjected to four types of perturbations: Dilution rate shifts, continuous-to-batch shifts, substrate pulses and substrate switches. Each of these perturbations has yielded unique insights into the variables that control the growth dynamics.

Dilution rate shift. In dilution rate shift-up experiments, the chemostat is allowed to reach steady state at some initial dilution rate, say, D_0, and the dilution rate is abruptly increased to $D > D_0$. These experiments show that chemostats display *excitable* dynamics; i.e., they return to the steady state rapidly when subjected to small perturbations, but undergo a large and prolonged excursion when subjected to large perturbations [33].

Mateles *et al.* demonstrated excitable dynamics in a chemostat by subjecting nitrogen-limited cultures of *E. coli* B to dilution rate shift-ups [34]. They observed that the specific growth rate increases *instantly* in response to the dilution rate shift-up, regardless of the initial dilution rate. If the shift-up, $D - D_0$, is small, the enhanced specific growth rate immediately equals the new dilution rate. If the dilution rate shift-up is large, the enhanced specific growth rate cannot match the new dilution rate (Figure 1–4). There now begins a period during which the specific growth rate increases slowly. During this period, the cell density

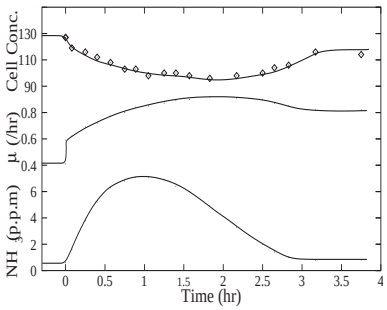

Figure 1–4: Response of nitrogen-limited culture of *E. coli* B to a dilution rate shift from $D = 0.41$ 1/hr to $D = 0.83$ 1/hr at a fixed feed concentration of 100 mg/L (from [34]).

decreases and the substrate concentration increases. This large excursion of the substrate concentration, which can last a few hours, is finally contained when the specific growth rate becomes equal to the new dilution rate. At this instant ($\hat{t}$) the substrate concentration reaches a maximum ($\hat{s}$) and the cell density reaches a minimum. This is followed by a period during which the specific growth rate exceeds the new dilution rate. During this period, the cell density increases and the substrate concentration decreases until they reach values consistent with the new steady state. The time taken to return to the steady state (t_∞) can be as long as 12.5 hours.

Similar transients have been obtained in carbon-limited [12, 35–37] and phosphate-limited cultures [38, 39].

Substrate switch. The substrate switch experiments reveal that *if the peripheral enzyme for the growth-limiting substrate are inducible and and if the concentration level of the enzyme is small, the growth is limited by the substrate uptake rate.* Herein, the culture is allowed to reach steady state at a given dilution rate and feed concentration on one substrate. Once the steady state is achieved, the identity of the growth-limiting substrate is switched abruptly to any other substrate.

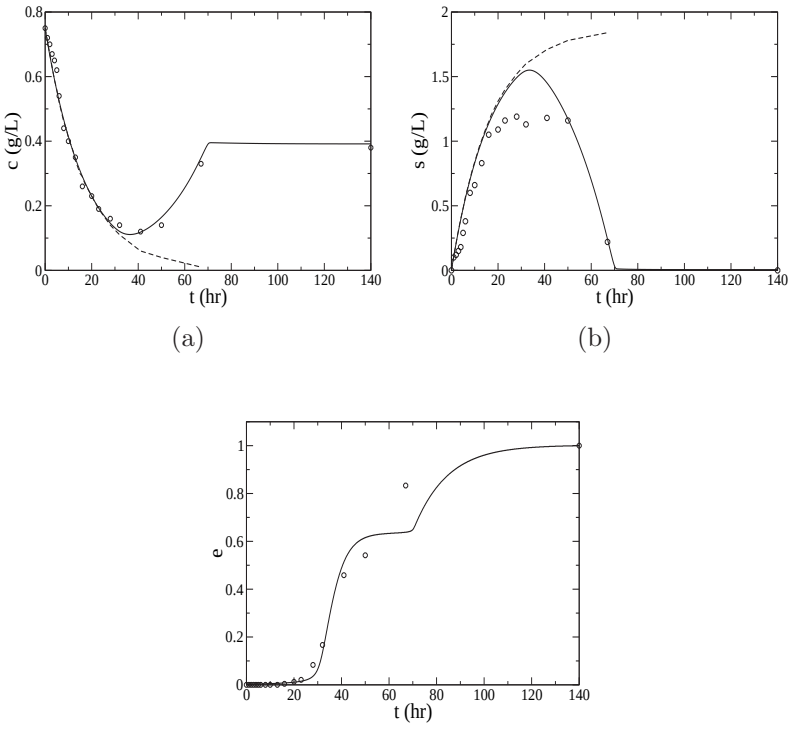

Figure 1–5: Response to a switch in the identity of the growth-limiting substrate from glucose to nitrilotriacetic acid (NTA) in a culture of *C. heintzii* (data from [40], simulations from [41]). The dilution rate was held fixed at 0.006 1/hr. The dashed line in (a, b) shows the profile that would be obtained if there was no substrate consumption.

Bally and Egli performed substrate switch experiments with *C. heintzii* cultures growing in a chemostat under glucose or nitrilotriacetic acid (NTA) limitation [40]. When the carbon source was switched from NTA to glucose, the rapid growth was observed after 2–3 hours. In contrast, when the carbon source was switched from glucose to NTA, *there was almost no substrate consumption for nearly 30 hours* (Figure 1–5a,b). The dramatic difference in the time required to consume significant amounts of substrate is due to the difference in the initial peripheral enzyme levels. The peripheral enzymes for glucose, being constitutive, are always present at high levels. Consequently, when the substrate is switched from NTA to glucose, consumption of glucose begins immediately. On the other hand, the peripheral enzymes for NTA, being inducible, have vanishingly small

concentrations during growth on glucose. When the culture is shifted from glucose to NTA, it takes several tens of hours before the peripheral enzymes for NTA build up to sufficiently high levels (Figure 1–5c).

Similar results were obtained when bacterial cultures were shifted from glucose to xylose and *vice versa* [37, 42]. Switching from glucose to xylose led to a prolonged decrease in the cell density lasting over 1 day during which xylose accumulated in the chemostat. Switching from xylose to glucose caused no measurable accumulation of glucose.

In substrate switches, the growth rate is limited by substrate uptake only because the cells have not been growing on the substrate, so that the initial levels of the peripheral enzymes are vanishingly small. However, if the cells have been growing on the substrate at some dilution rate, the initial enzyme level is relatively large at all but the smallest dilution rates (see curve for β-galactosidase in Figure 1–3b). It follows that the transient response of cells growing at very low dilution rates will be controlled by peripheral enzyme synthesis. Moreover, the transient will be characterized by long recovery times (on the order of days) and the absence of excretion and storage [12]. A systematic study has never been done, but it seems likely that the transient response of cells growing at medium to large dilution rates will be controlled by rRNA synthesis. This transient will be characterized by short recovery times (on the order of hours) and it will be accompanied by significant excretion or/and storage.

Continuous-to-batch shift. In dilution rate shift-ups, the substrate concentration instantly increases to supersaturating levels. The specific growth rate also increases instantly but does not reach the maximum specific growth rate despite the presence of supersaturating substrate concentrations. This raises two questions: (1) What is responsible for the instantaneous increase in the specific growth rate?

(2) What prevents the specific growth rate from instantly achieving the maximum value? The answers to both questions are provided by continuous-to-batch shifts.

In these experiments, a sample of cells is withdrawn from a steady state continuous culture growing at a certain dilution rate. The sample is immediately exposed to supersaturating substrate concentrations in a batch reactor, and the initial rates of various processes (substrate uptake, growth, respiration and excretion) are measured. These experiments show that regardless of the dilution rate at which cells are growing before their withdrawal from the chemostat:

- The specific substrate uptake rate immediately accelerates to its maximal value. This is the value that would be observed in batch cultures growing exponentially under substrate-excess conditions [43–45] (Figure 1–6a).
- The specific respiration rate also increases rapidly to the maximal level expressed under substrate-excess conditions [14, 46] (Figure 1–6b).

It follows that there is an adequate supply of precursors and energy immediately after the shift-up.

In contrast, the specific biosynthesis rate (of RNA and protein) depends crucially on the dilution rate at which cells are growing before their withdrawal from the chemostat [14]. When exposed to supersaturating substrate concentrations (Figure 1–6c)

- The specific biosynthesis rate of cultures growing at low dilution rates ($D < 0.3$ 1/hr) increases instantly, but does not reach the maximum value.
- The specific biosynthesis rate of cultures growing at high dilution rates ($D > 0.3$ 1/hr) does *not* improve immediately. The RNA content increases markedly after 30 minutes, and the protein content increases after 60 minutes.

This answers the second question raised above. *It is the slow synthesis of RNA and proteins that prevents the specific growth rate from instantly achieving its maximum value.* Also consistent with this conclusion is the observation that

- The specific excretion rate instantly increases to very high levels [29, 45] (Figure 1–6d).
- The specific glycogen synthesis rate also increases to very high levels [14].

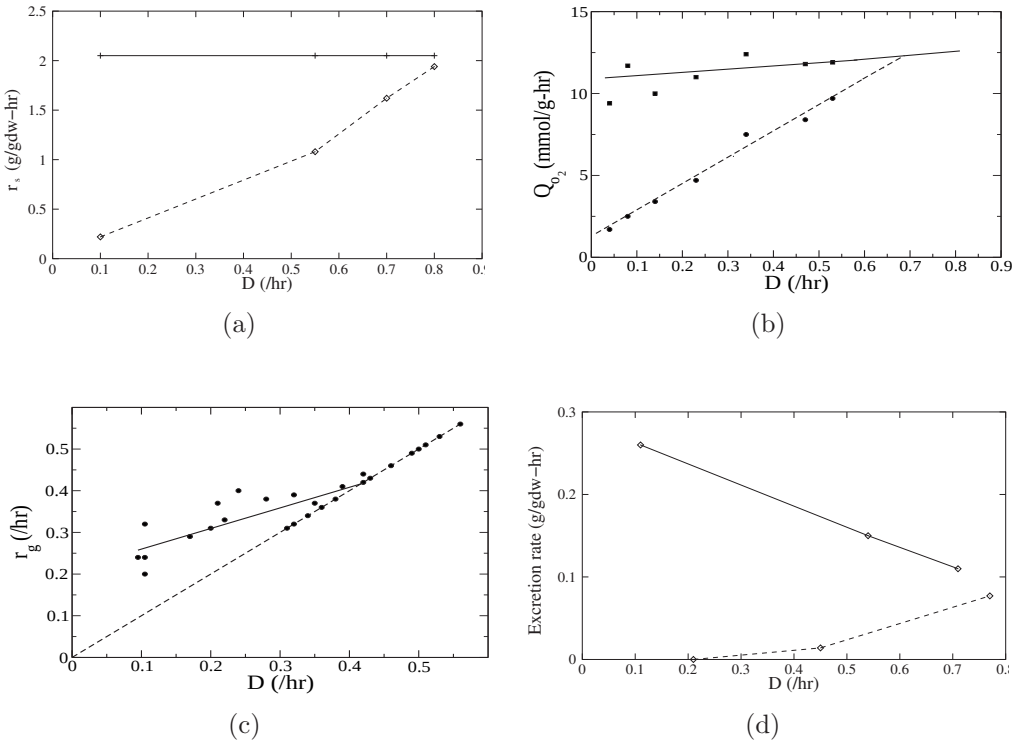

Figure 1–6: Initial response of glucose-limited steady state continuous cultures growing at various dilution rates to supersaturating glucose concentrations. The dashed line shows the rate of a process during steady state growth in a chemostat. The full line shows the *initial* rate of the same process when the culture is abruptly exposed to supersaturating glucose concentrations. (a) Specific substrate uptake rate [45] (b) Specific respiration rate [46] (c) Specific biosynthesis rate [14] (d) Specific excretion rate [29, 45]). The data in (c) was obtained with *glycogenless* mutants of *E. coli* B. All other data was obtained with wild-type *K. aerogenes*.

This indicates that the substrate uptake and respiration rates immediately increase to their maximal levels, whereas the specific biosynthesis rate increases only partially. Consequently, there is rapid accumulation of precursors, resulting in storage and excretion. *The instantaneous improvement in the specific growth rate of cultures growing at low dilution rates is due to rapid synthesis of RNA, protein, and glycogen. The instantaneous improvement in the specific growth rate of cultures growing at high dilution rates is due to rapid synthesis of glycogen, since the RNA and protein synthesis rates of such cultures increase only after a lag of 30–60 minutes.* Based on these experimental data and the mechanisms described in

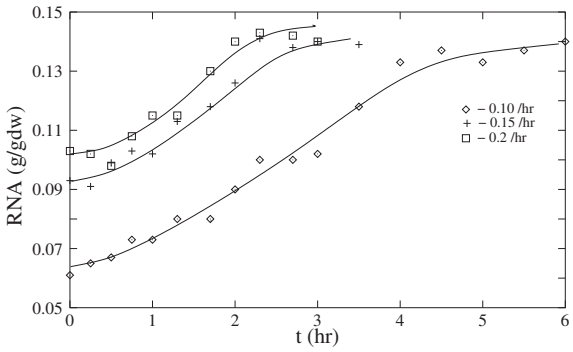

Figure 1–7: Autocatalytic kinetics of RNA synthesis in glucose-limited cultures of *Azotobacter vinelandii* in response continuous-to-batch transitions [47]. The three curves shown correspond to initial dilution rates of 0.1, 0.15 and 0.20 1/hr. The maximum specific growth rate on glucose is 0.275 1/hr.

Section 1.3.1, we can synthesize the following picture of the chemostat transients in response to substrate-excess conditions.

In cultures growing at **low** dilution rates, biosynthetic enzymes, RNA polymerase (RNAP) and ribosomes are subsaturated with respect to precursors, nucleoside triphosphates (NTPs) and amino acids, respectively. When the exogenous substrate concentration increases in response to a shift-up, the specific substrate rate immediately increases causing rapid acceleration in the synthesis rates of all the intracellular components. During this *fast* transient, the concentrations of the fast variables (precursors, NTPs, and amino acids) increase instantaneously, while the concentrations of the slow variables (biosynthetic enzymes, RNAP, ribosomes, RNA and proteins) remain essentially constant. The rapid increase of NTPs or/and amino acids triggers rRNA synthesis by the mechanisms described in Section 1.3.1. The fast transient is followed by a *slow* dynamic during which the concentration of RNA increases sigmoidally (Figure 1–7) [14, 47, 48]. The sigmoidal kinetics reflect the autocatalytic kinetics of RNA synthesis. Indeed, an increase in the concentration of RNA implies an increase in the concentration of ribosomes. This promotes the synthesis of proteins in general and RNAP in particular, which results in the synthesis of even more RNA.

In cultures growing at **high** dilution rates, the RNA and protein synthesis rates show no improvement on the fast time scale. It follows that either the biosynthetic enzymes are saturated with precursors or the ribosomes are saturated with amino acids. There is evidence supporting both conclusions. Harvey has shown that the specific growth rate is proportional to the activity of glutamate dehydrogenase throughout the transient response in a continuous-to-batch shift [14]. On the other hand, it has been shown that when amino acids are added to a culture growing on excess glucose, there is no change in the protein synthesis rate until additional ribosomes are synthesized [2, 14, 49]. Although both hypotheses are tenable, they imply different consequences. If the biosynthetic enzyme(s) are saturated with precursors, there should be no change in the concentration of amino acid monomers. However, there should be a rapid accumulation of precursors (leading to excretion or/and storage) and NTPs. Accumulation of NTPs would stimulate RNA synthesis which in turn would promote synthesis of the biosynthetic enzyme(s). If the ribosomes are saturated with amino acid monomers, there should be accumulation of amino acid monomers which in turn would stimulate synthesis of rRNA. High concentrations of amino acids should persist until ribosomal concentrations build up to sufficiently large levels.

Substrate pulse. In the substrate pulse experiments, the reactor is maintained at steady state at a fixed dilution rate. A small perturbation is given to the glucose concentration by injecting a pulse of extra glucose in the reactor. The glucose concentration instantly increases to supersaturating level, and the cell displays the dynamics similar to continuous to batch shifts for first few minutes. As glucose is being consumed and washing out together, the glucose concentration decreases continuously and became subsaturating. Thus, the reactor comes back to the initial steady state in the next few hours. This type of perturbation has been widely used to study the role of adenine nucleotides (ATP) as energy molecules in the cell.

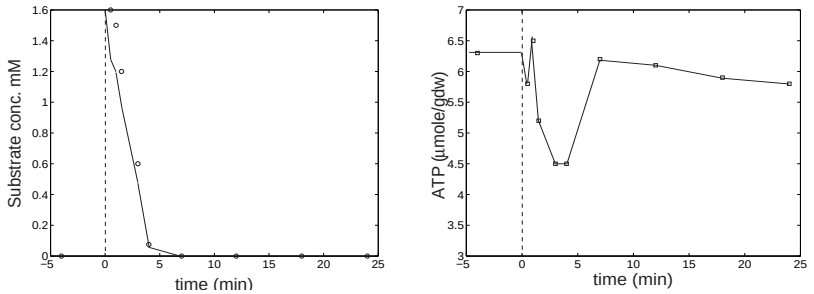

(a) (b)

Figure 1–8: Transient response to a substrate pulse in minutes time scale. At $t < 0$, the culture was at steady state corresponding to dilution rate $d = 0.21$/hr. Glucose was injected at time $t = 0$ to the chemostat.

The cell uses ATP as energy molecule in the protein, polysaccharides synthesis etc, and as raw material in the RNA, DNA, Protein synthesis. The ATP concentration is very small 6- 10 $\mu mole/gdw$ for most bacterial cell and yeast cell at steady state. Atkinson has calculated the ATP turnover rates for Salmonella typhimurium and Escherichia coli and concluded that ATP exhibits fast dynamics. The ATP pool was consumed and further replenished in less than $38 - 381$ seconds at different growth rates [50].

Harrison and Mitra have used a substrate pulse experiments to examine the status of ATP concentration inside the cell for the first 10 mins [17]. As the initial transients are same as continuous to batch shift, the substrate uptake rate and respiration rate jumps instantaneously. Hence, the ATP concentration should also increase, however the fall in ATP concentration was observed (Figure 1–8). At initial consideration, the fall in ATP concentration with an increased availability of substrate and increase respiration rate seems anomalous. But it was explained by an increased utilization of ATP for the synthesis of polysaccharides and other cell components.

To capture the fast dynamics in seconds time scale, the pulse experiments have been done using rapid sample collection technique [51, 52]. The drop in ATP

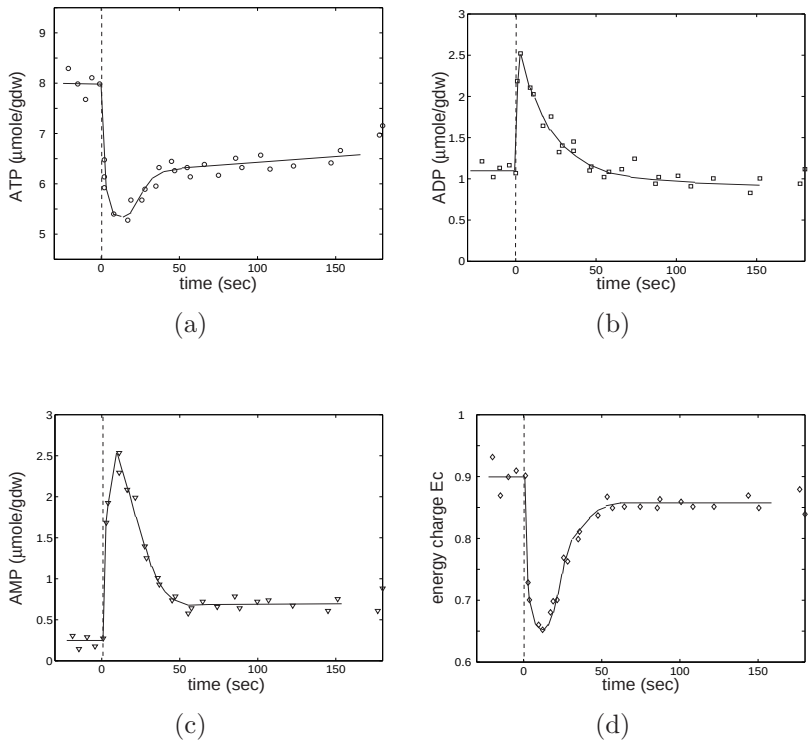

Figure 1–9: Transient response to a substrate pulse in seconds time scale. At $t < 0$, the culture was at steady state corresponding to dilution rate $d = 0.11$/hr. Glucose was injected at time $t = 0$ to the chemostat culture. The figure show the evolution of the (a) Adenine triphosphate, (b) Adenine diphosphate, (c) Adenine monophosphate concentration and (d) Energy charge. Energy charge was calculated by using ATP, ADP and AMP concentration.

concentration with subsequent recovery was observed in first 40 seconds (Figure 1–9). The drop in ATP concentration immediately after increased injection of the glucose pulse was attributed to sudden increase in ATP consumption caused by increased in the glucose transport process. At steady state, the transport enzymes are subsaturated with respect to glucose. When the glucose concentration increases in response to a pulse, the transport enzyme becomes saturated resulting in immediate increase in the specific substrate uptake rate. Glucose gets phosphorylated in glucose-6-phosphate by consuming phosphate from ATP in the process of transport. This ATP consumption results in the decrease in ATP concentration, thereby increasing the ADP concentration and decreasing the energy charge.

CHAPTER 2
THE ROLE OF TRANSPORT ENZYME

Overshoot in the substrate concentration occurs when the starved cells are suddenly exposed to large substrate concentrations by increasing the flow rate or the substrate concentration in the feed. Two factors could contribute to this phenomenon. Either the starved cells lack the enzyme which transports the substrate from the medium into the cell, and a considerable length of time is required to synthesize the enzyme to a level that is high enough to match the increased supply of substrate. Or the starved cells lack the ribosomal machinery required to convert the catabolic products derived from the substrate into biomass. The resultant accumulation of the catabolic products represses substrate uptake by inhibiting the transport enzyme. Furthermore, it takes a long time to build the ribosomal machinery to a level consistent with the higher specific growth rate that is required to match the increased supply of substrate [2].

We are addressing this question by systematically investigating the role of potential candidates. In this chapter, we studied the role of *peripheral enzymes,* i.e., the enzymes that catalyze the transport and peripheral catabolism of substrates [41]. This study was motivated by the dynamics of *substrate switches*. Figure 1–5 shows an example of such an experiment. When the growth-limiting carbon source of a *C. heintzii* culture is switched from glucose to nitrilotriacetic acid (NTA), there is almost no substrate uptake, and hence, no growth for ∼30 hours (see Figures 1–5a,b). We argued that this is because the synthesis of the peripheral enzymes for NTA is inducible, and hence, autocatalytic. Since the cells have not seen NTA until the substrate is switched, the initial level of the peripheral enzymes for NTA is vanishingly small (Figure 1–5c). Because inducible enzyme

synthesis is autocatalytic, it takes several hours to build sufficiently high levels of these enzymes.

Several structured models have been proposed in order to capture single-substrate dynamics. These include highly structured models accounting for maintenance, storage, and synthesis of ribosomes and various enzymes [53, 54]. The goal of this work is to study the role of transport enzyme in single-substrate growth. The model has been developed to explain the dilution rate shift-up and substrate switch experiments, where the sluggish response of a chemostat, whenever it occurs, is exclusively due to low transport enzyme levels in the cells. We assume, that there is no maintenance, and "excess" ribosomes are always available for these cases. This assumption is not to deny the roles of maintenance and ribosomal synthesis, but to determine the extent to which enzyme synthesis alone can account for the observed lags. Experiments show that in *E. coli*, the assumption of "excess" ribosomes is valid for dilution rates up to 0.4 1/hr.

2.1 The Model

The kinetic scheme is shown in Figure 2–1. Here, S denotes the substrate, E denotes the inducible enzyme or "lumped" system of inducible enzymes catalyzing the uptake and peripheral catabolism of S, X denotes the inducer for E, P denotes the "lumped" pool of biosynthetic precursors, and C^- denotes all constituents of cell mass except E, X, and P. The entire cell consisting of E, X, P and C^- is denoted by C. The concentrations of these entities are denoted by the corresponding lower-case letters s, c, e, x, p, and c^-. Here, s g/L and c gdw/L are based on the volume of the chemostat, whereas x, e, p and c^- g/gdw are based on the dry weight of the biomass. Steady state and quasi-steady state concentrations are denoted by overlaying these letters with $\sim$ and $-$, respectively (for instance, $\tilde{x}$ and $\bar{x}$). The yield, denoted Y, is the mass of P produced per unit mass of X.

The following assumptions are made about the kinetics of the various processes

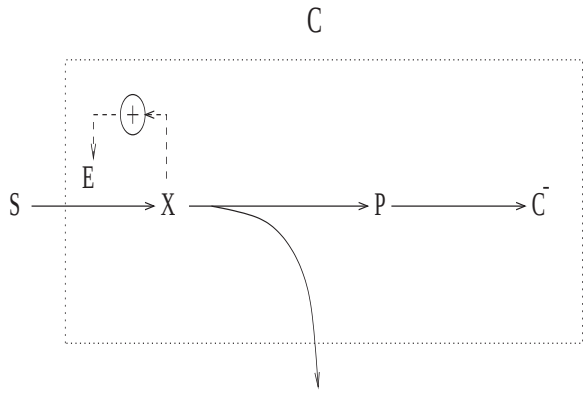

Figure 2–1: Kinetic scheme of the transport enzyme model. Here, S denotes the substrate, X denotes the inducer, E denotes the inducible enzyme(s) catalyzing the uptake and peripheral catabolism of S, P denotes the biosynthetic precursors derived from catabolism of X, C^- denotes the remaining components of biomass, and C denotes the entire cell consisting of E, X, P and C^-. The positive feedback loop represents the induction of enzyme synthesis.

The specific substrate uptake rate, denoted r_s, satisfies the kinetic law

$$r_s \equiv V_s e \frac{s}{K_s + s}$$

The specific rate of breakdown of X into energy and precursors P, denoted r_x, is given by

$$r_x \equiv k_x x$$

The specific rate of formation of C^- is given by

$$r_c \equiv k_g p$$

The specific rate of enzyme synthesis, denoted r_e, is

$$r_e \equiv V_e \frac{1 + K_1 x + K_2 x^2}{K_3 + K_1 x + K_2 x^2}$$

This kinetic is obtained because the repressor can bind to two inducer molecules [55]. Thus, K_1 is the equilibrium constant for binding of a repressor to one inducer molecule, K_2 is the equilibrium constant for binding of a repressor to two inducer

molecules, and K_3 is proportional to the equilibrium constant for binding of a repressor to an operator.

In what follows, we shall appeal to the following two facts. First, since repressor-operator binding is not perfectly tight, ie., K_3 is finite, the enzyme is synthesized even in the absence of the inducer; this phenomenon is referred to as *constitutive* enzyme synthesis. Second, if $K_2 \gg K_1^2$, as is the case for the *lac* operon, binding of the first inducer molecule to a repressor facilitates the binding of the second inducer molecule, resulting in cooperative or sigmoidal kinetics.

The specific rate of enzyme degradation, denoted r_d, follows first-order kinetics

$$r_d \equiv k_d e$$

The yield, Y, is a fixed "stoichiometric" coefficient. That is, the rates of non-biosynthetic processes, such as overflow metabolism, energy spillage, and maintenance, are proportional to the biosynthetic rate.

A mass balance on the state variables yields

$$\frac{ds}{dt} = D(s_f - s) - r_s c \tag{2.1}$$

$$\frac{dx}{dt} = r_s - r_x - \left(D + \frac{1}{c}\frac{dc}{dt}\right) x \tag{2.2}$$

$$\frac{dp}{dt} = Y r_x - r_e + r_d - r_p - \left(D + \frac{1}{c}\frac{dc}{dt}\right) p \tag{2.3}$$

$$\frac{de}{dt} = r_e - r_d - \left(D + \frac{1}{c}\frac{dc}{dt}\right) e \tag{2.4}$$

$$\frac{dc^-}{dt} = r_c - \left(D + \frac{1}{c}\frac{dc}{dt}\right) c^- \tag{2.5}$$

where the last term in (2.2–2.5) represents the dilution of X, P, E, and C^-, respectively, by effluent flow and growth, s_f denotes the concentration of S in the feed, and D denotes the dilution rate. It is shown in [56] that since

The mass fraction of all intracellular entities equals unity

$$x + p + e + c^{-} = 1\, g/gdw$$

The inducer and precursor concentrations rapidly achieve quasi-steady state

$$\frac{dx}{dt} = \frac{dp}{dt} = 0 \quad \Rightarrow \quad r_x \approx r_s, \;\; r_c \approx Y r_x$$

equations (2.1–2.5) are approximated by the following equations

$$\frac{ds}{dt} = D(s_f - s) - \left(V_s e \frac{s}{K_s + s}\right) c \tag{2.6}$$

$$\frac{de}{dt} = V_e \frac{1 + K_1\bar{x} + K_2\bar{x}^2}{K_3 + K_1\bar{x} + K_2\bar{x}^2} - \left(Y V_s e \frac{s}{K_s + s} + k_d\right) e \tag{2.7}$$

$$\frac{dc}{dt} = \left(Y V_s e \frac{s}{K_s + s} - D\right) c \tag{2.8}$$

$$k_x\bar{x} = V_s e \frac{s}{K_s + s} \tag{2.9}$$

$$k_g\bar{p} = Y V_s e \frac{s}{K_s + s} \tag{2.10}$$

for all but a negligibly small initial time interval.

2.2 Simulations

The simulations were done with parameter values in Table 2–1.

Table 2–1: Parameter values used in the transport enzyme model simulations.

$V_s = 10^4 \frac{g}{gdw-hr}$	$K_s = 10^{-2} \frac{g}{L}$	$Y = 0.4 \frac{gdw}{g}$
$k_x = 900 \frac{1}{hr}$	$V_e = 2 \times 10^{-4} \frac{g}{gdw-hr}$	$K_1 = 10^5 \frac{gdw}{g}$
$K_2 = 10^{11} \left(\frac{gdw}{g}\right)^2$	$K_3 = 10^5$	$k_d = 10^{-2} \frac{1}{hr}$

2.2.1 Steady States

Equations (2.6–2.10) admit two types of steady states, namely, the persistence ($\tilde{c} \neq 0$) and the washout ($\tilde{c} = 0$) steady states; we denote them by ϕ_1 and ϕ_0, respectively.

The persistence steady state, ϕ_1, is unique, no matter what the parameter values. At the persistence steady state, the specific growth rate equals the dilution rate; that is

$$YV_s\tilde{e}\frac{\tilde{s}}{K_s+\tilde{s}} = D \tag{2.11}$$

It immediately follows that

$$\begin{aligned}
\tilde{x}(D) &= \frac{D}{Yk_x} && (2.12)\\
\tilde{p}(D) &= \frac{D}{k_g} && (2.13)\\
\tilde{e}(D) &= \frac{1}{D+k_d}\left[V_e\frac{1+K_1\tilde{x}+K_2\tilde{x}^2}{K_3+K_1\tilde{x}+K_2\tilde{x}^2}\right] && (2.14)\\
\tilde{s}(D) &= K_s\frac{D}{YV_s\tilde{e}-D} && (2.15)\\
\tilde{c}(D,s_f) &= Y(s_f-\tilde{s}) && (2.16)
\end{aligned}$$

At feed concentrations ($s_f = 1.5$ g/L), there is a unique washout dilution rate at $D_w = 0.8$ 1/hr, and the bifurcation diagram is formally similar to the bifurcation diagram for the Monod model (Figure 2–2). Below the (unique) washout dilution rate, the persistence steady state is globally stable; above the washout dilution rate, the washout steady state is globally stable.

2.2.2 Transients

2.2.2.1 Dilution rate shifts

In these experiments, at $t < 0$, the culture is in a steady state at some dilution rate, sayD_0, and feed concentration, s_f. At $t = 0$, the dilution rate is shifted up to a new value, $D > D_0$, while the feed concentration, s_f, is held fixed. If the shift-up, $D - D_0$, is small, the higher specific growth rate thus achieved equals the higher dilution rate, D. In this case, the change in the substrate concentration and cell density is imperceptibly small. If the shift-up, $D - D_0$, is large, the higher specific growth rate achieved on the fast time scale falls short of the dilution rate, D. The rapid increase of the specific growth rate is followed by a period of slow increase

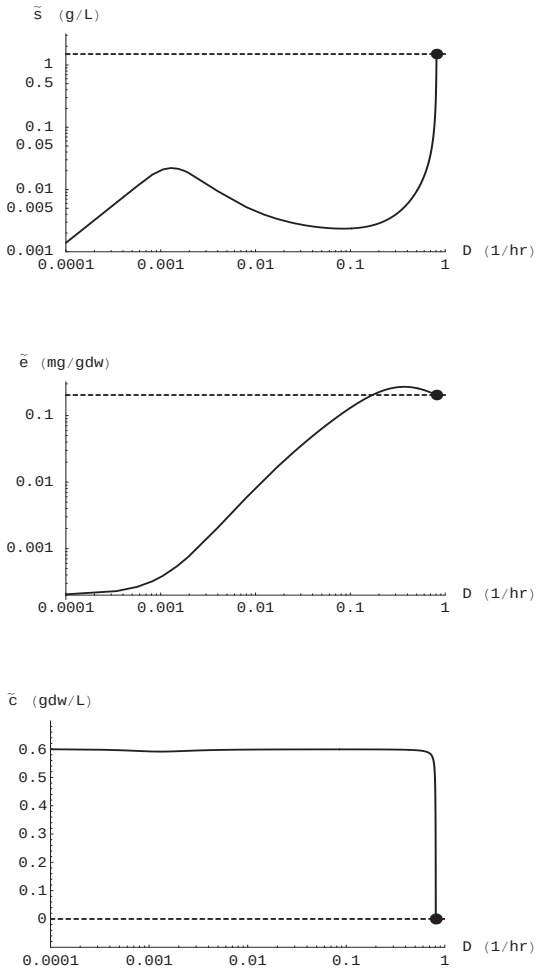

Figure 2–2: Variation of steady states with D at $s_f = 1.5$ g/L. The washout bifurcation point is denoted by the symbol •. Stable and unstable steady states are denoted by full and dashed lines, respectively.

during which s increases and c decreases. After several hours or days, the specific growth rate of the culture catches up with the increased dilution rate. At this instant, s reaches a maximum and c attains a minimum. Thereafter, the specific growth rate is higher than D; during this period, s decreases and c increases until the culture reaches a new steady state consistent with the new dilution rate D.

We show that all three features are mirrored by the model. If D_0 is small compared to D, the initial enzyme level is so small that the specific growth rate

cannot match the new dilution rate even after the substrate concentration has reached supersaturating levels ($s \gg K_s$). To mitigate this growth rate deficit, the cells begin the slow process of enzyme synthesis under supersaturating substrate concentrations. During this period, which lasts several hours (see Figure 2–3), s increases and c decreases. This continues until the specific growth rate becomes equal to D. The orbit then enters the region in which the specific growth rate exceeds D, and begins its final approach to the steady state. During this period, e continues to grow, but s decreases until the steady state is achieved.

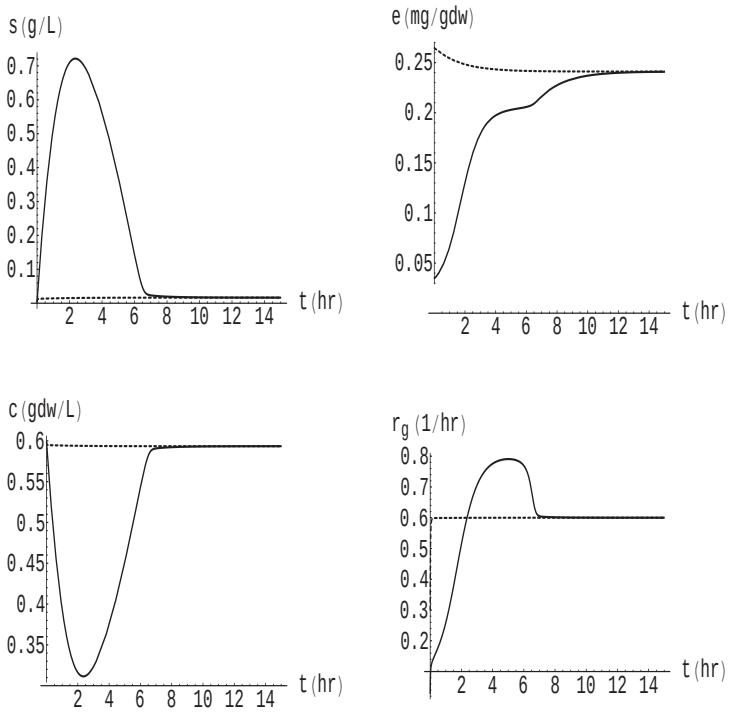

Figure 2–3: Trajectories for dilution rate shifts to the final dilution rate, $D = 0.6$ 1/hr, from initial dilution rates, $D_0 = 0.03$ 1/hr (full lines) and $D_0 = 0.3$ 1/hr (dashed lines); the feed concentration, s_f, is held fixed at 1.5 g/L.

2.2.2.2 Feed switches

In these experiments, at time $t < 0$, the culture is allowed to reach a steady state. At time $t = 0$, the identity of the growth-limiting substrate is changed while

holding the dilution rate and the feed concentration fixed at their original values. Under such perturbations, it is observed that [37, 40, 43]

- The substrate concentration immediately increases, and the cell density rapidly decreases.
- The magnitude of the response depends on the nature of the substrate and the dilution rate at which the identity of the substrate is switched.

If the new substrate supports a relatively large constitutive enzyme synthesis rate, the culture recovers rapidly and there is no observable substrate overshoot; if the new substrate supports a relatively small constitutive enzyme synthesis rate, there is a very pronounced lag before the excursion of the substrate concentration can be contained.

To consider the dynamics of the model, the full system consisting of equations (2.6–2.8) must be considered along with the initial conditions

$$s(0) = 0, e(0) = e_0 = \frac{V_e}{K_3}\frac{1}{D + k_d}, c(0) = c_0$$

Here, e_0 is the steady state enzyme level in cells growing at a dilution rate, D, in the absence of the substrate, and c_0 is the cell density of the culture on the previous substrate. The larger the value of K_3, the smaller the initial enzyme level.

Simulations show that the time required for the chemostat to achieve the new steady state depends very strongly on K_3. When $K_3 = 10^5$, it takes 1000 hours for the substrate concentration to reach values comparable to K_s. Such long lags have, and will, never be observed; therefore, we assumed that $K_3 \sim 10^4$. When $K_3 = 10^4$, the recovery time is on the order of 10 hours (Figure 2–4); when $K_3 = 5 \times 10^4$, the recovery time increases by an order of magnitude (Figure 2–5). Both figures also show that the recovery time depends on the dilution rate at which the identity of the substrate is switched. In terms of our model, this phenomenon has a simple explanation. At large dilution rates, the mass flow rate of the new substrate is

higher and the initial enzyme level is lower; that is, a higher substrate burden is imposed upon cells that are even less capable of consuming the substrate.

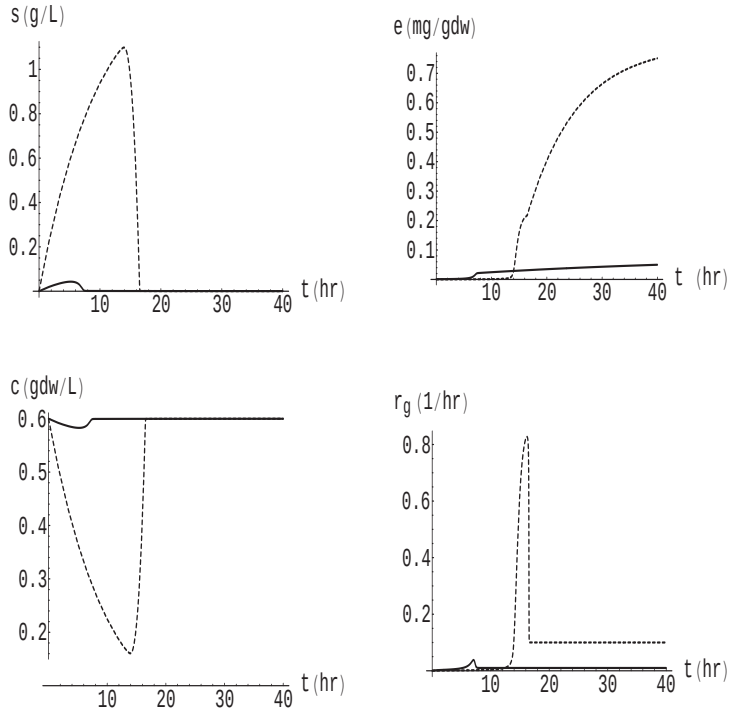

Figure 2–4: Trajectories for a switch in the identity of the substrate at $D = 0.01$ 1/hr (full lines) and $D = 0.1$ 1/hr (dashed lines); K_3 was assumed to be 10^4.

2.3 Discussion

The goal of this work is to advance our understanding of dynamics of a chemostat in response to sudden changes in the flow rate, or identity of a single growth-limiting substrate. To this end, we have analyzed a simple model accounting for induction and dilution of the transport enzyme. The parameter values of the model are based on the *lac* operon. Despite the simplicity of the model, the results are promising. We show that At high feed concentrations ($s_f \sim 1$ g/L), the simulations agree qualitatively with known experimental data for perturbations, namely, abrupt increases in flow rate, and change in the identity of the substrate. We find that in all cases, the substrate concentration increases for several hours

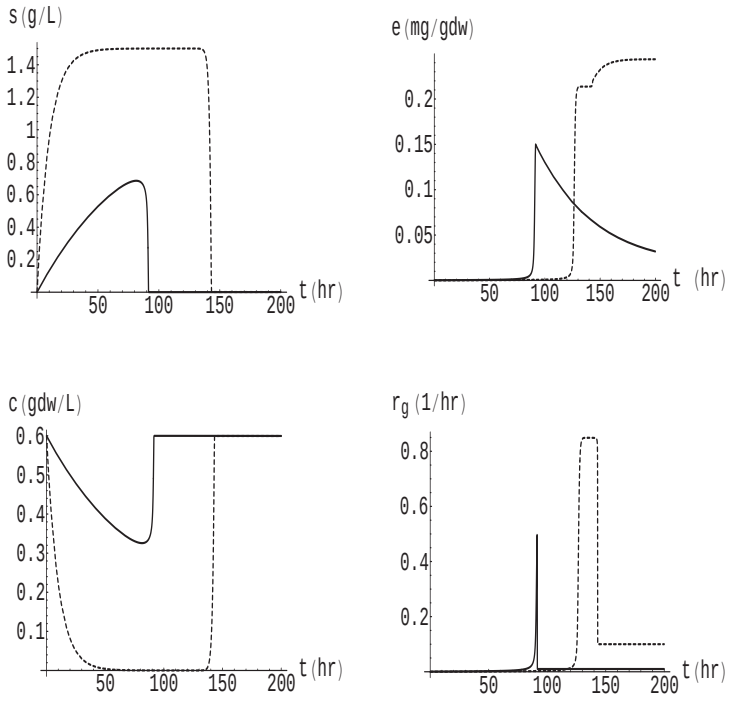

Figure 2–5: Trajectories for a switch in the identity of the substrate at $D = 0.01$ 1/hr (full lines) and $D = 0.1$ 1/hr (dashed lines); K_3 was assumed to be 5×10^4.

before it can be contained. According to our model, this occurs because the initial transport enzyme levels are too small to cope with the increased substrate supply. The magnitude of the substrate excursion is most striking when one changes the identity of the substrate feeding into the chemostat. In this case, the initial enzyme level is at its smallest since there is no prior adaptation to the new substrate; the resulting lags are on the order of several days.

More data is needed to test quantitative predictions of the model. We know that Powell's model, which is formally similar to the model presented here, yields results that agree quantitatively with the data, provided the parameter values for synthesis of the "Q-substance" are suitably chosen [36, 57]. However, to rigorously test the quantitative predictions of the model, it is necessary to obtain transient data for a substrate such as lactose whose enzyme induction kinetics

are independently measurable. Work to this effect is currently in progress in our laboratory.

CHAPTER 3
THE ROLE OF RIBOSOMES

In previous chapter, we studied the role of transport enzymes to explain the dilution rate shift-up and substrate switch experiments in which the low level of transport enzyme limits the growth. It was shown that the long lag could occur because of autocatalytic synthesis of transport enzyme, and the model accounting for transport enzyme synthesis can capture the experimental data quantitatively.

It is well known that similar dynamics are observed even if the glucose-limited chemostat is subjected to *dilution rate shift-ups.* When a glucose-limited culture of *E. coli* is subjected to a dilution rate shift-up, the cell density decreases and the substrate concentration increases (Figure 3–1). But the steady state peripheral enzyme levels are high at all $D > 0.1$ 1/hr (Figure 1–3b). In fact, the enzyme levels are even higher than the levels observed at the maximum (washout) dilution rate. The existence of such high peripheral enzyme levels suggests that the dynamics of dilution rate shift-ups starting from sufficiently large initial dilution rates cannot be due to slow substrate uptake. Then what is responsible for the sluggish response in such dilution rate shift-ups?

The source of the slow dynamics in dilution rate shift-ups is revealed by examining the initial response to *continuous-to-batch shifts.* In these experiments, the cells, maintained at steady state in a chemostat, are abruptly exposed to excess substrate concentrations. The initial response is obtained by measuring the rates of various processes within 10–15 minutes of the shift to substrate-excess conditions. Figure 1–6 shows the initial response of the substrate uptake, biosynthesis, respiration, and excretion in continuous-to-batch shifts of glucose-limited cells. It is evident that the specific substrate uptake rate increases to the

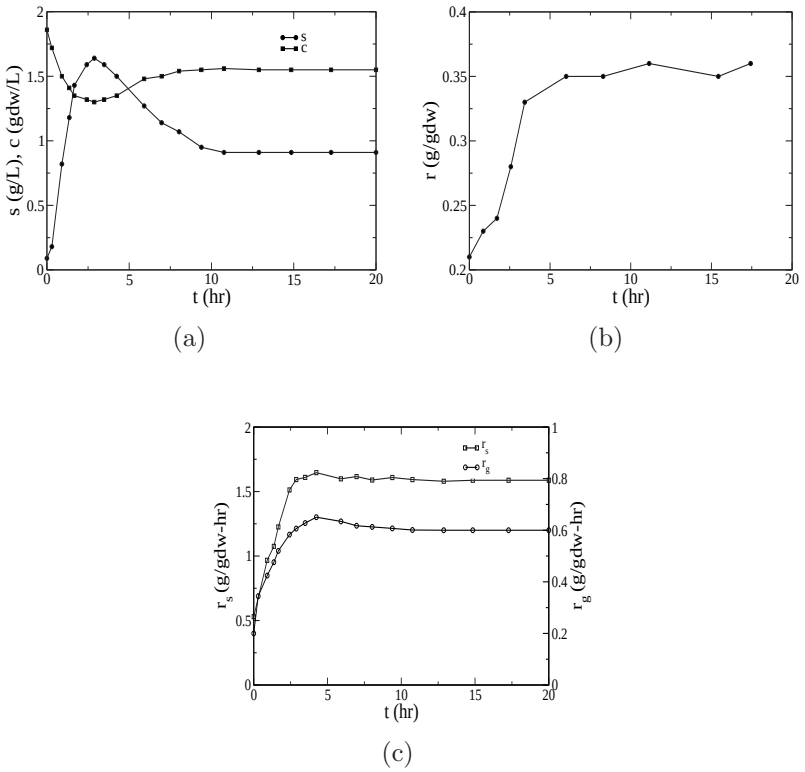

Figure 3–1: Transient response of a glucose-limited culture of *E. coli* K12 to a dilution rate shift-up (from [48]). At $t < 0$, the culture is at the steady state corresponding to the dilution rate, $D_0 = 0.2$ 1/hr, and feed concentration, $s_f = 5$ g/L. At $t = 0$, the dilution rate is shifted up to $D = 0.6$ 1/hr, while the feed concentration is held constant. The figures show the evolution of the (a) Cell density and substrate concentration (b) Ribosome level (c) Specific substrate uptake and growth rates calculated from the curves in (a) by appealing to the formulas, $r_s = [D(s_f - s) - ds/dt]/c$ and $r_g = (dc/dt - Dc)/c$, which follow from the mass balances for the substrate and cells.

maximal levels obtained near the washout dilution rate (Figure 1–6a). However, the specific rate of RNA and protein synthesis increases only partially if the culture has been growing at low dilution rates, and shows no perceptible increase if the culture has been growing at high dilution rates (Figure 1–6b). It follows that when cells growing at steady state in a chemostat are exposed to substrate-excess conditions, the substrate enters the cell at near-maximal rates, but the catabolic products derived from it are, at best, only partially channeled into biosynthesis. The excess substrate is eliminated by instantly increasing the rates of respiration

(Figure 1–6c), excretion (Figure 1–6d), and storage [12, 14]. Thus, we conclude that the response is sluggish in dilution rate shift-ups because the specific RNA and protein synthesis rates do not achieve maximal levels instantly.

The initial response of continuous-to-batch shifts reveals the identity of the variables that prevent the biosynthesis rate from increasing instantly, but sheds no light on the reason for the slow response of the variables. We gain some insight into the mechanism of the slow response by examining the evolution of ribosome levels in continuous-to-batch shifts (Figures 1–7). These transients suggest that the synthesis of ribosomes is autocatalytic. The synthesis rates are small initially, accelerate subsequently, and subside finally after passing through an inflection point. It is conceivable that these autocatalytic kinetics occur because an increase in the activity of RNA results in elevated synthesis of protein, which activates the synthesis of ribosomal RNA and ribosomes [4, 5, 58]. In what follows, we assume that synthesis of RNA is autocatalytic without making any attempt to model the underlying molecular mechanism.[1]

The goal of this work is to study whether an extended model taking due account of peripheral enzymes and ribosomes can capture and explain the data shown in Figures 1–6,3–1 and additional data discussed below. We begin by formulating the extended model (Section 3.1). We then simulate and analyze

[1] This assumption is not new. It was made implicitly by Bremer [59] and Koch [60], who assumed that the protein synthesis rate was proportional to the concentration of RNA, and the RNA synthesis rate, in turn, was proportional to the concentration of proteins. It was made explicitly by Powell [57] and Yun e*t al* [48], who simply assumed that the synthesis rate of RNA is proportional to the concentration of RNA. However, Bremer and Koch did not account for the dynamics of the substrate concentration. Powell and Yun *et al* accounted for substrate dynamics by assuming a constant yield. This couples substrate uptake and growth, thus precluding the cell density overshoot observed in dilution rate shift-downs (see [48, Figure 6]).

the model to show that it yields results in qualitative agreement with the data (Section 3.2). Finally, we discuss the extent to which the model captures the key results of the experimental literature (Section 3.3).

3.1 The Model

Figure 3–2 shows the kinetic scheme of the model. Here, S denotes the growth-limiting carbon and energy source, E denotes the peripheral enzymes that catalyze the transport and peripheral catabolism of the carbon source and X denotes the internalized form of the substrate that induces the synthesis of E; P denotes the pool of precursors produced by catabolism of X; R denotes ribosomes or ribosomal RNA (rRNA);[2] and C^- denotes proteins. The entire cell consisting of E, X, P, R, and C^- is denoted by C. The term *biosynthesis* will be used to refer to the synthesis of RNA and proteins, and *growth* will refer to the synthesis of all intracellular components.

Throughout this work, the instantaneous concentrations of the variables are denoted by the corresponding lower-case letters s, e, x, p, r, c^-, and c, while steady state and quasisteady state concentrations are denoted by overlaying the letters with $\sim$ and $-$, respectively (for instance, $\tilde{x}$ and $\bar{x}$). The concentrations of the *environmental* variables, s and c, are based on the volume of chemostat (g/L and gdw/L, respectively), and the concentrations of the *physiological* variables, e, x, p, r, and c^- are based on the dry weight of biomass (g/gdw).

We make the following assumptions regarding the kinetics of the processes.

[2] We use the terms ribosome and rRNA interchangeably. This seems appropriate because rRNA constitutes $\sim$ 60% of a ribosome. But, more importantly, the synthesis of ribosomal RNA and ribosomes is tightly coupled through a negative feedback loop involving regulation of ribosomal protein synthesis [3].

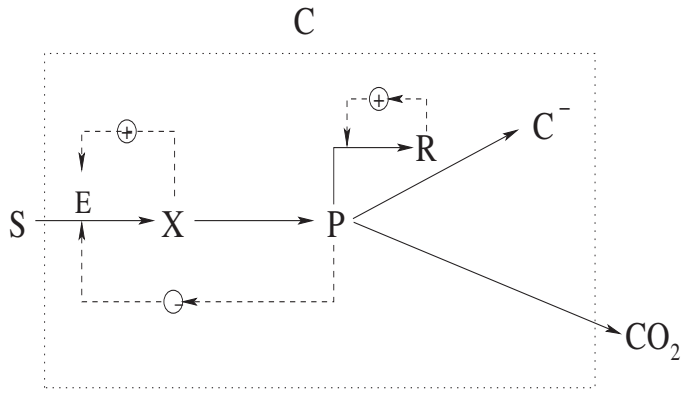

Figure 3–2: Kinetic scheme of the model. Here, S denotes the substrate, E denotes the inducible enzyme(s) catalyzing the uptake and peripheral catabolism of S, X denotes the inducer for E, P denotes the biosynthetic precursors derived from catabolism of X, R denotes rRNA, C^- denotes proteins, and C denotes the entire cell consisting of E, X, P, R, and C^-. The positive feedback loops represent induction of enzyme synthesis and autocatalytic synthesis of RNA. The negative feedback loop represents the inhibition of substrate uptake by precursors.

1. The specific substrate uptake rate, denoted r_s, satisfies the kinetic law

$$r_s \equiv V_s e \frac{s}{K_s + s} \frac{1}{1 + p/K_i}$$

where the factor $1/(1 + p/K_i)$ denotes the inhibition of substrate uptake by precursors. The experimental data suggests that such feedback inhibition exists. Indeed, if there were no feedback inhibition, the specific substrate uptake immediately after a continuous-to-batch shift would be proportional to the preexisting steady state enzyme level ($\bar{r}_s \approx V_s \tilde{e}$). Since $\tilde{e}$ increases three-fold as D decreases from 0.6 1/hr to 0.2 1/hr (Figure 1–3b), $\bar{r}_s$ should be three-fold higher for cultures growing at $D = 0.2$ 1/hr compared to cultures growing at $D = 0.6$ 1/hr. But Figure 1–6a shows that $\bar{r}_s$ is the same for cultures growing at dilution rates between 0.2 and 0.6 1/hr . This suggests that in cultures growing at low dilution rates, feedback inhibition acts to prevent the specific substrate rate from exceeding its value at high dilution rates.

2. The specific rate of breakdown of X into energy and precursors P, denoted r_x, is given by

$$r_x \equiv k_x x$$

3. The specific rate of respiration is

$$r_{co_2} \equiv k_{co_2} p$$

4. The specific rate of enzyme synthesis, denoted r_e^+, is

$$r_e^+ \equiv V_e \frac{r}{K_e + r} \frac{1 + K_2 x^2}{K_3 + K_2 x^2}. \tag{3.1}$$

Underlying these kinetics is the fact that the enzyme synthesis rate is precisely the rate at which the messenger RNA (mRNA) for the enzyme is translated by the ribosomes. We assume that the specific translation rate of the enzyme is $k_e m r/(K_e + r)$, where m and r denote the concentration of mRNA and ribosomes, respectively. Now, the evolution of mRNA is given by the equation $dm/dt = r_m^+ - r_m^- - r_g m$, where $r_m^+ \equiv V_m(1 + K_2 x^2)/(K_3 + K_2 x^2)$ is the specific transcription rate,[3] $r_m^- \equiv k_m^- m$ is the specific degradation rate, and $r_g m$ is the dilution rate. Since mRNA has a half-life of ∼2 min ($k_m^- \approx 20$ 1/hr) [61], it rapidly reaches the quasisteady state concentration, $\bar{m} \approx r_m^+/k_m^-$. Substituting this concentration in the expression for the specific translation rate yields (3.1) with $V_e \equiv k_e V_m/k_m^-$.

5. The specific rate of (ribosomal) RNA synthesis is given by

$$r_r^+ \equiv k_r^+ r p$$

where the dependence on r reflects the assumption that rRNA synthesis is autocatalytic.

6. The specific rate of protein (C^-) synthesis is given by

$$r_c^+ \equiv V_c r \frac{p}{K_c + p}$$

where the dependence on r accounts for the fact that ribosomes catalyze protein synthesis.

7. The specific rates of peripheral enzyme, rRNA, and protein degradation, denoted r_e^-, r_r^-, and r_c^-, respectively, are given by

$$r_e^- \equiv k_e^- e,\ r_r^- \equiv k_r^- r,\ r_c^- \equiv k_c^- c^-$$

[3] These kinetics reflect the fact that transcription of the mRNA for the peripheral enzymes involves the binding of a repressor molecule to two inducer molecules [55]. Thus, K_2 is the equilibrium constant for binding of a repressor to two inducer molecules, and K_3 is proportional to the equilibrium constant for binding of the repressor to the operator. Note that since repressor-operator binding is not perfect, K_3 is finite, so that mRNA is transcribed even in the absence of the inducer ($r_m^+|_{x=0} = (V_m/K_3) > 0$). This phenomenon is called *constitutive* enzyme synthesis.

8. The synthesis of peripheral enzymes, rRNA and proteins depletes the pool of precursors. Likewise, their degradation replenishes the pool of precursors.

A mass balance on the state variables yields

$$\begin{aligned}
\frac{ds}{dt} &= D(s_f - s) - r_s c && (3.2)\\
\frac{dc^-}{dt} &= r_c^+ - r_c^- - \left(D + \frac{1}{c}\frac{dc}{dt}\right) c^- && (3.3)\\
\frac{de}{dt} &= r_e^+ - r_e^- - \left(D + \frac{1}{c}\frac{dc}{dt}\right) e && (3.4)\\
\frac{dr}{dt} &= r_r^+ - r_r^- - \left(D + \frac{1}{c}\frac{dc}{dt}\right) r && (3.5)\\
\frac{dx}{dt} &= r_s - r_x - \left(D + \frac{1}{c}\frac{dc}{dt}\right) x && (3.6)\\
\frac{dp}{dt} &= r_x - r_{\mathrm{co}_2} - (r_c^+ - r_c^-) - (r_e^+ - r_e^-) - (r_r^+ - r_r^-) - \left(D + \frac{1}{c}\frac{dc}{dt}\right) p && (3.7)
\end{aligned}$$

where s_f denotes the concentration of S in the feed, and D denotes the dilution rate. These equations define $(1/c)(dc/dt)$ implicitly in terms of the other derivatives. We can solve for $(1/c)(dc/dt)$ explicitly by observing that the mass fraction of all intracellular entities equals unity, i.e.

$$c^- + e + r + x + p = 1. \tag{3.8}$$

Hence, addition of (3.3–3.7) yields the equation

$$D + \frac{1}{c}\frac{dc}{dt} = r_s - r_{\mathrm{co}_2} \tag{3.9}$$

which can be rewritten in the more familiar form

$$\frac{dc}{dt} = (r_g - D)c$$

where r_g denotes the specific growth rate, and is defined as

$$r_g \equiv r_s - r_{\mathrm{co}_2}. \tag{3.10}$$

Equations (3.9) and (3.10) imply that the last term in equations (3.3–3.7) represents the dilution of the corresponding physiological concentration due to growth.

Thus, we arrive at the equations

$$\frac{ds}{dt} = D(s_f - s) - r_s c \tag{3.11}$$
$$\frac{dc}{dt} = (r_g - D)c \tag{3.12}$$
$$\frac{dc^-}{dt} = r_c^+ - r_c^- - r_g c^- \tag{3.13}$$
$$\frac{de}{dt} = r_e^+ - r_e^- - r_g e \tag{3.14}$$
$$\frac{dr}{dt} = r_r^+ - r_r^- - r_g r \tag{3.15}$$
$$\frac{dx}{dt} = r_s - r_x - r_g x \tag{3.16}$$
$$\frac{dp}{dt} = r_x - r_{co_2} - (r_c^+ - r_c^-) - (r_e^+ - r_e^-) - (r_r^+ - r_r^-) - r_g p \tag{3.17}$$

where r_g is given by (3.10). It is worth noting that (3.8) implies that equations (3.13–3.17) are linearly dependent. Hence, we can replace any one of these equations with (3.8).

3.2 Simulations

The simulations were done with the parameter values in Table 3–1.

Table 3–1: Parameter values used in the ribosome model simulations.

$V_s = 2 \times 10^4 \ \frac{g}{g-hr}$	$K_s = 10^{-2} \ \frac{g}{L}$	$K_i = 5 \times 10^{-3}$	$k_x = 10^3 \ \frac{g}{g-hr}$
$V_e = 5 \times 10^{-4} \ \frac{g}{gdw-hr}$	$K_e = 0.1 \ \frac{g}{gdw}$	$K_2 = 10^{10} \left(\frac{gdw}{g}\right)^2$	$K_3 = 5 \times 10^3$
$k_e^- = 0.075 \ \frac{g}{g-hr}$	$k_r^+ = 100 \ \frac{gdw}{g-hr}$	$k_r^- = 0.1 \ \frac{g}{g-hr}$	$V_c = 3 \ \frac{g}{g-hr}$
$K_c = 0.002 \ \frac{g}{gdw}$	$k_c^- = 0.05 \ \frac{g}{g-hr}$	$k_{co_2} = 150 \ \frac{g}{g-hr}$	

3.2.1 Steady States

To analyze the steady states, we replace (3.17) with (3.8). Thus, we consider the equations

$$\begin{aligned}
\frac{ds}{dt} &= D(s_f - s) - \left(V_s e \frac{s}{K_s + s} \frac{1}{1 + p/K_i}\right) c = 0 && (3.18)\\
\frac{dc}{dt} &= (r_g - D)c = 0 && (3.19)\\
\frac{dc^-}{dt} &= V_c r \frac{p}{K_c + p} - \left(r_g + k_c^-\right) c^- = 0 && (3.20)\\
\frac{de}{dt} &= V_e \frac{r}{K_e + r} \frac{1 + K_2 x^2}{K_3 + K_2 x^2} - \left(r_g + k_e^-\right) e = 0 && (3.21)\\
\frac{dr}{dt} &= \left(k_r^+ p - r_g - k_r^-\right) r = 0 && (3.22)\\
\frac{dx}{dt} &= V_s e \frac{s}{K_s + s} \frac{1}{1 + p/K_i} - (r_g + k_x)\, x = 0 && (3.23)\\
p &= 1 - (c^- + e + r + x) && (3.24)
\end{aligned}$$

where r_g is given by (3.10). These equations admit two types of steady states — the *persistence* steady state ($\tilde{c} > 0$), and the *washout* steady state ($\tilde{c} = 0$). For a given microbial species and growth-limiting substrate, these steady states can depend on two parameters — the dilution rate and the feed concentration.

3.2.1.1 Persistence steady state

The variation of the persistence steady state with respect to the feed concentration is simple. If the feed concentration is increased at a fixed dilution rate, the cell density increases, but there is no perceptible change in the substrate concentration [11, 62]. There is no data on the variation of the physiological steady states with respect to the feed concentration. However, since the physiological state is completely determined by the substrate concentration, these steady states should also be independent of the feed concentration. We show below that this property is inherent in the model.

The variation of the persistence steady state with respect to the dilution rate is more complex. The substrate concentration and ribosome levels increase

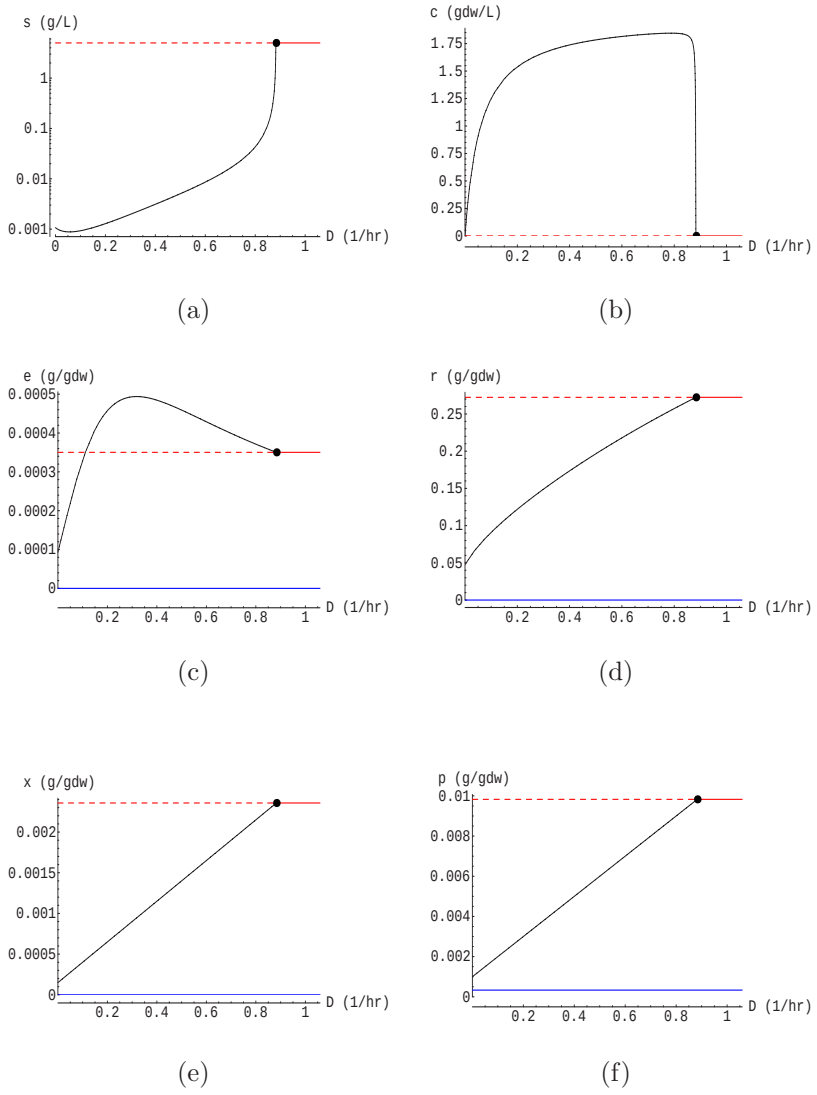

Figure 3–3: Variation of the steady states with D at $s_f = 5$ g/L. The persistence, and washout are represented by black, and red lines, respectively. Stable and unstable steady states are denoted by full and dashed lines, respectively. The full circle shows the bifurcation point at which the persistence and washout steady state exchange stability.

monotonically (Figure 1–3a,d). On the other hand, the cell density and peripheral enzyme levels pass through a maximum (Figure 1–3a,b). Figure 3–3 shows that the model simulations are in good agreement with this data. In what follows, we shed more light on these simulations by deriving explicit expressions for the steady state values of all the variables.

To this end, observe that since $\tilde{c}, \tilde{r} > 0$ at the persistence steady state, (3.19) and (3.22) imply that $\tilde{r}_g = D$ and

$$\tilde{p}(D) = \frac{D + k_r^-}{k_r^+}. \tag{3.25}$$

Thus, $\tilde{p}$ increases linearly with D (Figure 3–3f). Interestingly, as D tends to zero, $\tilde{p}$ approaches a positive limit. Thus, we obtain "maintenance effects," even though no maintenance was explicitly postulated. Indeed, substituting (3.25) in (3.10) yields

$$\tilde{r}_s = D + \tilde{r}_{co_2} = D + k_{co_2}\tilde{p} = D + k_{co_2}\left(\frac{D + k_r^-}{k_r^+}\right) = \frac{D}{\hat{Y}} + m \tag{3.26}$$

where $\hat{Y} \equiv k_r^+/(k_r^+ + k_{co_2})$ is the *maximum yield of biomass*, and $m \equiv k_{co_2}(k_r^-/k_r^+)$ is the *maintenance coefficient* (which reflects the "futile cycling" of rRNA at vanishingly small dilution rates).

It follows immediately from (3.23) and (3.26) that

$$\tilde{x}(D) = \frac{\tilde{r}_s}{k_x + D} = \frac{D/\hat{Y} + m}{k_x + D} \approx \frac{D/\hat{Y} + m}{k_x} \tag{3.27}$$

so that $\tilde{x}$ increases linearly with the dilution rate (Figure 3–3e). To find the concentrations of the remaining physiological variables, we observe that (3.20) and (3.21) imply that

$$\tilde{c}^-(\tilde{r}) = \frac{\tilde{r}_c^-}{D + k_c^-} = \frac{V_c}{D + k_c^-}\tilde{r}\frac{\tilde{p}}{K_c + \tilde{p}},\ \tilde{e}(\tilde{r}) = \frac{\tilde{r}_e^+}{D + k_e^-} = \frac{V_e}{D + k_e^-}\frac{\tilde{r}}{K_e + \tilde{r}}\frac{1 + K_2\tilde{x}^2}{K_3 + K_2\tilde{x}^2}. \tag{3.28}$$

Substituting these relations in (3.24) yields

$$\tilde{r} + \frac{V_c}{D + k_c^-}\tilde{r}\frac{\tilde{p}}{K_c + \tilde{p}} + \frac{V_e}{D + k_e^-}\frac{\tilde{r}}{K_e + \tilde{r}}\frac{1 + K_2\tilde{x}^2}{K_3 + K_2\tilde{x}^2} = 1 - \tilde{x} - \tilde{p} \tag{3.29}$$

which is a quadratic in $\tilde{r}$. Since the LHS is an increasing function of $\tilde{r}$, and the RHS is independent of $\tilde{r}$, (3.29) has at most one positive root at any given D. A simple approximation to $\tilde{r}(D)$ is obtained by recognizing that $\tilde{e}, \tilde{x}, \tilde{p} \ll 1$. In this case, (3.29) yields the relation

$$\frac{\tilde{r}}{1 - \tilde{r}} \approx \frac{\tilde{r}}{\tilde{c}^-} = \frac{D + k_c^-}{V_c}\frac{K_c + \tilde{p}}{\tilde{p}} = \frac{k_r^+}{V_c}\frac{D + k_c^-}{D + k_r^-}(K_c + \tilde{p}). \tag{3.30}$$

At high dilution rates, $D \gg k_c^-, k_r^-$ and protein synthesis is saturated ($p \gg K_c$), so that

$$\frac{\tilde{r}}{1 - \tilde{r}} \approx \frac{\tilde{r}}{\tilde{c}^-} = \frac{D}{V_c + D}$$

which implies that $\tilde{r}$ increases (and $\tilde{c}^-$ decreases) with D (Figure 3–3d). The steady state enzyme level is obtained by substituting $\tilde{r}(D)$ in (3.28). It passes through a maximum since the enzyme synthesis rate saturates at large D, i.e., $\tilde{r}_e^+ \approx V_e$ (Figure 3–3c).

The steady state substrate concentration can be derived by appealing to the definition of r_s. Thus

$$\frac{\tilde{s}}{K_s + \tilde{s}} = \frac{\tilde{r}_s}{V_s\tilde{e}/(1 + \tilde{p}/K_i)}. \tag{3.31}$$

We gain some insight into the variation of $\tilde{s}$ with respect to D (Figure 3–3a) by recalling that $\tilde{r}_s$ and $\tilde{p}$ increase linearly with D. At high dilution rates, $\tilde{e} \approx V_e/D$, so that $\tilde{s}/(K_s + \tilde{s})$, and hence, $\tilde{s}$, increases with D.

The variation of the steady state cell density with D (Figure 3–3b) follows immediately from (3.18). Thus

$$\tilde{c} = \frac{D(s_f - \tilde{s})}{\tilde{r}_s} \tag{3.32}$$

At low dilution rates, $\tilde{s} \ll s_f$ and $\tilde{r}_s \approx m$; hence, $\tilde{c} \approx (s_f/m)D$. At high dilution rates, $\tilde{r}_s \approx D/\hat{Y}$, so that $\tilde{c} \approx \hat{Y}(s_f - \tilde{s})$.

Note that the steady state concentrations of the substrate and the physiological variables are independent of the feed concentration, s_f. This is because the steady state concentrations of S and the five physiological variables (C^-, E, R, X, and P) are completely determined by the six equations (3.19–3.24), which are independent of the feed concentration.

3.2.1.2 Washout steady state

As noted above, at high dilution rates, the substrate concentration corresponding to the persistent steady steady is an increasing function of D. When D becomes sufficiently large, $\tilde{s} = s_f$ and $\tilde{c} = 0$, i.e., the cells wash out of the chemostat. We refer to this steady state as the *washout steady state,* and the corresponding dilution rate, denoted D_w, as the *washout dilution rate.* The physiological variables corresponding to this steady state are determined by equations (3.20–3.24) with $r_g = r_s - r_{\mathrm{co}_2}$ and $\tilde{s} = s_f$. It follows that the washout steady state is independent of the dilution rate.

Since the washout steady state is achieved when the substrate concentration corresponding to the persistent steady state equals s_f, the washout dilution rate satisfies the following equation obtained by letting $\tilde{s} = s_f$ in (3.31)

$$\frac{s_f}{K_s + s_f} = \frac{\tilde{r}_s}{V_s \tilde{e}/(1 + \tilde{p}/K_i)} \tag{3.33}$$

where $\tilde{p}$, $\tilde{r}_s$, and $\tilde{e}$ are given by (3.25), (3.26) and (3.28), respectively. Now, in typical experiments, $s_f \sim 1$ g/L, so that $s_f/(K_s + s_f) \approx 1$. Moreover, at large dilution rates ($D \approx D_w$), $\tilde{p}$, $\tilde{r}_s$, and $\tilde{e}$ can be approximated by the relations

$$\tilde{p} \approx \frac{D}{k_r^+},\ \tilde{r}_s \approx \frac{D}{\hat{Y}},\ \tilde{e} \approx \frac{V_e}{D}$$

since the loss of enzyme and rRNA by degradation is negligible compared to their loss by dilution due to growth ($k_e^-, k_r^- \ll D$); substrate consumption for maintenance (as opposed to growth) is negligibly small ($m \ll D/\hat{Y}$); and enzyme induction is near-maximal ($r_e^+ \approx V_e$). We substitute these relations in (3.33) to conclude that the washout dilution rate satisfies the approximate relation

$$\frac{1}{k_r^+ K_i} D_w^3 + D_w^2 \approx \hat{Y} V_s V_e,$$

which has a unique positive solution. In the absence of feedback inhibition ($K_i \to \infty$), we obtain a simple approximation, $D_w \approx \sqrt{\hat{Y} V_s V_e}$, which provides a convenient upper bound for the washout dilution rate.

3.2.2 Transients

To simulate and analyze the transients, we replace (3.13) with (3.8). Thus, we consider the equations.

$$\begin{aligned}
\frac{ds}{dt} &= D(s_f - s) - r_s c \\
\frac{dc}{dt} &= (r_g - D)c \\
\frac{de}{dt} &= r_e^+ - r_e^- - r_g e \\
\frac{dr}{dt} &= r_r^+ - r_r^- - r_g r \\
\frac{dx}{dt} &= r_s - r_x - r_g x \\
\frac{dp}{dt} &= r_x - r_{\mathrm{co}_2} - (r_c^+ - r_c^-) - (r_e^+ - r_e^-) - (r_r^+ - r_r^-) - r_g p \\
c^- &= 1 - e - r - x - p
\end{aligned}$$

The inducer and precursor concentrations rapidly achieve quasi-steady state

$$\frac{dx}{dt} = \frac{dp}{dt} = 0$$

the quasi-state implies that for all but a negligibly small time interval, these equations can be approximated by the *reduced* equations

$$\frac{ds}{dt} = D(s_f - s) - \left(V_s e \frac{s}{K_s + s} \frac{1}{1 + \bar{p}/K_i}\right) c \tag{3.34}$$

$$\frac{dc}{dt} = (r_g - D)\, c \tag{3.35}$$

$$\frac{de}{dt} = V_e \frac{r}{K_e + r} \frac{1 + K_2 \bar{x}^2}{K_3 + K_2 \bar{x}^2} - k_e^- e - r_g e \tag{3.36}$$

$$\frac{dr}{dt} = k_r^+ r \bar{p} - k_r^- r - r_g r \tag{3.37}$$

$$0 \approx V_s e \frac{s}{K_s + s} \frac{1}{1 + \bar{p}/K_i} - k_x \bar{x} \tag{3.38}$$

$$0 \approx k_x \bar{x} - k_{co_2} \bar{p} - r_g \tag{3.39}$$

where r_g is given by

$$r_g \approx V_c r \frac{\bar{p}}{K_c + \bar{p}} - k_c^-(1 - r) + k_r^+ r \bar{p} - k_r^- r. \tag{3.40}$$

That is, the specific growth rate is effectively equal to the specific rate of net rRNA and protein biosynthesis.

3.2.2.1 Continuous-to-batch shifts

In continuous-to-batch shifts, the initial rates of various processes are measured within 10–15 minutes of exposing the culture to substrate-excess conditions (Figure 1–6). To simulate these experiments with the model, we observe that in this short time period, the peripheral enzyme and ribosome levels remain essentially unchanged, but the inducer and precursor concentrations rapidly move to the new quasisteady state corresponding to substrate-excess conditions. This new quasisteady state is obtained by letting $s/(K_s + s) \approx 1$ in (3.38–3.39), while the peripheral enzyme and ribosome levels are held at their initial steady state values, $e_0 = \tilde{e}(D)$ and $r_0 = \tilde{r}(D)$. Thus

$$\bar{x} \approx \frac{V_s e_0/(1 + \bar{p}/K_i)}{k_x} \tag{3.41}$$

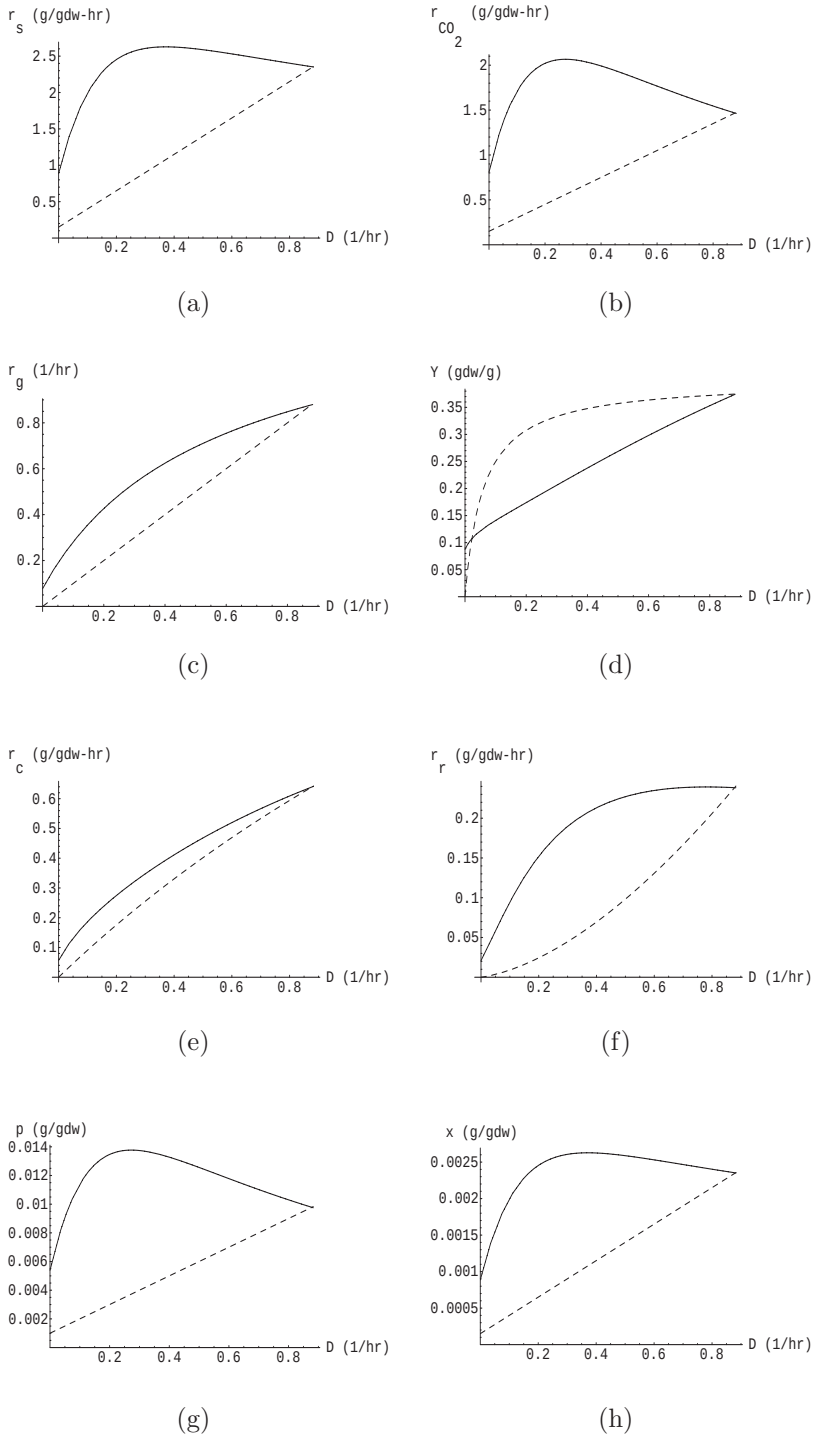

Figure 3–4: Initial response following a continuous-to-batch shift. The dashed line shows the initial steady state value. The full line shows the value after the cells have been exposed to substrate-excess conditions: (a) Specific substrate uptake rate (b) Specific respiration rate (c) Specific growth rate (d) Yield of biomass (e) Net specific protein synthesis rate ($r_c \equiv r_c^+ - r_c^-$) (f) Net specific rRNA synthesis rate ($r_r \equiv r_r^+ - r_r^-$) (g) Precursor concentration (h) Inducer concentration.

and $\bar{p}$ satisfies the equation

$$V_s e_0 \frac{1}{1+\bar{p}/K_i} \approx k_{co_2}\bar{p} + V_c r_0 \frac{\bar{p}}{K_c+\bar{p}} - k_c^-(1-r_0) + k_r^+ r_0 \bar{p} - k_r^- r_0 \tag{3.42}$$

If we assume that the degradation rates of rRNA and protein are negligibly small compared to their synthesis rates, and protein synthesis is saturated ($\bar{p} \gg K_c$), (3.42) can be solved to yield the approximate solution

$$\bar{p} \approx \frac{K_i}{2}\left(\sqrt{\left(1+\frac{V_c r_0}{(k_{co_2}+k_r^+ r_0)\,K_i}\right)^2 + 4\frac{V_s e_0 - V_c r_0}{(k_{co_2}+k_r^+ r_0)\,K_i}} - \frac{V_c r_0}{(k_{co_2}+k_r^+ r_0)\,K_i}\right) \tag{3.43}$$

which is accurate to within 10% of the exact (numerical) solution for all e_0 and r_0. The rates of various processes immediately after a continuous-to-batch shift can now be obtained by substituting the above concentrations into the appropriate kinetic expressions (for example, $\bar{r}_s = V_s e_0/(1+\bar{p}/K_i)$ and $\bar{r}_{co_2} = k_{co_2}\bar{p}$).

Figure 3–4 shows the rates of various processes and the quasisteady state concentrations ($\bar{x}$,$\bar{p}$) immediately after the continuous-to-batch shift. The simulated rates are consistent with the experimental data shown in Figure 1–6. At all but the smallest dilution rates, the specific substrate uptake and respiration rates immediately jump to high levels (Figure 3–4a,b), but the specific growth rate increases only partially (Figure 3–4c). Thus, substrate uptake and growth become uncoupled immediately after the shift, resulting in a reduction of the instantaneous yield, $Y \equiv r_g/r_s$ (Figure 3–4d). The increase in the specific substrate uptake and growth rates is largest at intermediate dilution rates, and decreases at low and high dilution rates. At high dilution rates, substrate uptake is already saturated before the cells are exposed to substrate-excess conditions ($s_0 \gg K_s$), so that further provision of the substrate provokes no additional response. At low dilution rates, the initial peripheral enzyme are too small to support a substantial increment in

the specific substrate uptake rate, and the initial rRNA levels are too small to support a substantial increment in the protein and rRNA synthesis rates (Figure 3–4e,f).

3.2.2.2 Substrate switch

The transient response to substrate switches could be captured by our earlier model (see Figure 1–5). Simulations of the extended model preserve these transients. The specific substrate uptake and growth rates remain at vanishingly small levels for the first ∼20 hours (Figure 3–5c,f). Consequently, the substrate concentration and cell density go through a massive overshoot and undershoot, respectively (Figure 3–5a,b). The peripheral enzyme level shows a biphasic response: After an initial increase, it becomes more or less constant at $t \approx 25$ hours before increasing once again (Figure 3–5d). These simulations are in good agreement with the data shown in Figure 1–5. In addition to these dynamics, the extended model also describes the evolution of rRNA (Figure 3–5e).

We can decompose these dynamics into four phases. It is worth examining these phases in more detail. As we show later, the dynamics of dilution rate shift-ups and shift-downs reproduce the dynamics of one or more of these phases.

Phase 1. During the *first* phase, the substrate attains supersaturating concentrations within 10–15 minutes. Indeed, since the initial enzyme level is negligibly small $[e_0 = (V_e/K_3)(D + k_e^-)r_0/(K_e + r_0) \sim 10^{-6}$ g/gdw], so is the initial substrate uptake rate. The initial motion of the substrate concentration is, therefore, approximated by the equation

$$\frac{ds}{dt} \approx Ds_f - Ds,\ s(0) = 0 \ \Rightarrow s(t) \approx s_f\left[1 - \exp(-Dt)\right]. \tag{3.44}$$

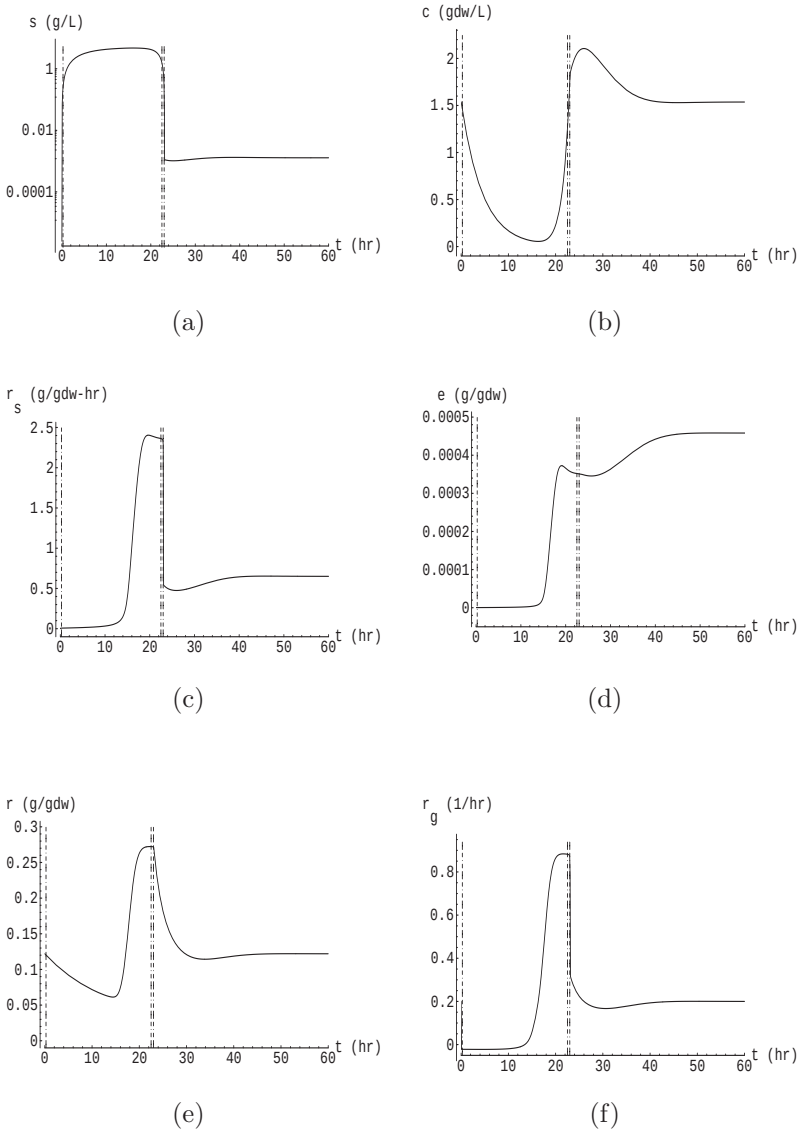

Figure 3–5: Transient response for a switch in the identity of the substrate at $D = 0.2$ 1/hr. Before the switch, the culture is in a steady state corresponding to the absence of the substrate. The vertical dashed lines mark the end of Phases 1, 2 and 3.

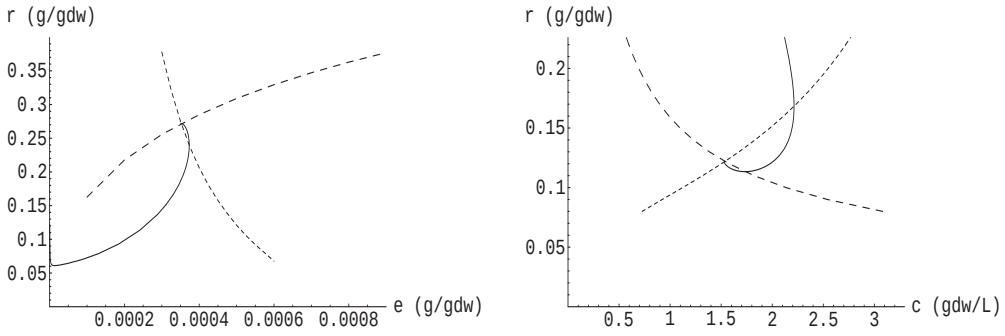

(a) (b)

Figure 3–6: Phase portraits of the slow motion during a feed switches. (a) The slow motion toward balanced growth. The line with short dashes shows the null-cline for e; the line with long dashes shows the null-cline for r; the intersection of the two null-clines represents the concentration of e and r at balanced growth; the full line shows the approach of e and r toward the state of balanced growth. (b) The slow motion away from balanced growth to the ultimate steady state. The line with short dashes shows the null-cline for c; the line with long dashes shows the null-cline for r; the intersection of the two null-clines represents the steady state concentrations of c and r at $D = 0.2$ 1/hr; and the full line shows the motion of c and r from balanced growth toward the final steady state.

This equation describes the theoretical washout curve shown as a dashed curve in Figure 1–6a. It implies that the substrate concentration increases to supersaturating levels ($s \sim K_s$) within

$$-\frac{\ln(1 - K_s/s_f)}{D} \approx \frac{K_s/s_f}{D} \sim 0.1 \text{ hrs.}$$

On this short time scale, the cell density, the peripheral enzyme level, and the ribosome level remain at their initial values, but the inducer and precursor concentrations constantly adjust to the rapidly increasing substrate concentration. Hence, at the end of this phase, $c = c_0$, $e = e_0$, $r = r_0$, but s reaches supersaturating levels, and x, p achieve the corresponding quasisteady state concentrations given by (3.41) and 3.43).

Phase 2. During the *second* phase, which lasts about 30 hours, the substrate concentration is supersaturating, i.e., $s/(K_s + s) \approx 1$. Under these conditions,

the substrate concentration and cell density change, but these changes cannot be discerned by the cells, since they see the environment through the ratio $s/(K_s + s)$, and this ratio is approximately constant. Given this quasiconstant environment, the physiological variables evolve toward a quasisteady state. We shall refer to this transient as *substrate-sufficient batch dynamics* because the quasisteady state reached by the physiological variables is identical to the physiological state attained by a substrate-sufficient batch culture during the exponential growth phase: All the physiological variables are constant, and the cells grow exponentially at their maximum specific growth rate (Figure 3–5f). In the microbiological literature, this quasisteady state is frequently referred to as the state of *balanced growth.*

The simulations show that during the approach to balanced growth, the enzyme and ribosome levels accumulate, pass through a maximum, and finally reach the constant level characteristic of balanced growth. To gain further insight into this transient, we observe that throughout the approach to balanced growth, the substrate concentration is supersaturating, so that the inducer and precursor levels are in the quasisteady state given by

$$\bar{x} \approx \frac{V_s e/(1 + \bar{p}/K_i)}{k_x} \tag{3.45}$$

$$\bar{p} \approx \frac{K_i}{2}\left(\sqrt{\left(1 + \frac{V_c r}{(k_{co_2} + k_r^+ r)\,K_i}\right)^2 + 4\frac{V_s e - V_c r}{(k_{co_2} + k_r^+ r)\,K_i}} - \frac{V_c r}{(k_{co_2} + k_r^+ r)\,K_i}\right) \tag{3.46}$$

The motion toward balanced growth is, therefore, two-dimensional: The slow variables, e and r, evolve gradually according to equations (3.36–3.37), while the fast variables, x and p, constantly adjust to the slow motion in accordance with (3.45–3.46). Figure 3–6a shows the phase portrait for this two-dimensional motion. Note that

- The phase path intersects both null-clines before reaching balanced growth. Hence, both e and r pass through extrema on their way to balanced growth. Indeed, the eigenvalues of the linearization about the quasisteady state

corresponding to balanced growth are imaginary with negative real parts ($\lambda_{1,2} = -1.1 \pm 0.5\iota$). The quasisteady state is, therefore, a stable focus, i.e., the phase path spirals into the quasisteady state.

- When the phase path crosses the null-cline for e (resp. r), the sign of $\dot{e}$ (resp. $\dot{r}$) changes from positive to negative. This implies that both e and r pass through a maximum before reaching balanced growth.
- The phase path intersects the null-cline for e before it intersects the null-cline for r. It follows that e reaches its maximum before r.

These dynamics reflect the fact that the specific enzyme synthesis rate increases first, followed by the specific ribosome synthesis rate, the specific protein synthesis rate, and finally, the specific growth rate. Thus, the peripheral enzyme and ribosome levels go through maxima because their synthesis rates increase too much before their dilution rates catch up, and the peripheral enzyme level reaches its maximum before the ribosome level because the synthesis rate of the enzyme increases before the synthesis rate of the ribosomes.

Phase 3. During the *third* phase, the substrate concentration switches from supersaturating to subsaturating levels. This transition, which marks the end of balanced growth, occurs on a time scale of 1 min. To see this, observe that at the beginning of this phase, the substrate concentration is on the order of K_s, and the substrate uptake rate, $r_s c$, is on the order of 1 g/(L-hr). It follows that within $K_s/(r_s c) \sim 0.01$ hrs of the end of balanced growth, the substrate reaches the quasisteady state concentration defined by the equation

$$r_s c \approx D s_f. \tag{3.47}$$

At the same time, the inducer and precursor levels, which constantly adjust to the exogenous substrate concentration, achieve the corresponding quasisteady state values

$$\bar{x} \approx \frac{D s_f / c}{k_x} \tag{3.48}$$

$$\bar{p} \approx \frac{K_c}{2}\left[\frac{Ds_f/c - V_c r}{(k_{co_2} + k_r^+ r)K_c} - 1 + \sqrt{\left(\frac{Ds_f/c - V_c r}{(k_{co_2} + k_r^+ r)K_c} - 1\right)^2 + 4\frac{Ds_f/c}{(k_{co_2} + k_r^+ r)K_c}}\right] \tag{3.49}$$

obtained by substituting (3.47) in equations (3.38–3.39). The achievement of these quasisteady states is so rapid that the cell density, the peripheral enzyme level and the ribosome level remain at the values achieved at the end of balanced growth.

Phase 4. During the *last* phase, s, x and p remain in the quasisteady states defined by (3.47–3.49), while e, r, and c evolve slowly according to the equations

$$\frac{de}{dt} \approx V_e \frac{1 + K_2\bar{x}^2}{K_3 + K_2\bar{x}^2} - k_e^- e - r_g e \tag{3.50}$$

$$\frac{dr}{dt} \approx k_r^+ r\bar{p} - k_r^- r - r_g r \tag{3.51}$$

$$\frac{dc}{dt} \approx (r_g - D)c \tag{3.52}$$

where r_g is given by (3.40) and and $\bar{x}, \bar{p}$ are given by (3.48–3.49).

The study of these dynamics is facilitated by observing that $\bar{p}$ is independent of the enzyme level [see (3.48–3.49)]. Thus, we can study the slow motion during this phase by confining our attention to the two-dimensional system (3.51–3.52). At the heart of this simplification is that the fact that during this phase, the cells consume nearly all the substrate entering the chemostat. This ensures that the specific substrate uptake rate is effectively independent of the peripheral enzyme level ($r_s \approx Ds_f/c$). Now, the precursor levels sense the enzyme level through the specific substrate uptake rate [see (3.39)]. Since the specific substrate uptake rate is independent of the enzyme level, so is $\bar{p}$. Thus, the ribosome level and cell density evolve without seeing the changes in the peripheral enzyme level.

Figure 3–6b shows the motion of c and r on the phase plane. Note that

1. The phase path intersects both null-clines before reaching balanced growth. Hence, both c and r pass through extrema as they approach the steady state. Here also, the steady state is a stable focus since the the eigenvalues of the linearization about the steady state are $\lambda_{1,2} = -0.2 \pm 0.1\iota$.

2. When the phase path crosses the null-cline for c, the sign of $\dot{c}$ changes from positive to negative. When it crosses the null-cline for r, the sign of $\dot{r}$ changes from negative to positive. This implies that c passes through a maximum while r passes through a minimum.

3. The phase path intersects the null-cline for c before it intersects the null-cline for r. It follows that c reaches its maximum before r attains its minimum.

These dynamics reflect that fact that the specific ribosome synthesis rate decreases first, followed by the specific protein synthesis and growth rates. Thus, at the beginning of Phase 4, $\dot{r} < 0$ because the synthesis rate of ribosomes has increased much more than their dilution rate, and $\dot{c} > 0$ because of the inertia in the specific growth rate. As r decreases, so does the specific growth rate until it becomes equal to $D = 0.2$ 1/hr. This is the point at which the cell density displays a maximum. As the ribosome levels, and hence, the specific growth rate, decrease further, the dilution rate of the ribosomes progressively decreases until their synthesis and dilution rates become equal. This is the point at which the ribosomes display a minimum.

We shall refer to these transients as *cell-sufficient fed-batch dynamics* because the fundamental property underlying these dynamics — the complete consumption of all the influent substrate ($Ds_f \approx r_s c$) — is characteristic of high-density fed-batch cultures.

3.2.2.3 Dilution rate shift-down

Figure 3–7 shows the dynamics of a dilution rate shift-down. We assume that the initial dilution rate is close to the washout dilution rate, but not too close to it, so that the initial substrate concentration satisfies the inequality $K_s \ll s_0 \ll s_f$. The first inequality, $s_0 \gg K_s$, implies that the initial substrate concentration is at supersaturating levels. Consequently, there is an initial phase during which the cells continue to consume substrate and grow at their pre-shift rates, $r_{s,0}$ and D_0. The evolution of the substrate concentration and cell density during this initial growth

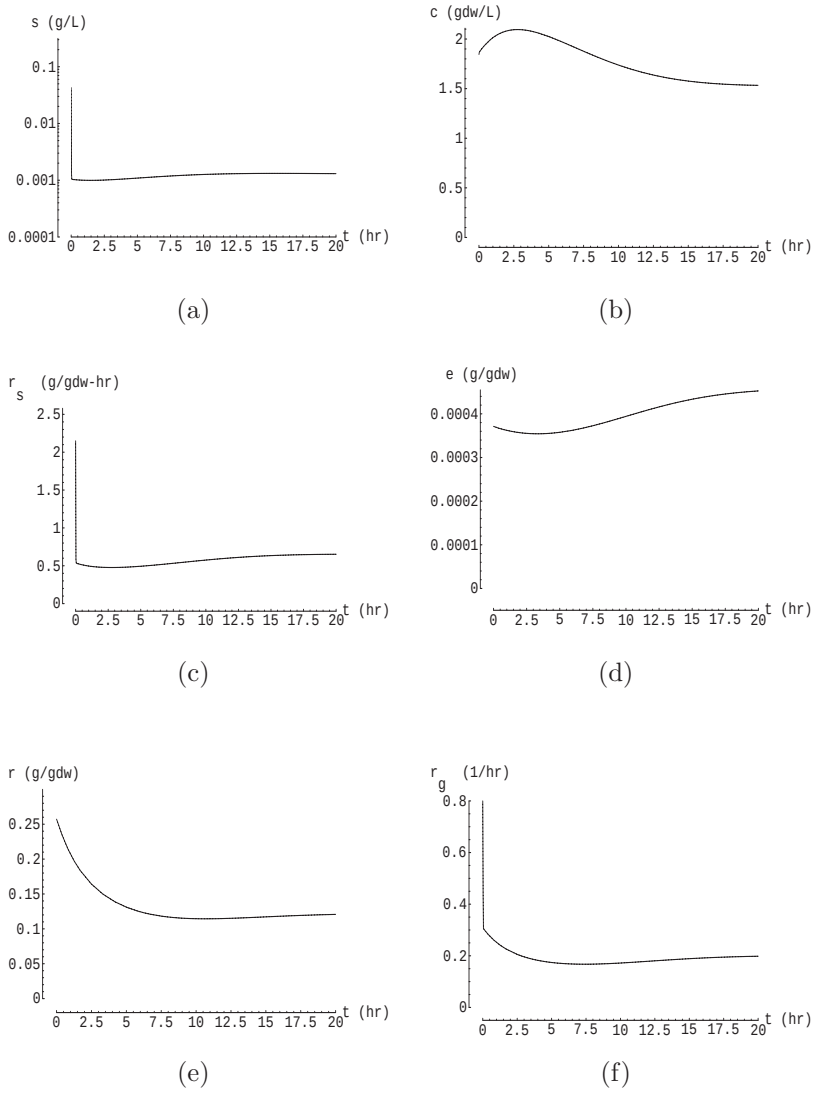

Figure 3–7: Transient response to a dilution rate shift-down. At $t < 0$, the culture is at the steady state corresponding to the dilution rate, $D_0 = 0.8$ 1/hr, and feed concentration, $s_f = 5$ g/L. At $t = 0$, the dilution rate is shifted down to $D = 0.2$ 1/hr, while the feed concentration is held constant.

phase is approximated by the equations

$$\frac{ds}{dt} \approx D(s_f - s) - r_{s,0}c$$
$$\frac{dc}{dt} \approx (D_0 - D)c.$$

Since $r_{s,0}c_0 = D_0(s_f - s_0)$, these equations imply that

$$s(t) \approx s_f - (s_f - s_0)\exp(D_0 - D)\,t \tag{3.53}$$

$$c(t) \approx c_0 \exp(D_0 - D)\,t. \tag{3.54}$$

The second inequality, $s_0 \ll s_f$, implies that the initial cell density, $c_0 \approx \hat{Y}(s_f - s_0) \approx \hat{Y}s_f$, is large compared to the initial substrate concentration. The initial growth phase should, therefore, last for a relatively short period of time. This is indeed the case. To see this, observe that the initial exponential growth phase persists until the substrate concentration drops to levels comparable to the saturation constant ($s \sim K_s$). It follows from (3.53) that the time taken to reach subsaturating substrate concentrations is given by the expression

$$\frac{1}{D_0 - D}\ln\left(\frac{1 - K_s/s_f}{1 - s_0/s_f}\right) \approx \frac{(s_0 - K_s)/s_f}{(D_0 - D)} \tag{3.55}$$

which is ~ 0.2 hrs if $s_0/s_f = 0.1$ and $D_0 - D = 0.5$ 1/hr.

Once the substrate concentration reaches levels on the order of K_s, the reactor replicates the dynamics of phase 3 and phase 4 above. The cell density, the peripheral enzyme level and the ribosome concentration evolve slowly from the values achieved at the end of balanced growth to their ultimate steady state values, while the substrate, inducer, and precursor levels remain at the quasisteady state concentrations defined by (3.47–3.49).

The simulations are in good agreement with the data shown in Figure 3–8, the only difference being that the predicted time interval of the initial exponential growth phase is smaller than the observed time interval of this phase. This is

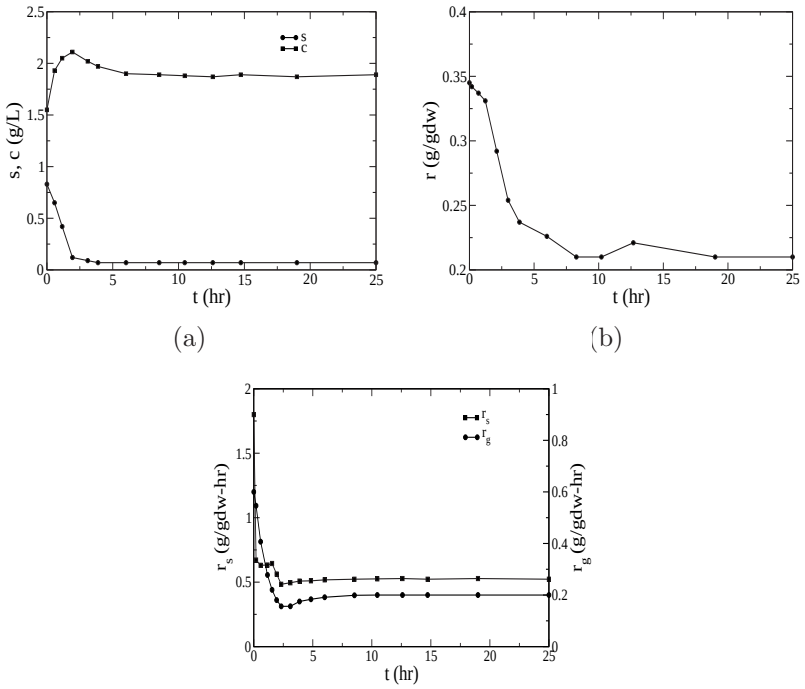

Figure 3–8: Response of a glucose-limited culture of *E. coli* K12 to a dilution rate shift-down (from [48]). At $t < 0$, the culture is at the steady state corresponding to the dilution rate, $D_0 = 0.6$ 1/hr, and feed concentration, $s_f = 5$ g/L. At $t = 0$, the dilution rate is shifted down to $D = 0.2$ 1/hr, while the feed concentration is held constant. The figures show the evolution of the (a) Cell density and substrate concentration (b) RNA level (c) Specific substrate uptake growth rates calculated from the curves in (a).

because in this experimental system, the initial substrate concentration and the saturation constant are relatively large ($s_0 \approx 1$ g/L, $K_s = 0.1$ g/L). The large initial substrate concentration increases the duration of the initial exponential growth phase [see (3.55)]. The high saturation constant increases the time required for the substrate to switch from supersaturating to subsaturating levels.

3.2.2.4 Dilution rate shift-up

The response to dilution rate shift-ups also replicates the dynamics observed in feed switches. Figure 3–9 shows the simulations of three dilution rate shift-ups from $D_0 = 0.1$ 1/hr to $D = 0.4$ 1/hr, $D = 0.6$ 1/hr, and $D = 0.8$ 1/hr, respectively. In all three cases, the substrate concentration, the specific substrate uptake, and

the specific growth rate rapidly increase within 10–15 minutes Figure (3–9a,c,f). However, the subsequent behavior of the three transients is quite different.

If the shift-up is small ($D = 0.4$ 1/hr), the substrate concentration never achieves supersaturating concentrations. This is because the shift-up is so small that the rapid increment of the specific substrate uptake rate is sufficient to match the increase in the substrate input rate, Ds_f. Thus, within 10–15 minutes, the substrate reaches the quasisteady state concentration given by (3.47). The subsequent evolution is given by equations (3.35–3.37), while s, x and p, are in the quasisteady states given by (3.47–3.49), respectively. The phase portrait for this motion is shown in Figure 3–10a.

If the shift-up is large ($D = 0.8$ 1/hr), the substrate concentration rapidly reaches supersaturating levels, and remains at these levels throughout the subsequent transient. In this case, the shift-up is so large that the substrate uptake rate, $\bar{r}_s c_0$, cannot match the substrate input, Ds_f, even when the substrate concentration has reached supersaturating levels. Thus, the substrate concentration continues to increase, and remains at supersaturating levels. The rapid attainment of supersaturating substrate concentrations also stimulates the specific growth rate. As expected from the earlier analysis of continuous-to-batch shifts (Figure 3–4), the specific growth immediately increases to 0.3 1/hr (Figure 3–10f). But this enhanced specific growth rate falls well below the new dilution rate ($D = 0.8$ 1/hr). Thus, in addition to accumulation of the substrate, there is a pronounced decline in the cell density which continues until the ribosome levels have been built up to sufficiently high levels. These dynamics are similar to the Phase 1 and Phase 2 dynamics of the feed switch. The phase portrait for this evolution is shown in Figure 3–10b.

If the shift-up is intermediate ($D = 0.6$ 1/hr), the substrate concentration saturates, and the physiological variables begin their approach to balanced growth, i.e., the cells go through Phase 1 and enter Phase 2. But before balanced growth is

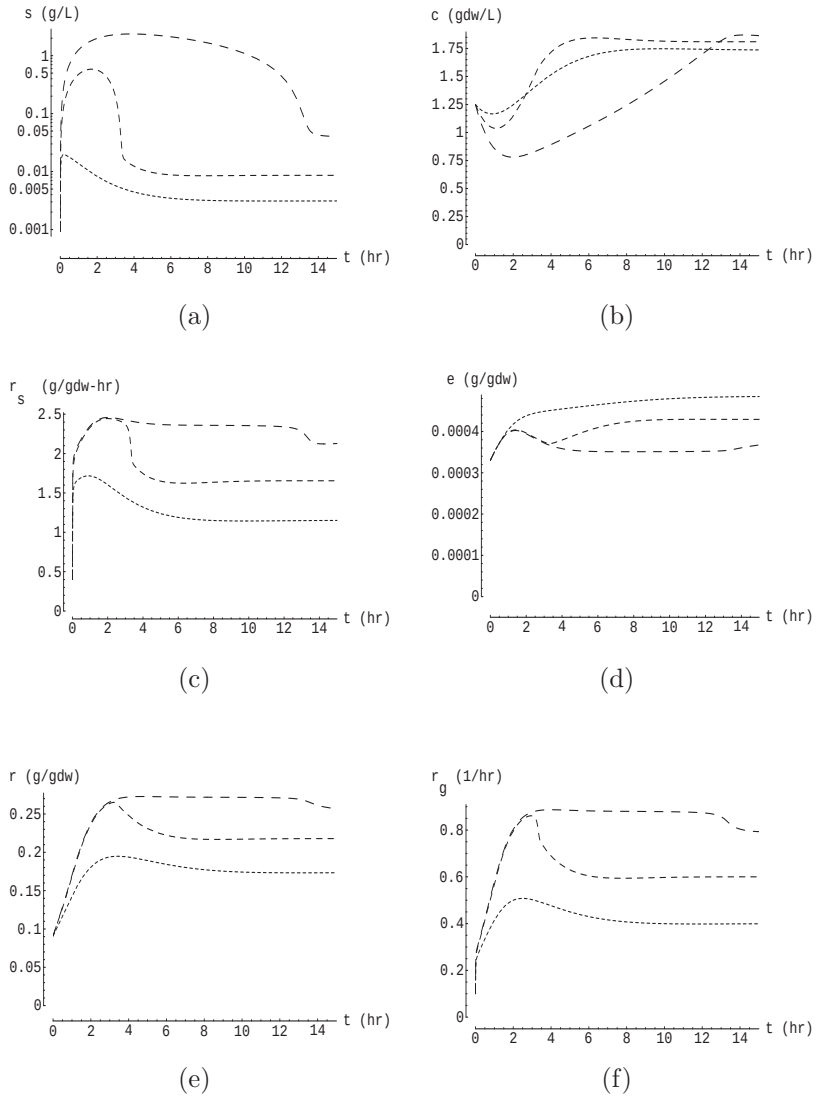

Figure 3–9: Transient response to dilution rate shift-ups. At $t < 0$, the culture is at the steady state corresponding to the dilution rate, $D_0 = 0.1$ 1/hr, and feed concentration, $s_f = 5$ g/L. At $t = 0$, the dilution rate is shifted up to $D = 0.4$ 1/hr (- -), $D = 0.6$ 1/hr (– –), and $D = 0.8$ 1/hr (— —).

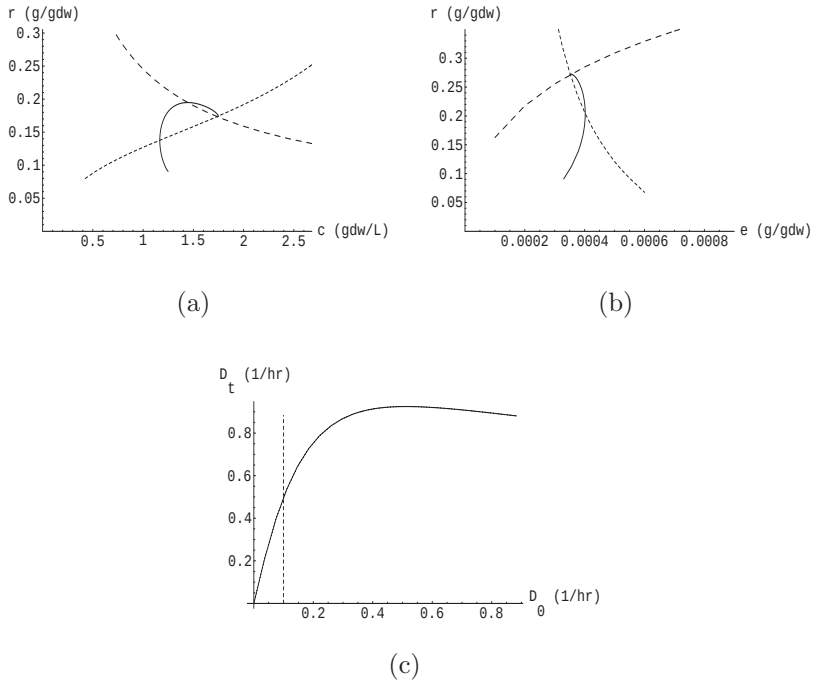

Figure 3–10: Phase portraits of the slow motion during dilution rate shifts. (a) The slow motion corresponding to the dilution rate shift-up from $D_0 = 0.1$ 1/hr to $D = 0.4$ 1/hr. (b) The slow motion corresponding to the large dilution rate shift-up from $D_0 = 0.1$ 1/hr to $D = 0.8$ 1/hr. (c) Classification of dilution rate shift-up dynamics.

reached, the substrate concentration returns to subsaturating levels, and the cells switch to Phase 3 and Phase 4 dynamics. Similar transients have been observed in experiments. Figure 3–11 shows the response of a glycerol-limited culture of *K. aerogenes* to a dilution rate shift-up from $D_0 = 0.004$ 1/hr to $D = 0.24$ 1/hr. The ribosome level, the specific growth rate, and the specific substrate uptake rate increase in a manner consistent with the approach to balanced growth (Figures 3–11b,c). However, balanced growth is not fully attained because the substrate concentration drops to subsaturating levels well before the cells achieve balanced growth. Indeed, the substrate concentration drops to subsaturating levels at $t \approx 10$ hrs (Figure 3–11a). At this point, the specific growth rate is ~ 0.6 1/hr, which is less than the maximum specific growth rate of 0.8 1/hr.

Intuition suggests that the magnitude of the dilution rate shift-up required to provoke these dynamics depends on the initial dilution rate. For, if the initial dilution rate is very small, so is the initial enzyme level. In this case, relatively small shift-ups should yield supersaturating substrate concentrations, resulting in Phase 1 and Phase 2 dynamics. On the other hand, if the dilution rate is large, the peripheral levels are so high that the substrate concentration should remain subsaturating throughout the transient, leading to Phase 3 and Phase 4 dynamics. This is indeed the case. In fact, given the response to continuous-to-batch shifts (Figure 1–6), one can predict the class of dynamics corresponding to any pre-assigned initial and final dilution rates. To see this, observe that the substrate concentration attains the quasisteady state given by (3.47) if and only if $\bar{r}_s(D_0)c_0 > Ds_f$, where $\bar{r}_s(D_0)$ denotes the specific substrate uptake rate achieved immediately after the cells have been exposed to supersaturating concentrations (see Figure 3–4a). But it follows from (3.19) that $c_0 \approx D_0 s_f/\tilde{r}_s(D_0)$ at all but the highest dilution rates. We conclude that s attains quasisteady state if and only if

$$\bar{r}_s \frac{D_0 s_f}{\tilde{r}_s(D_0)} > Ds_f \Rightarrow D < D_0 \frac{\bar{r}_s(D_0)}{\tilde{r}_s(D_0)}$$

In words, the substrate concentration attains quasisteady state if and only if the ratio by which the dilution rate increases, D/D_0, is less than ratio by which the specific uptake rate increases in response to a continuous-to-batch transition, $\bar{r}_s(D_0)/\tilde{r}_s(D_0)$. Thus, we can classify the dynamics by plotting the *transition* dilution rate

$$D_t \equiv D_0 \frac{\bar{r}_s(D_0)}{\tilde{r}_s(D_0)}$$

as a function of the initial dilution rate, D_0 (Figure 3–10c). Given any D_0, Phase 1 and 2 dynamics are obtained if D lies above the curve; Phase 3 and 4 dynamics are obtained if D lies below the curve. In particular, one can see that the simulations shown in Figure 3–9 are consistent with this classification.

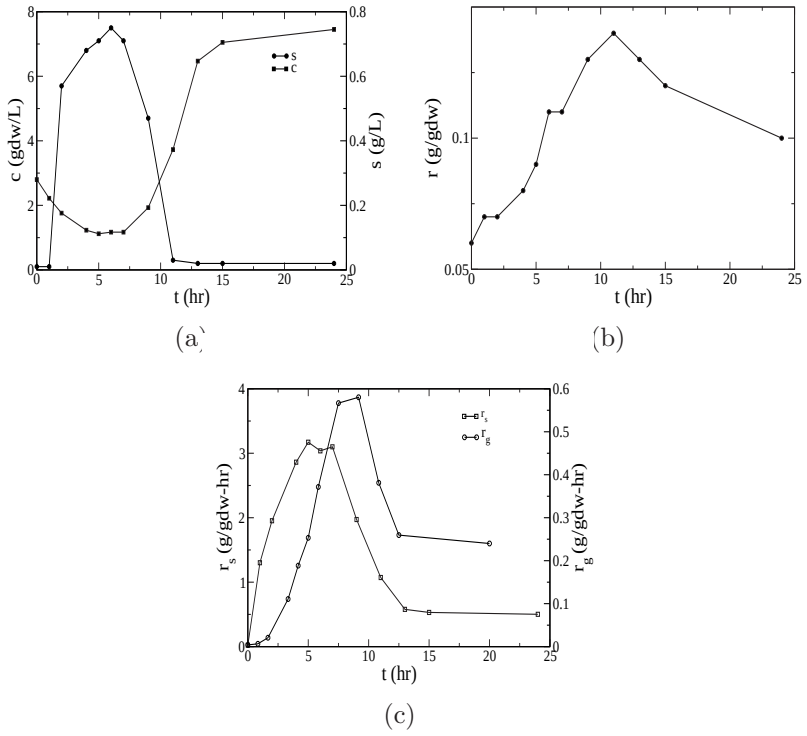

Figure 3–11: Response of a glycerol-limited culture of *K. aerogenes* to a dilution rate shift-up (from [12]). At $t < 0$, the culture is at the steady state corresponding to the dilution rate, $D_0 = 0.004$ 1/hr, and feed concentration, $s_f = 15$ g/L. At $t = 0$, the dilution rate is shifted up to $D = 0.24$ 1/hr, while the feed concentration is held constant. The figures show the evolution of the (a) Cell density and substrate concentration (b) RNA level (c) Specific substrate uptake and growth rates calculated from the curves in (a).

3.3 Discussion

Chemostat dynamics have been the subject of numerous experimental studies. From this formidable body of literature, Daigger & Grady [63] and Duboc *et al* [64] have distilled the key generalizations. We begin by reiterating these generalizations and interpreting them in terms of our model.

Based on an extensive review of the literature prior to 1980, Daigger & Grady classified the transients into two categories: growth responses and storage responses. Since our model does not account for storage, we confine attention to the growth responses. They state that

1. The growth responses possess the following properties

   (a) *Growth rate hysteresis (GRH):* During periods of varying substrate concentration, the specific growth rate of the culture lags behind the value predicted by the steady state specific growth rate. During periods of decreasing concentration, the specific growth rate will be more than predicted, while during periods of increasing substrate concentration, it will be less than predicted.
   The model exhibits growth rate hysteresis. Indeed, Figure 3–7f shows that immediately after the dilution rate shift-down, the culture settles into a specific growth rate that is higher than its final value. Conversely, the specific growth rate immediately after a dilution rate shift-up is lower than its ultimate value (Figure 3–9f).

   (b) *Available growth potential (AGP):* Microbial cultures possess the ability to rapidly increase their growth and substrate uptake rates during a transient response. As a general rule, the degree to which a culture can immediately increase its growth and substrate removal rates increases as the steady state specific growth rate of the culture is decreased.
   Simulations of the continuous-to-batch shifts show that the specific substrate uptake and growth rates do increase immediately (Figure 3–4a,c). Moreover, the increments in these rates increase as the dilution rate of the culture decreases. But this is true only up to a point. At sufficiently low dilution rates, the increments decrease once again because at very low dilution rates, the peripheral enzyme and ribosome levels become small.

2. In many instances, both phenomena are observed. For example, the specific growth rate immediately after exposure to substrate-excess conditions is greater than the rate before (AGP), but less than the maximum rate which the culture could attain. However, with the passage of time, the specific growth rate gradually increases, and eventually reaches the maximum rate. Throughout this period, the specific growth rate is less than the maximum specific growth rate (GRH).
   This property is evident in Figures 3–5f and 3–9f.

3. The concept of physiological adaptation may be used to understand these growth responses. When a microbial culture is grown at a submaximal specific growth rate, the culture adapts to that growth environment. In particular, the RNA content, the enzyme levels, and concentration of intracellular metabolites are lower than the values attained at the maximum specific growth rate. When the cells are exposed to a substrate-excess environment, the culture is unable to grow at its maximum rate. This is because the physiological adaptation is not complete, so that the culture possesses only a limited ability to immediately increase its specific growth rate (AGP). As time passes, the levels of RNA, enzymes, and intracellular metabolites

gradually increase. Thus, the specific growth rate of the culture increases progressively until it eventually reaches its maximum value (GRH).
This train of events is precisely what transpires in the model (see Figures 3–5 and 3–9).

More recently, Duboc *et al* arrived at the following conclusions based on extensive dilution rate shift-up experiments with *S. cerevisiae* [64].

1. There is an immediate increase in the catabolic activity. Moreover, the increase in the catabolic activity is always larger than the increase in the growth rate, leading to a transient uncoupling of catabolism and growth. This model displays this characteristic as is evident from Figures 3–4a,c,d. To capture the different response times of the catabolic and anabolic rates, Duboc *et al* assumed that these rates followed the phenomenological equations
$$\tau_{\text{cat}}\frac{dr_{\text{cat}}}{dt} = (r_{\text{cat}}^{\max} - r_{\text{cat}}),\ \tau_{\text{g}}\frac{dr_g}{dt} = (r_{\text{g}}^{\max} - r_g)$$
and unique time constants, τ_{cat} and τ_g were chosen for each experiment in order to fit the data. Our model may be viewed as an attempt to give a physiological basis for the foregoing phenomenological equations.

2. In some experiments, such as the dilution rate shift-up of aerobic cultures limited by acetic acid, the transient behavior of the culture is similar to the adaptation of the metabolism during a batch experiment where substrate is in large excess and does not influence the specific growth rate. In yet other experiments, such as the dilution rate shift-up of glucose-limited aerobic cultures, the substrate did not accumulate.
According to our model, these two transients reflect Phase1/Phase 2 and Phase 3/Phase 4 dynamics, respectively. Since the maximum specific growth rate on acetic acid is much lower than the maximum specific growth rate on glucose, the very same dilution rate shift-up, i.e., the very same D_0 and D, could lead to substrate-sufficient batch dynamics in the first case, and cell-sufficient fed-batch dynamics in the second case.

The model yields further insights into these observations.

1. The substrate concentration exists in either one of two states. It is either at supersaturating levels or at the subsaturating levels attained when the substrate reaches quasisteady state. Transitions between these two states are so fast (on the order of minutes) that they may be ignored on the time scale of interest (on the order of hours).

2. The dynamics corresponding to these two states are canonical in the following sense. The transients observed in response to a wide variety of perturbations are a combination of these two classes of dynamics. Thus, in dilution rate shift-ups, the substrate is supersaturating throughout the transient if the final

dilution rate is close to the maximum specific growth rate. It is subsaturating throughout the transient if the final dilution rate is close to the initial dilution rate. It switches from supersaturating to subsaturating levels when the shift-ups are moderate. The latter is also the case in feed switches where the substrate concentration is supersaturating at first, but switches to subsaturating concentrations later. It follows that a complete understanding of these two classes of dynamics is sufficient for understanding all other dynamics.

3. These two classes of dynamics possess the following experimentally testable properties

   (a) During the approach to balanced growth, the peripheral enzyme and ribosome levels pass through a maximum, but the enzyme level reaches a maximum before the ribosome level.

   (b) During the approach to the final steady state, the cell density passes through a maximum and the ribosome level passes through a minimum. The cell density reaches its maximum before the ribosome level reaches its minimum.

We can express these observations more concisely in the parlance of nonlinear dynamics. We have shown, in effect, that the chemostat displays *excitable* dynamics. In other words, there are two "slow" submanifolds (surfaces) embedded within the space of all variables in the model . The motion into and out of these submanifolds is very fast. The dynamics on the time scale of interest (hours) occur only when the variables lie in one of the submanifolds. The motion on these two submanifolds corresponds to Phase 1/Phase 2 and Phase 3/Phase 4 dynamics, respectively.

CHAPTER 4
THE ROLE OF ADENINE NUCLEOTIDE

We have characterized the sluggish response in the chemostat to the environmental perturbation in two categories. Firstly, the lags were observed due to substrate uptake rate limitation, which were assigned to the insufficient transport enzyme level. The role of transport enzyme was studied in chapter 2. It was demonstrated that the model accounting for transport enzyme captures the experimental data quantitatively (Figure 1–5). Secondly, in the case where the growth was limited by protein synthesis, the phenomena was encompassed using the autocatalytic synthesis of Ribosome or RNA. The role of ribosomes was studied in chapter 3. We argued that a lower concentration of RNA at a low dilution rate would limit the specific growth rate. We assumed that the biosynthesis was limited by ribosomes, and further explained these dynamics qualitatively.

This study is motivated by the metabolic regulation of the specific growth rate. When the cell picks up the substrate, the different enzymes inside the cell brakes down the incoming substrate into precursor molecules i.e. glucose-6-phosphate, fructose-6-phosphate, pyruvate etc. The precursor molecules have an opportunity to go either to biosynthesis, respiration, storage products, or excretion. The question now arises that how the cell decides where to send the incoming substrate? To solve this discrepancy, we have used energy charged particle, adenosine triphosphate (ATP), as an energy source and as a major regulatory factor in controlling the metabolic flux distribution. The energy charged particle (ATP) converts into energy uncharged particle, adenosine diphosphate (ADP), in energy consuming processes and the energy uncharged particle (ADP) converts back to energy charged particle (ATP) in energy generating processes. For this

purpose, we have defined energy charge as the ratio of the charged adenosine nucleotides to total adenosine nucleotides and will be used to show how the ratio of ATP and ATP plus ADP regulates the metabolic fluxes. We wish to extend our previous model to account for these observations by including ATP in the model. We have incorporated the concentration of ATP and ADP in different kinetic expressions to explain the metabolic regulation in various transient dynamics in the chemostat including the stationary phase in the batch culture.

The goal of this work is to study an extended model taking due account of ATP to capture and explain the metabolic flux distribution, and additional data discussed below while keeping the various dynamics of previous model intact. We begin by formulating the extended model (Section 4.1). We then simulate the model to show that it yields results in qualitative agreement with the data (Section 4.2). Finally, we compare the key results of the model to those summarized in reviews of the experimental literature.

4.1 The Model

Figure 4–1 shows the kinetic scheme of the model. Here, S denotes the growth-limiting carbon source, E denotes the peripheral enzymes that catalyze the transport and peripheral catabolism of the carbon source and X denotes the internalized form of the substrate that induces the synthesis of E; P denotes the pool of precursors produced by catabolism of X; R denotes ribosomes or rRNA; C^- denotes proteins; E_a denotes the enzymes required to synthesize adenosine diphosphate (ADP)[1] and A_3, A_2 and A_t denotes adenosine triphosphate (ATP), adenosine diphosphate (ADP) and total adenine nucleotides respectively. The

[1] In the cell, the function of adenine nucleotide synthesis enzyme is to produce adenosine monophosphate (AMP). As AMP is not incorporated in the model to retain the simplicity, adenine nucleotide synthesis enzyme is used for the synthesis of ADP.

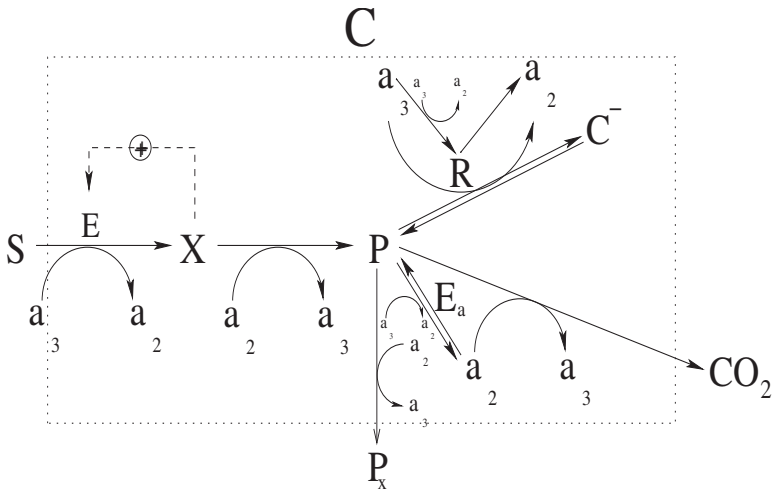

Figure 4–1: Kinetic scheme of the ATP model. Here, S denotes the substrate, E denotes the inducible enzyme(s) catalyzing the uptake and peripheral catabolism of S, X denotes the inducer for E, P denotes the biosynthetic precursors derived from catabolism of X, R denotes RNA, C^- denotes proteins, A_3 denotes the the *charged* nucleotides, A_2 denotes the *uncharged* nucleotides, E_a denotes the uncharged nucleotides synthesis enzyme and C denotes the entire cell consisting of E, X, P, R, A_3, A_2, E_a and C^-.

role of adenosine monophosphate (AMP) has been omitted to avoid complexity in the model. As AMP is not a part of this model, ATP and ADP are defined as energy charged and energy uncharged nucleotides. Thus energy charge, E_c, is defined as the concentration of A_3/A_t. The entire cell consisting of E, X, P, R, C^-, E_a,A_3, and A_2 is denoted by C. The term *biosynthesis* will be used to refer the synthesis of RNA (R), and proteins (C^-), while *growth* will refer the synthesis of all intracellular components.

Throughout this work, the instantaneous concentrations of the variables are denoted by the corresponding lower-case letters s, e, x, p, r, c^-, e_a, a_3,a_2, a_t and c, while steady state and quasisteady state concentrations are denoted by overlaying the letters with $\sim$ and $-$, respectively (for instance, $\tilde{x}$ and $\bar{x}$). The concentrations of the *environmental* variables, s and c, are based on the volume of chemostat (g/L and gdw/L respectively), the concentrations of the *physiological* variables, e, x, p, r, a, c^-, e_a, a_3, a_2, and a_t are based on the dry weight of biomass (g/gdw).

We make the following assumptions regarding the kinetics of the processes.

1. The specific substrate uptake rate, denoted r_s, satisfies the kinetic law

$$r_s \equiv V_s a_3 e \frac{s}{K_s + s} \frac{1}{1 + \left(\frac{p}{K_i}\right)^2}$$

where the factor $\frac{1}{1+\left(\frac{p}{K_i}\right)^2}$ denotes the inhibition of substrate uptake by precursors.

2. The specific rate of breakdown of X into energy and precursors P, denoted r_x, is given by

$$r_x \equiv k_x a_2 x$$

3. The specific rate of respiration is

$$r_{\mathrm{co}_2} \equiv k_{\mathrm{co}_2} a_2 p$$

4. The specific rate of enzyme synthesis, denoted r_e^+, is

$$r_e^+ \equiv V_e \frac{r}{k_e + r} \frac{1 + K_2 x^2}{K_3 + K_2 x^2}$$

The derivation of this reaction kinetic has been described in chapter 3.

5. The specific rate of excretion is

$$r_{p_x} \equiv k_{p_x} a_2 p^3$$

6. The specific rate of rRNA synthesis is

$$r_r^+ \equiv k_r^+ a_3^2 p r$$

7. The specific rate of protein (C^-) synthesis is

$$r_c^+ \equiv V_c a_3 r \frac{p}{K_c + p}$$

8. The specific rate of nucleotide synthesis enzyme is

$$r_{e_a}^+ \equiv k_{e_a}^+ p r$$

9. The specific rate of *de novo* nucleotide synthesis is

$$r_{a_2}^+ \equiv k_{a_2}^+ a_3 p e_a$$

10. The specific rates of peripheral enzyme, nucleotide, rRNA, nucleotide synthesis enzyme, and protein denoted r_e^-, $r_{a_2}^-$, r_r^-, $r_{e_a}^-$and r_c^- respectively, are given by

$$r_e^- \equiv k_e^- e,\ r_{a_2}^- \equiv k_{a_2}^- a_2,\ r_r^- \equiv k_r^- r,\ r_{e_a}^- \equiv k_{e_a}^- e_a,\ r_c^- \equiv k_c^- c^-$$

11. The synthesis of peripheral enzymes, uncharged nucleotides, nucleotide synthesis enzyme, and proteins depletes the pool of precursors and their degradation replenishes the pool of precursors.

12. The synthesis of RNA depletes the pool of charged nucleotides and their degradation replenishes the pool of uncharged nucleotides.

A mass balance on the state variables yields

$$\frac{ds}{dt} = D(s_f - s) - r_s c \tag{4.1}$$

$$\frac{dc^-}{dt} = r_c^+ - r_c^- - \left(D + \frac{1}{c}\frac{dc}{dt}\right) c^- \tag{4.2}$$

$$\frac{de}{dt} = r_e^+ - r_e^- - \left(D + \frac{1}{c}\frac{dc}{dt}\right) e \tag{4.3}$$

$$\frac{de_a}{dt} = r_{e_a}^+ - r_{e_a}^- - \left(D + \frac{1}{c}\frac{dc}{dt}\right) e_a \tag{4.4}$$

$$\frac{dr}{dt} = r_r^+ - r_r^- - \left(D + \frac{1}{c}\frac{dc}{dt}\right) r \tag{4.5}$$

$$\frac{da_2}{dt} = \gamma_s r_s - \gamma_x r_x - \gamma_{\mathrm{co}_2} r_{\mathrm{co}_2} + \sum_{i=c^-,r,a_2} (\gamma_i^+ r_i^+ - \gamma_i^- r_i^-) + (r_{a_2}^+ - r_{a_2}^-) + r_r^- - \left(D + \frac{1}{c}\frac{dc}{dt}\right) a_2 \tag{4.6}$$

$$\frac{da_3}{dt} = -\gamma_s r_s + \gamma_x r_x + \gamma_{\mathrm{co}_2} r_{\mathrm{co}_2} - \sum_{i=c^-,r,a_2} (\gamma_i^+ r_i^+ - \gamma_i^- r_i^-) - r_r^+ - \left(D + \frac{1}{c}\frac{dc}{dt}\right) a_3 \tag{4.7}$$

$$\frac{dx}{dt} = r_s - r_x - \left(D + \frac{1}{c}\frac{dc}{dt}\right) x \tag{4.8}$$

$$\frac{dp}{dt} = r_x - r_{\mathrm{co}_2} - r_{p_x} - \sum_{i=a_2,c,e,e_a} (r_i^+ - r_i^-) - \left(D + \frac{1}{c}\frac{dc}{dt}\right) p \tag{4.9}$$

$$\frac{dp_x}{dt} = r_{p_x} c - D p_x \tag{4.10}$$

where s_f denotes the concentration of S in the feed, and D denotes the dilution rate. γ_s denotes the energy required to transport the substrate inside the

cell, γ_x denotes energy generated in the process of producing precursors, $\gamma_i^+$and γ_i^-denote the energy required to generate the different cellular components and energy generated while degrading the cellular components respectively, and γ_{co_2} denotes energy generated from utilizing the precursors in the TCA cycle .

To derive the reduced equations from the original equations (4.20–4.28), we appeal to the following facts

1. The mass fraction of all intracellular entities equals unity, i.e.,

$$c^- + e + r + e_a + a_2 + a_3 + x + p = 1 \;\; g/gdw. \tag{4.11}$$

Then, adding equations (4.2–4.9) yields

$$D + \frac{1}{c}\frac{dc}{dt} = r_s - r_{\mathrm{co}_2} - r_{p_x} \tag{4.12}$$

We define

$$r_g \equiv r_s - r_{\mathrm{co}_2} - r_{p_x} \tag{4.13}$$

where r_g denotes the specific growth rate of the cells. It follows from (4.12–4.13) that the last term in equations (4.2–4.9) represents the dilution of the intracellular variables due to cell growth, and (4.12) can be rewritten in the more familiar form

$$\frac{dc}{dt} = (r_g - D)c \tag{4.14}$$

To derive the reduced equations, we substitute equation (4.2) with equation (4.14), and replace the expression $D + (1/c)(dc/dt)$ in equations (4.2–4.9) with r_g.

2. Although both variables, a_2 and a_3, change rapidly. The total concentration a_t evolves slower than a_2 and a_3.

$$a_t \equiv a_2 + a_3.$$

The addition of equations (4.6) and (4.7) yields the following equation

$$\frac{da_t}{dt} = r_{a_2}^+ - r_{a_2}^- - r_r^+ + r_r^- - r_g a_t \tag{4.15}$$

To derive the reduced equations, we replace (4.6) with (4.15).

3. Since A_3, A_t, X and P are present in small concentrations, but participate in rapid reactions, they achieve quasi-steady state almost instantly. Thus

$$\frac{da_3}{dt} = 0 \Rightarrow (\gamma_x - \gamma_s) r_s + \gamma_{\mathrm{co}_2} r_{\mathrm{co}_2} + \gamma_{p_x} r_{p_x} - \sum_{i=c,r,a_2} (\gamma_i^+ r_i^+ - \gamma_i^- r_i^-) \approx 0 \quad (4.16)$$

$$\frac{da_t}{dt} = 0 \Rightarrow (r_{a_2}^+ - r_{a_2}^-) \approx (r_r^+ - r_r^-) \quad (4.17)$$

$$\frac{dx}{dt} = 0 \Rightarrow r_x \approx r_s \quad (4.18)$$

$$\frac{dp}{dt} = 0 \Rightarrow r_x - r_{\mathrm{co}_2} - r_{p_x} \approx (r_c^+ - r_c^-) + (r_{a_2}^+ - r_{a_2}^-) \quad (4.19)$$

where we have assumed that the dilution rates of A_3, X, P and A_t are negligibly small compared to the rates at which these entities are produced/consumed by various catabolic and anabolic reactions.
To derive the reduced equations, we replace the differential equations (4.7–4.9) with the algebraic relations (4.16–4.19).

4. Further simplification of the expression obtains by observing that (4.17–4.19) imply the relation

$$r_g \equiv r_s - r_{\mathrm{co}_2} - r_{p_x} \approx (r_c^+ - r_c^-) + (r_r^+ - r_r^-)$$

where we have assumed that $\sum_{i=e,e_a} (r_i^+ - r_i^-) \ll (r_c^+ - r_c^-)$ This expression is consistent with our intuition that since $x, p, e, a_2, a_3 \ll r, c^-$, the specific growth rate is effectively equal to the sum of the net specific rates of RNA and protein synthesis rates.

5. Finally, note that since $e, x, p, a_2, a_3 \ll 1$, equation (4.11) implies that

$$c^- + r \approx 1 \Rightarrow c^- \approx 1 - r$$

Hence, equations (4.1–4.10) can be approximated by the *reduced* equations

$$\frac{ds}{dt} = D(s_f - s) - \left(V_s \bar{a}_3 e \frac{s}{K_s + s} \right) c \quad (4.20)$$

$$\frac{dc}{dt} = (r_g - D)\, c \quad (4.21)$$

$$\frac{de}{dt} = V_e \frac{r}{k_e + r} \frac{1 + K_2 \bar{x}^2}{K_3 + K_2 \bar{x}^2} - k_e^- e - r_g e \quad (4.22)$$

$$\frac{de_a}{dt} = k_{e_a}^+ p r - k_{e_a}^- e_a - r_g e_a \quad (4.23)$$

$$\frac{dr}{dt} = k_r^+ r \bar{a}_3^2 \bar{p} - k_r^- r - r_g r \quad (4.24)$$

$$0 \approx (\gamma_x - \gamma_s) r_s + \gamma_{\mathrm{co}_2} r_{\mathrm{co}_2} - \sum_{i=c^-,r,a_2} (\gamma_i^+ r_i^+ - \gamma_i^- r_i^-) - r_r^+ \tag{4.25}$$

$$0 \approx r_{a_2}^+ - r_{a_2}^- - r_r^+ + r_r^- \tag{4.26}$$

$$0 \approx V_s \bar{a}_3 e \frac{s}{K_s + s} - k_x \bar{a}_2 \bar{x} \tag{4.27}$$

$$0 \approx k_x \bar{a}_2 \bar{x} - k_{\mathrm{co}_2} \bar{a}_2 \bar{p} - k_{\mathrm{p_x}} \bar{a}_2 \bar{p}^3 - r_g \tag{4.28}$$

$$\frac{dp_x}{dt} = r_{p_x} c - D p_x \tag{4.29}$$

where r_g, the specific growth rate, is given by

$$r_g \approx V_c r \bar{a}_3 \frac{\bar{p}}{K_c + \bar{p}} - k_c^- c^- + k_r^+ r \bar{a}_3 \bar{p} - k_r^- r \tag{4.30}$$

$$1 \approx c^- + r \tag{4.31}$$

It is effectively equal to the specific rate of net rRNA and protein.

4.2 Simulations

The simulations were done with the parameter values in Table 4–1.

Table 4–1: Parameter values used in the ATP model simulations.

$V_s = 2 \times 10^7 \ \frac{\mathrm{gdw}}{\mathrm{g-hr}}$	$K_s = 10^{-2} \ \frac{\mathrm{g}}{\mathrm{L}}$	$K_i = 0.02 \ \frac{\mathrm{g}}{\mathrm{gdw}}$	$k_x = 10^6 \ \frac{\mathrm{gdw}}{\mathrm{g-hr}}$
$V_e = 1 \times 10^{-4} \ \frac{\mathrm{g}}{\mathrm{gdw-hr}}$	$K_2 = 10^{11} \left(\frac{\mathrm{gdw}}{\mathrm{g}}\right)^2$	$K_3 = 10^4$	$k_e^- = 0.01 \ \frac{1}{\mathrm{hr}}$
$k_e = 0.1 \ \frac{\mathrm{g}}{\mathrm{gdw}}$	$k_{\mathrm{co}_2} = 10^5 \ \frac{\mathrm{g}}{\mathrm{g-hr}}$	$k_r^+ = 3 \times 10^6 \ \frac{\mathrm{gdw}^3}{\mathrm{g}^3-\mathrm{hr}}$	$k_r^- = 0.03 \ \frac{1}{\mathrm{hr}}$
$V_c = 10^3 \ \frac{\mathrm{gdw}}{\mathrm{g-hr}}$	$k_c^- = 0.03 \ \frac{1}{\mathrm{hr}}$	$K_c = 0.002 \ \frac{\mathrm{g}}{\mathrm{gdw}}$	$k_{p_x} = 5 \times 10^7$
$k_{e_a}^+ = 0.01 \ \frac{gdw}{g-hr}$	$k_{e_a}^- = 0.06 \ \frac{1}{\mathrm{hr}}$	$k_{a_2}^+ = 3 \times 10^7 \ \frac{gdw^2}{g^2-hr}$	$k_{a_2}^- = 6 \ \frac{1}{hr}$
$\gamma_s = 3 \ \frac{g}{gdw}$	$\gamma_x = 10 \ \frac{g}{gdw}$	$\gamma_{p_x} = 0 \ \frac{g}{gdw}$	$\gamma_{a_2} = 20 \ \frac{g}{gdw}$
$\gamma_c = 40 \ \frac{g}{gdw}$	$\gamma_{co_2} = 23 \ \frac{g}{gdw}$	$\gamma_r = 8 \ \frac{g}{gdw}$	

4.2.1 Steady States

The equations (4.20–4.29) permit two types of steady states, namely, the persistence steady state ($\tilde{c} \neq 0$) and the washout steady state ($\tilde{c} = 0$). For a given microbial species and growth-limiting substrate, these steady states can depend on two parameters — the dilution rate and the feed concentration.

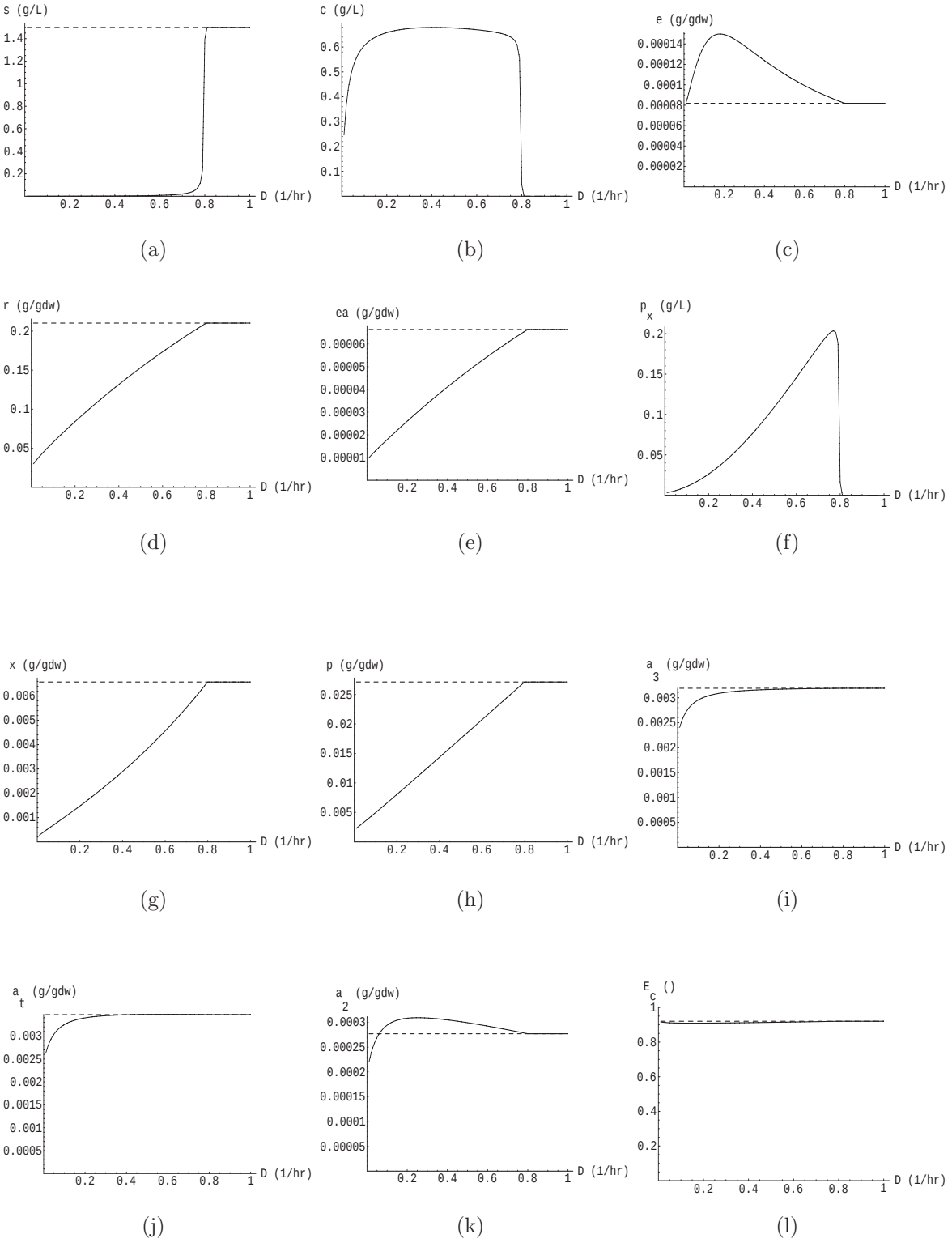

Figure 4–2: Variation of the steady states with D at $s_f = 1.5$ g/L. Stable and unstable steady states are denoted by full and dashed lines, respectively.

Under this condition, there exists washout steady state for all dilution rate and critical washout dilution rate at $D_w = 0.81$ 1/hr where the maximum growth rate is unable to balance the dilution rate, consequently the cell washes out.The washout steady state is stable above the critical washout dilution rate and unstable below the critical washout dilution rate. There exists a unique persistence steady state for all dilution rates. The persistence steady state is stable below the washout dilution rate and is unstable above the washout dilution rate. The steady state figures (Figure 4–2) are formally similar to the results obtained in experiments (Figure 1–3). The substrate concentration and ribosome levels increase monotonically (Figure 4–2a,d). The cell density and transport enzyme levels pass through a maximum(Figure 4–2b,c). At low dilution rate, the cell produces small concentration of excretory products compare to high dilution rate(Figure 4–2f). The concentrations of ATP, and total nucleotides show a hyperbolic profile and energy charge stays approximately constant for all dilution rates(Figure 4–2i,j,l). The concentration of ADP passes through maxima at $D_w = 0.2$ 1/hr (Figure 4–2k).

Note that the steady state concentrations of the substrate and the physiological variables are independent of the feed concentration, s_f. This is because the steady state concentrations of S and the eight physiological variables (E,E_a, R, X, P, E_a, A_3 and A_t) are completely determined by the eight equations (4.21–4.28). These equations depend only on the dilution rate; and are independent of the feed concentration.

4.2.2 Transients

The calculation of energy charge raises the question of its potential utility? The answer lies in the structure of the model. The absolute concentrations of charged and uncharged nucleotides define only the rate of all the reactions. The metabolic distribution of the incoming flux is defined by the energy charge as the growth rate is only initiated by the concentration of charged nucleotides, ATP, and

the rate of carbon dioxide evolution and excretory products are only dictated by the concentration of uncharged nucleotides, ADP. The ratio of charged nucleotides to total nucleotides helps the cell to make the decisions regarding the distribution of the incoming substrate either for creating biomass or for energy generation in TCA cycle depending on the concentration of ribosomes and the availability of the substrate. When the energy charge is high, implies the ATP concentration is high, the cell diverts the incoming substrate towards energy consuming pathways, i.e., protein synthesis and ribosome synthesis. Conversely, when the energy charge is low, the cell diverts the substrate flux to respiration to generate energy. This regulation is occurring because of inter conversion between charged nucleotides, ATP, and uncharged nucleotides ADP, hence the time period of this regulation lies in seconds. Thus, the cell utilizes the concentration of ribosomes for the regulation of the cell growth in a slow time scale and the concentration of charged and uncharged nucleotides in a fast time scale.

4.2.2.1 Substrate pulse

In substrate pulse experiment, the reactor was maintained at steady state at fixed dilution rate and a small perturbation was given to the glucose concentration by injecting a pulse of extra glucose. The transient concentration of ATP was measured for 180 seconds (see Figure 1–9)[51]. The fast drop in the concentration of ATP in seconds time scale immediately after the glucose pulse was attributed to the response of the ATP consumption in phosphorylation of the substrate. To replicate this experiment, the simulation was started with the steady state values at fixed dilution $D = 0.2$ 1/hr. At $t = 0$, the substrate concentration in the reactor was shifted to a higher value than the substrate concentration at steady state. In this simulation, the substrate concentration has been increased to 0.1 g/L. As soon as the cell perceives an excess substrate in the environment, the unsaturated transport enzyme becomes saturated with substrate, hence, the substrate uptake

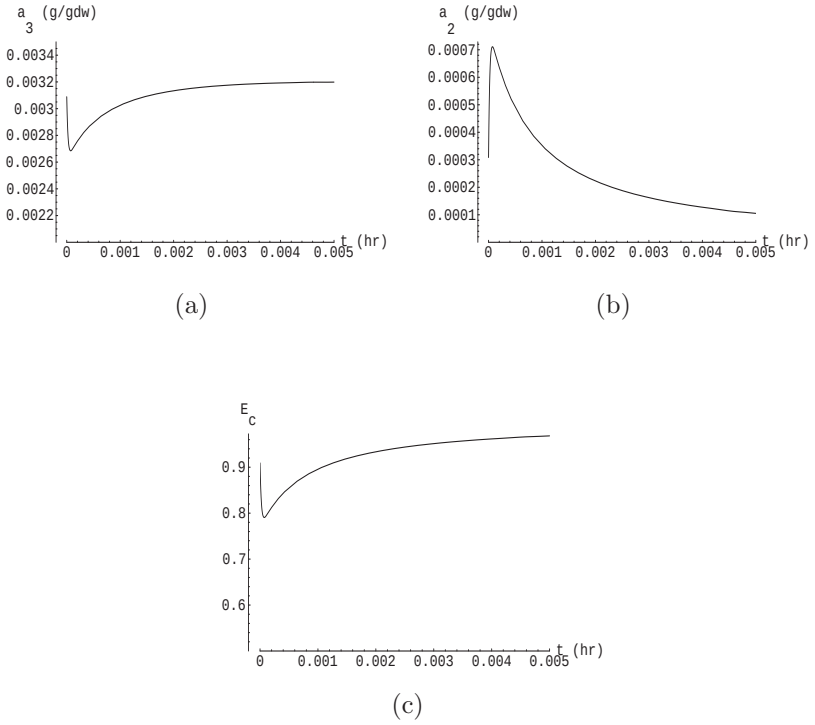

Figure 4–3: Transient response to substrate pulse in seconds time scale.At $t < 0$, the culture was at steady state corresponding to dilution rate $d = 0.21$/hr. At time $t = 0$, the substrate concentration, s, in the reactor is increased to $s = 0.1$g/l while feed concentration and dilution rate were held constant.

rate reaches to maximal level. The cell phosphorylates the incoming substrate in the process of substrate transport. The phosphorylation of the substrate uses adenosine triphosphate, ATP, and converts into adenosine diphosphate, ADP. As the total nucleotide concentration is really low inside the cell, this transport process causes the concentration of charged nucleotides, ATP, to drop in seconds time scale. The drop in ATP concentration recovers back only when the substrate starts accumulating as the inducer molecule inside the cell and commences energy generation from glycolysis in the process of producing precursors (see Figure 4–3).

The time period of this transient is so small that the incoming substrate does not reach biosynthesis especially the synthesis of ribosome and influences the total nucleotide concentration, hence the total nucleotide concentration stays constant. The conservation of total nucleotides helps in explaining the simulation

results. The inter conversion between the charged nucleotide, ATP, and uncharged nucleotide, ADP, in the process of substrate transport and glycolysis projects a light not only for the observed minima in ATP concentration, but also the observed maxima in ADP concentration and minima in energy charge. Energy charge is an increasing function of the charged nucleotide, ATP, and decreasing function of the uncharged nucleotide, ADP. As ATP converts to ADP in transport, this process decreases the ATP concentration and increases ADP concentration, hence, decreases energy charge. When concentration of ATP recovers back in the process of glycolysis, it increases the concentration of ATP and decreases the concentration of ADP, hence increases energy charge.

When the incoming substrate influences the biomass synthesis, the slow drop in the concentration of ATP within 30 minute was observed [17]. This further drop in ATP concentration was explained by an increased utilization of ATP for the synthesis of biomass especially the synthesis of ribosome or RNA. To replicate this experiment the above simulation was continued to run for 30 minutes. When the substrate converts into the precursor molecules, the slow ribosomal kinetics divert the incoming substrate to respiration or excretion resulting in an increase in the concentration of charged nucleotides, hence energy charge increases above the steady state value (Figure 4–4f). As the synthesis of RNA depends on the higher order of the charged nucleotides, a_3^2, than the *de novo* synthesis of uncharged nucleotides on the charged nucleotides, a_3, the increase in the charged nucleotide causes the higher jump in RNA synthesis rate than the uncharged nucleotides. This difference between the synthesis of RNA and uncharged nucleotides results in the decrease in the concentration of total nucleotides and consequently the slow drop in the charged nucleotides (see Figure 4–4d,e). If the substrate pulse is sufficient enough to sustain the perturbation for a while, then it increases the concentration of ribosomes above the steady state level. The higher levels ribosome concentration

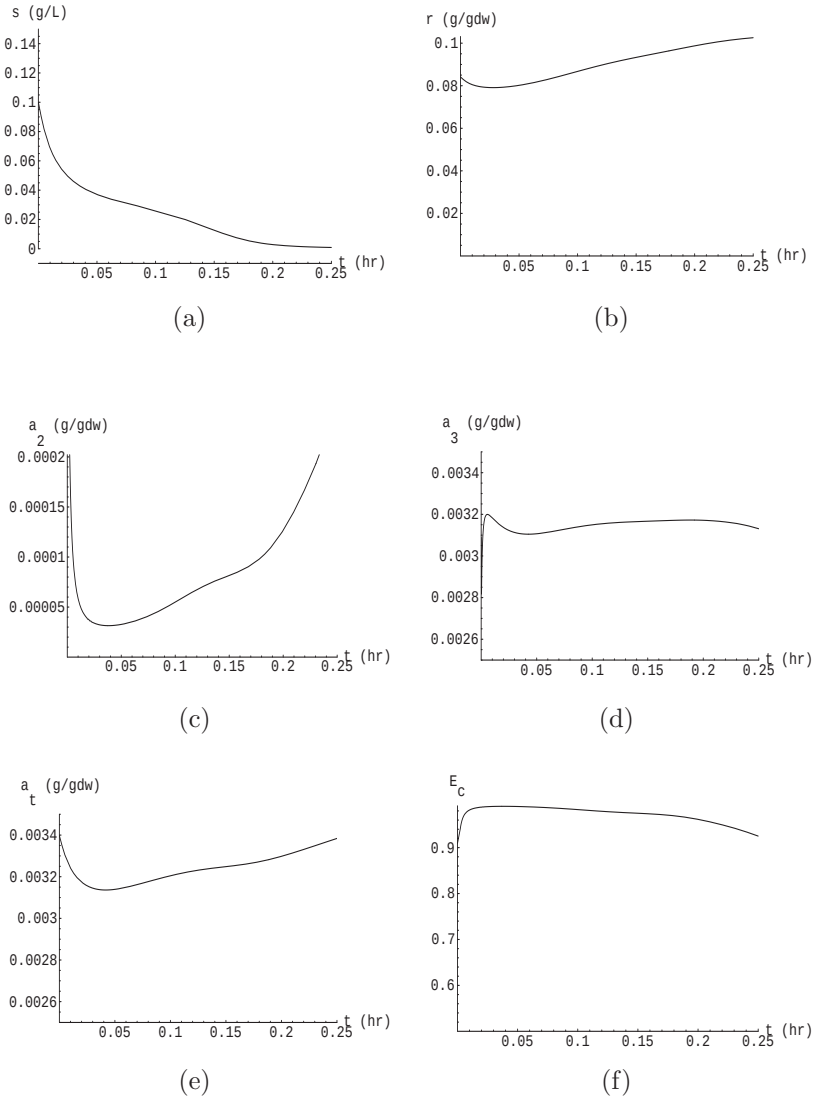

Figure 4–4: Transient response to substrate pulse in minute time scale. At $t < 0$, the culture was at the steady state corresponding to the dilution rate, $D_0 = 0.2$ 1/hr, and feed concentration, $s_f = 1.5$ g/L. At $t = 0$, the substrate concentration in the reactor was shifted up to $s = 0.1$ g/L, while the dilution rate was held constant.

can also produce a drop in charged nucleotides after the exhaustion of the substrate (simulations are not shown).

4.2.2.2 Continuous-to-batch shifts

In continuous-to-batch shifts, at $t < 0$, the culture is in steady state at some dilution rate, D. At time $t = 0$, a small sample of the culture is rapidly transferred to the batch reactor containing a high substrate concentration. The initial rates of biochemical processes are measured within 10–15 minutes of exposing the culture to excess substrate conditions (see Figure 1–6). To simulate these experiments with the model, we observe that in this short time period, the concentrations of the peripheral enzymes, ribosomes, and nucleotides synthesis enzyme levels essentially remain unchanged because of the slow kinetics. The inducer, precursor, ATP and total nucleotides concentrations rapidly move to new quasisteady states corresponding to substrate-excess conditions. This new quasisteady state is obtained by letting $s/(K_s + s) \approx 1$ in (4.25–4.28), while the peripheral enzyme, nucleotide synthesis enzyme and ribosome levels are held at their initial steady state values, $e_0 = \tilde{e}(D)$, $r_0 = \tilde{r}(D)$ and $e_{a0} = \tilde{e_a}(D)$.

Figure 4–5 shows that simulation results are consistent with the experiments (Figure 1–6). As soon as the cells are exposed to excess substrate conditions, the substrate uptake rate goes to its maximum value depending upon the enzyme concentration at that dilution rate (Figure 4–5a). This increase in r_s increases the inducer concentration, hence the precursor concentration which further results in the increase of the respiration rate, $r_{co_2}$and excretion rate, r_{p_x} (Figure 4–5b,e,h). The increase in the respiration rate, r_{co_2} increases the energy charge (Figure 4–5l), hence diverts the incoming substrate flux to the biomass synthesis. But the generation of nucleotide, $r^+_{a_2}$, and the consumption of nucleotides in RNA synthesis, r^+_r, maintains the constant concentration of ATP, a_3, which makes the ADP concentration, a_2, to go down (Figure 4–5i,j).

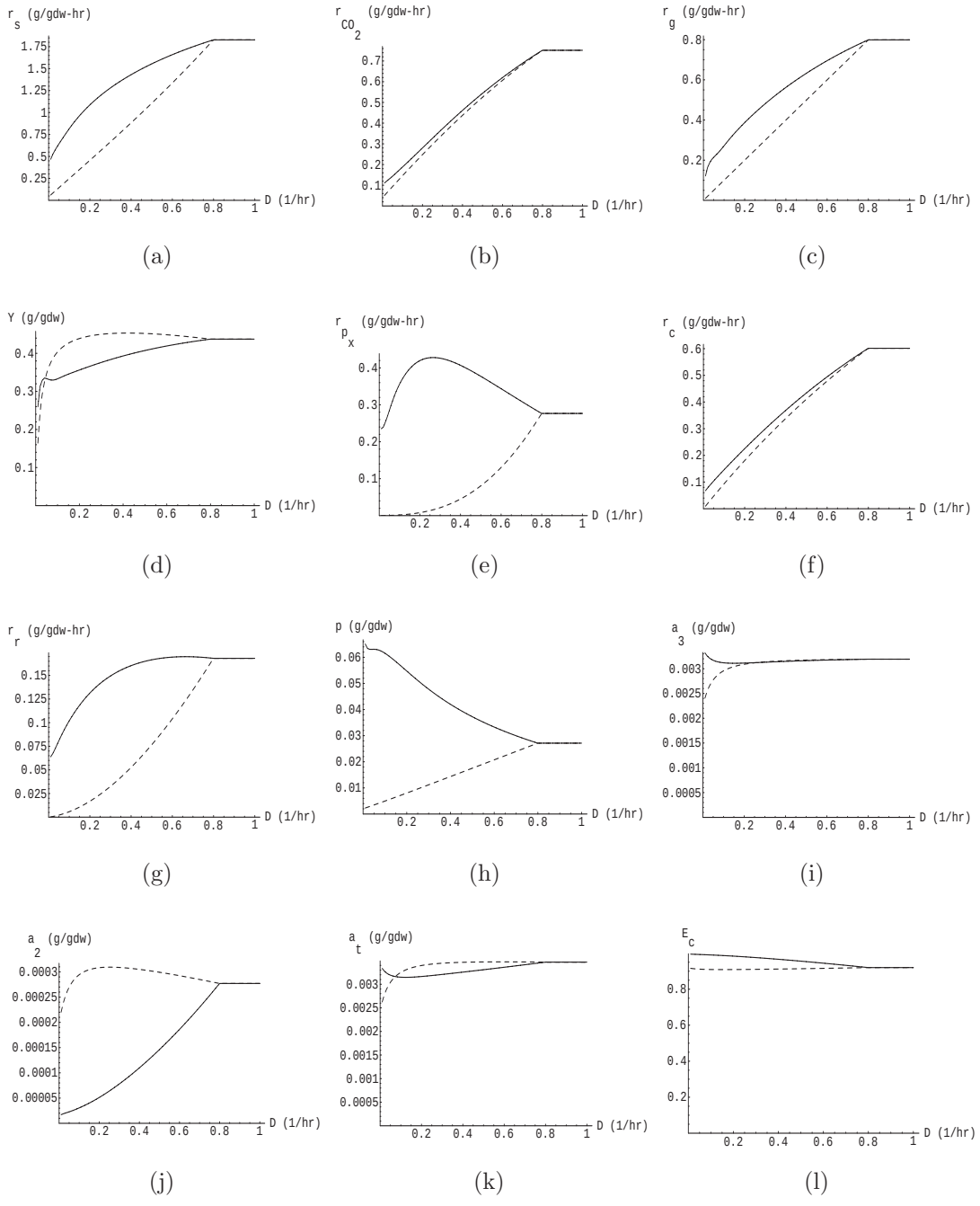

Figure 4–5: Initial response following a continuous-to-batch shift. The dashed line shows the initial steady state value. The full line shows the value after the cells have been exposed to substrate-excess conditions: (a) Specific substrate uptake rate (b) Specific respiration rate (c) Specific growth rate (d) Yield of biomass (e) Specific respiration rate (f) Net specific protein synthesis rate ($r_c \equiv r_c^+ - r_c^-$) (g) Net specific RNA synthesis rate ($r_r \equiv r_r^+ - r_r^-$) (h) Precursor concentration (i) ATP concentration (j) ADP concentration (k) Total nucleotide concentration (l) Energy charge.

4.2.2.3 Substrate switch

The transient response to a substrate switch could be captured using our earlier model (see Figure 1–5). Simulations of the extended model preserve these transients. This transient depends on the inducible nature of the transport enzyme synthesis. When the substrate is not present in the environment, the cell does not synthesize the transport enzyme corresponding to that substrate. In the absence of the substrate, the synthesis of the corresponding transport enzyme continues only at really small constitutive level. After the substrate switch, the trace level of transport enzyme corresponding to a new substrate, limits the specific substrate uptake rate, r_s, at vanishingly small levels for approximately the first 30 hours (Figure 4–6). During this time period, the intercellular variables show the response similar to the starvation phase (Figure 4–8). The ribosome concentration decreases gradually (Figure 4–8e). Similarly, the ATP concentration, a_3, shows a biphasic starvation response. Initially, the ATP concentration drops instantaneous because of the consumption of ATP in RNA and protein synthesis, and shows a gradual decrease after that because of the gradual degradation of the total nucleotide, a_t (Figure 4–8f,g). The slow synthesis of transport enzyme takes long time to build up its concentration to the desire level (Figure 4–8c), hence, the transient response shows massive loss of the cells and accumulation of substrate concentration in the reactor (Figure 4–6a,b). The utilization of charged nucleotides by the substrate transport enzymes makes the substrate uptake rate kinetics even more nonlinear than the previous models [41] and enhances the lag period. These simulations are in good agreement with the data shown in Figure 1–5.

4.2.2.4 Dilution rate shift-up

The response to dilution rate shift-ups is also preserved for both cases, the transport enzyme deficient culture [41] and RNA deficient culture [65]. In this model, the specific growth rate can be limited by either the transport enzyme

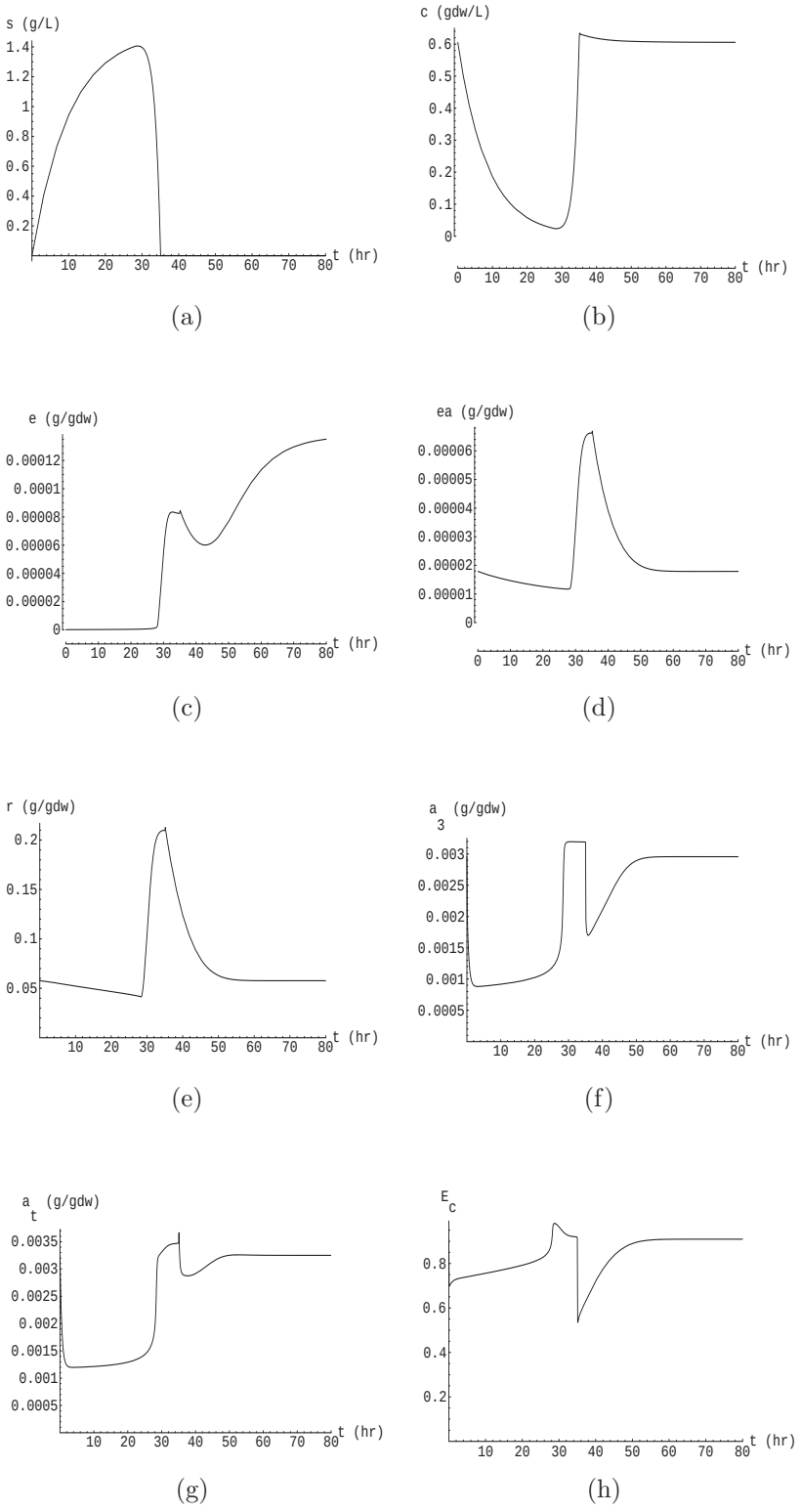

Figure 4–6: Transient response for a switch in the identity of the substrate at $D = 0.1$ 1/hr. Before the switch, the culture is in a steady state corresponding to the absence of the substrate.

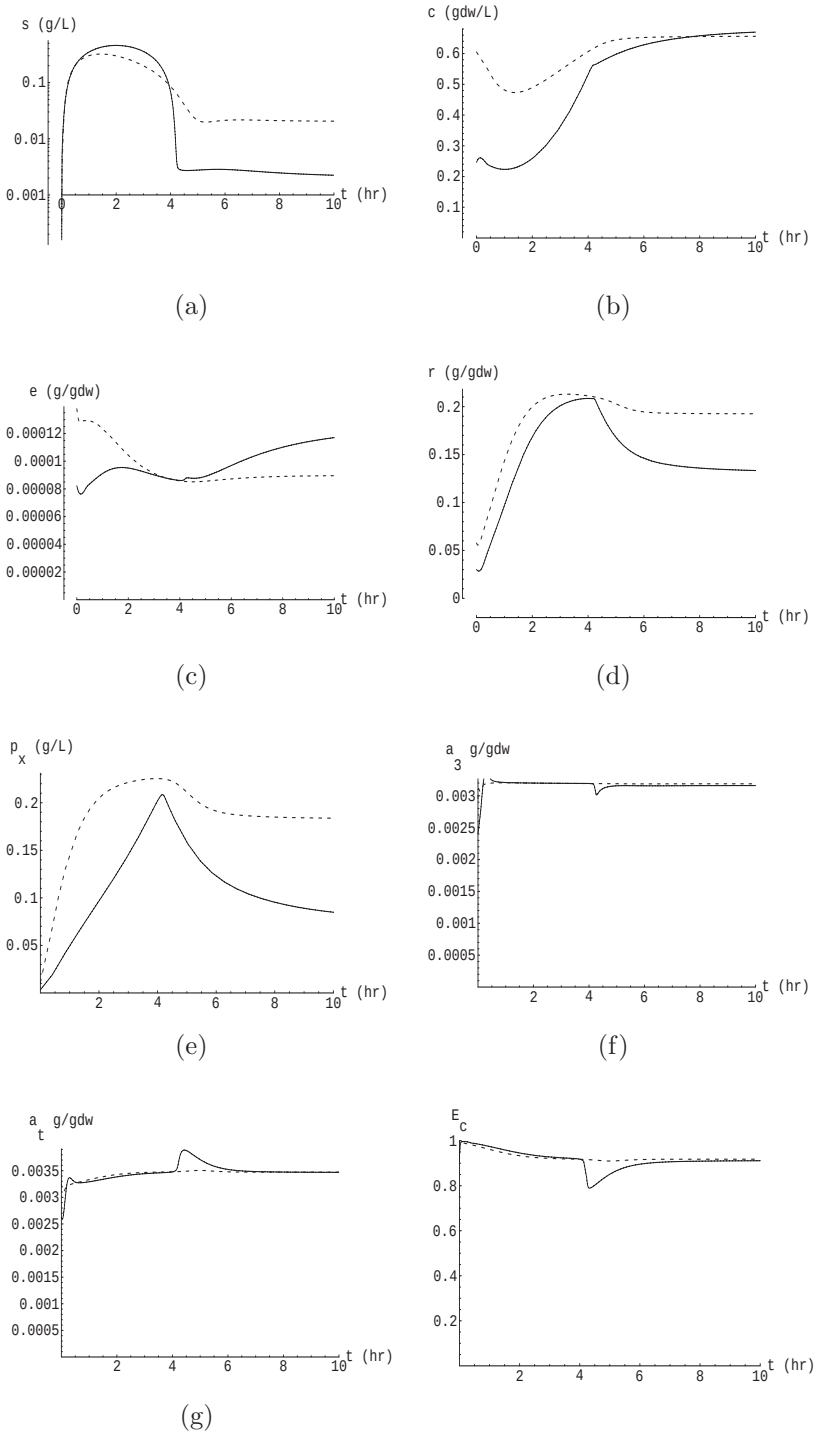

Figure 4–7: Transient response to a dilution rate shift-up. At $t < 0$, the culture is at the steady state corresponding to the dilution rate, $D_0 = 0.01$ 1/hr (solid line) and $D_0 = 0.1$ 1/hr (dash line), and feed concentration, $s_f = 1.5$ g/L. At $t = 0$, the dilution rate is shifted up to $D = 0.4$ 1/hr and $D = 0.7$ 1/hr respectively, while the feed concentration is held constant.

concentration or ribosome concentration. Figure 4–7 shows the simulations of the dilution rate shift-up for both limiting cases.

The dilution rate shift up from $D_0 = 0.011$/hr to $D = 0.4$ 1/hr (solid line) is an example of limitation caused by the transport enzyme. The low initial concentration of transport enzyme limits the instantaneous increase in the specific substrate uptake rate and consequently the instantaneous increase in the specific growth rate. When the instantaneous increase in the specific growth rate does not match with the increase in the dilution rate, the substrate concentration increases and the cell density decreases in the reactor. The slow kinetics of the transport enzyme takes several hours to build up to the desired level causing the long lag in the reactor.

The dilution rate shift up from $D_0 = 0.11$/hr to $D = 0.7$ 1/hr (dash line) is an example of the ribosomes limitation. The high concentration of transport enzyme let the substrate uptake rate goes up, but the low concentration of ribosomes limits the increase in instantaneous specific growth rate. The ribosome limitation results in accumulation of precursors inside the cell hence, increase in the specific respiration rate and specific excretion rate. The high concentration of precursors also inhibits the specific substrate uptake rate and thus results in the accumulation of the substrate in the reactor.

4.2.2.5 Starvation

The starvation is define as the state when the cell exhausts the growth limiting substrate and stops the growth. In this transient experiment, the culture is grown in single growth limiting substrate. The concentrations of physiological variables are measured for the growth phase and even after the exhaustion of the substrate in the batch reactor. It was observed that cell density stays constant for hours whereas ATP concentration and energy charge suddenly drop to the lower level and stay there [66]. To replicate this experiment, the simulation is computed even

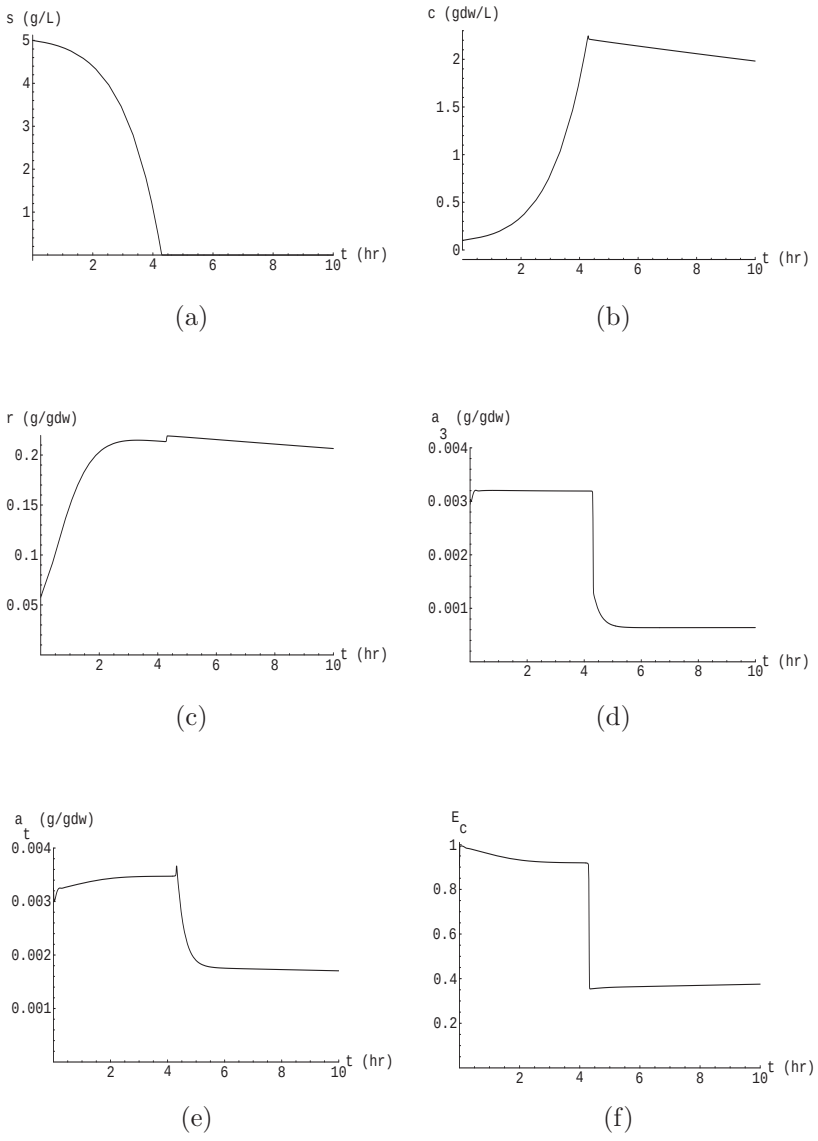

Figure 4–8: Simulation results of the batch culture during exhaustion of the substrate.

after the substrate concentration goes to zero. The simulation results (Figure 4–8) qualitatively matches the experimental data.

Several papers[67] suggest that the maintenance of constant cell density in the stationary phase is due to the consumption of excretory byproducts (i.e acetate). Since this model does not incorporate the consumption of excretory products; as the substrate concentration reaches zero, the decay in protein and RNA make the specific growth rate negative, and the cell density decreases in the culture (Figure 4–8b). In order to account for the decrease in the concentration of ATP and energy charge, refer to Figure 4–1, when the cell picks up the substrate, there are two ways to generate precursor molecules and energy, either from the uptake of substrate or from the degradation of the biomass. The cell generates the energy in glycolysis and respiration, and the total generated energy is used in the production of the biomass. At the exhaustion of the growth limiting substrate, precursors are generated only by the degradation of the biomass. The generated precursors redistribute themselves either by going into the respiration to generate energy or by polymerizing back into the biomass using the energy generated in the respiration. This process results in the net decay of the biomass known as futile cycle. Thus, this futile cycle degrades biomass. Since the cell no longer picks up the substrate, it lacks the energy generated through glycolysis. This loses of energy results in the sudden decrease in the concentration of charged nucleotides and consequently energy charge. The advantage of futile cycle is in maintaining the the low concentration of charged nucleotide, hence the viability of the cell.

4.2.2.6 Resumption of the growth in the starvation state

This experiment is an extension of starvation experiment. In this experiment, the cells were grown in a batch reactor. At the exhaustion of the substrate, the culture was allowed to enter into the starvation phase and glucose was resupplied after 45 minutes of starvation (Figure 4–10)[66]. The energy charge of exponentially

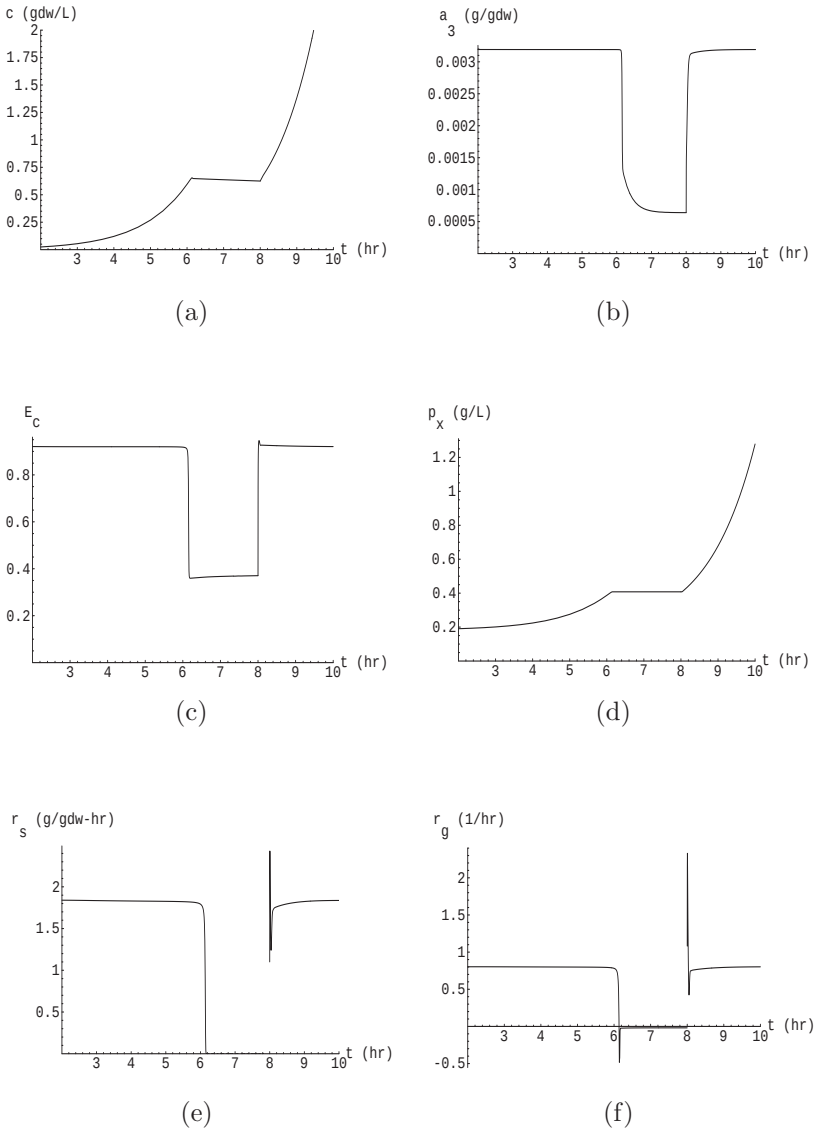

Figure 4–9: Simulation results of the batch culture with resupply of the substrate during starvation.

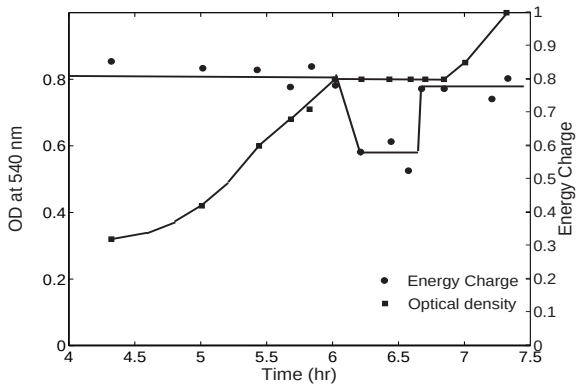

Figure 4–10: Transient response of the glucose limited batch culture with supply of glucose after 45 minutes of starvation.

growing cells was near 0.8. At the exhaustion of glucose, the cessation of growth causes energy charge to decrease to 0.6. When glucose was resupplied to the same culture after 45 minutes of starvation, the value of the energy charge jumps to the level characteristic of the growing culture. To replicate this experiment, the simulation was performed for an exponential growth in batch culture and continued even after the exhaustion of the substrate. At the starvation phase, the cell stops the growth and the energy charge comes down suddenly (see Figure 4–9b) because of the reason as mentioned in Section 4.2.2.5. The substrate concentration was shifted to some positive value after approximately 2 hours of starvation. The concentration of transport enzyme and ribosome stay high because of the slow degradation during all of this period. The energy level was maintained in the cell by the degradation of the biomass. Thus, as soon as the substrate is added to the reactor, the substrate uptake rate goes up (see Figure 4–9e). Initially, the incoming substrate diverts to respiration because of low energy charge, consequently, the concentration of charged nucleotides and energy charge goes up. The sudden increase in the concentration of charged nucleotides and availability of high concentration of ribosomes puts the growth rate to a higher level (see Figure 4–9f).

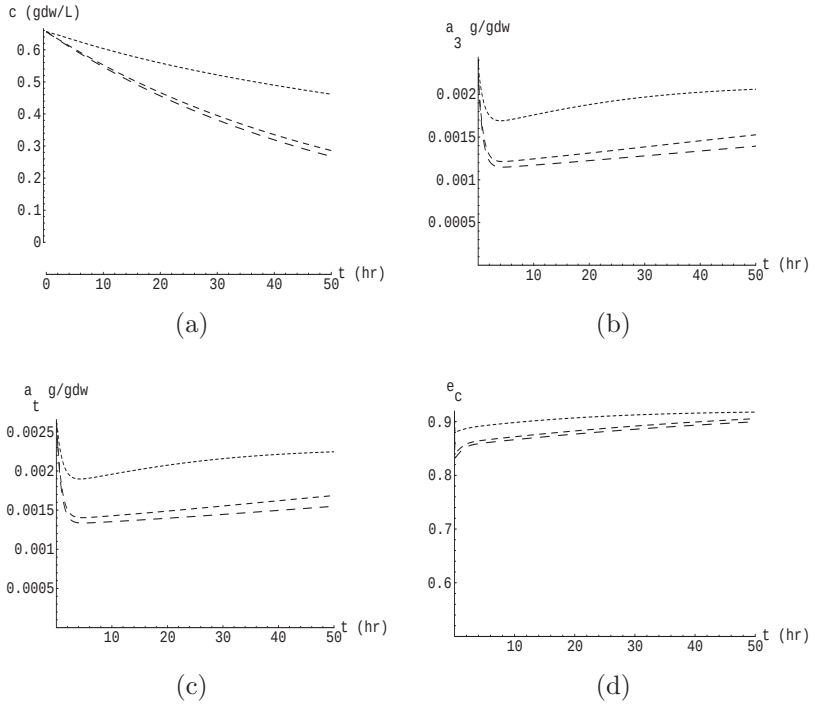

Figure 4–11: Simulation results of the batch culture with the slow supply of the substrate during starvation.

4.2.2.7 Slow supply of the substrate during starvation

The starvation experiments indicate that energy charge can be maintained between 0.8 and 0.9 as long as there is substrate in the environment. As soon as the substrate is exhausted, energy charge goes down. People were able to extend this maintenance of energy charge at 0.8 for days by continuous slow supply of glucose to a glucose limited culture in the starvation state (Figure 4–12)[67]. After cessation of the growth, glucose was added at the rate of 0.15μmole of glucose/mg of protein per h. When glucose was added at higher rate; a higher energy charge was maintained, similarly, at lower glucose addition rates; a lower energy charge was maintained. To replicate these results, it is assumed that the volumetric flow rate of the slow supply of glucose used in the experiment is so small that the volume of the culture does not change. This implies that the role of slow glucose supply is to maintain a constant small level of substrate concentration in the

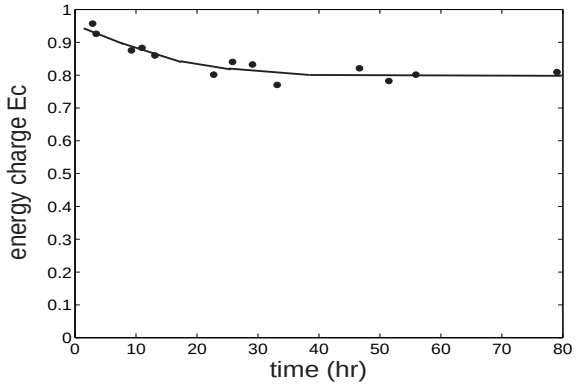

Figure 4–12: Transient response of a glucose limited batch culture with the slow supply of glucose during starvation to maintain energy charge.

reactor. Simulations were performed at constant substrate concentration without worrying the fact that reactor dilution occurs because of flow into the reactor. The resulting energy charge profile (Figure 4–11) was similar to the results obtained in the experiment (Figure 4–12). The concentrations of the cells, charged nucleotides, and total nucleotides stay constant or come down depending upon the substrate supply rate. The explanation behind this dynamic is that if the cells are exposed to some constant substrate concentration they will maintain a constant energy charge inside the cell. According to the model construction, the energy charge is an increasing function of substrate concentration bounded by the values corresponding to starvation and substrate abundance conditions. For this simulation, energy charge lies between 0.4 and 1 respectively. The energy charge profile saturate out at a very small value of substrate concentration in the environment. The simulation uses different values of the substrate concentration between zero and substrate concentration corresponding to saturation level of energy charge to generate different energy charges.

4.3 Discussion

The model accounting adenine nucleotides, ATP and ADP, captures a wide variety of experimental data. The simulation results qualitatively matches with

the experimental data. The incorporation of ATP in our previous model not only preserves the dynamics of transport enzyme and ribosome model but also includes the fast dynamics of ATP in a substrate pulse experiment and the slow evolution of ATP in various starvation experiments. The fast dynamics of ATP was attributed to its low concentration involved in the fast reaction kinetics, hence, the fast turnover time. However, the slow dynamics of ATP is a resultant of the transition of ATP into quasisteady state manifold of slow variables. This model also contradicts the hypothesis that cell always tries to maintain ATP and ADP concentration such that it maintains the constant energy charge. According to our formulation, the maintenance of constant level of ATP concentration is purely balance between *de novo* synthesis of nucleotide and consumption of nucleotides in RNA synthesis. The homeostasis of energy charge is maintained because of the balance between energy generation processes i.e. glycolysis, respiration and energy consumption processes i.e. synthesis of protein and RNA.

CHAPTER 5
CONCLUSIONS

We have formulated a model of microbial growth accounting for transport enzyme synthesis, ribosome-mediated protein synthesis and adenine nucleotide as energy molecule. Based on the experimental observation, the fundamental assumption was made that the synthesis of transport enzyme and ribosome is autocatalytic. Both the steady states and the transients of the model show remarkable agreement with a wide variety of experimental data. The model yields simple explanations of seemingly complex behavior.

1. Steady states

   (a) The cell density decreases at low dilution rates. This behavior does not stem from an *ad hoc* maintenance. It falls out naturally as a consequence of the futile cycling of RNA at low dilution rates.

   (b) The peripheral enzyme level passes through a maximum. This reflects the competing effects of enzyme induction and dilution. At low dilution rates, induction dominates, so that the peripheral enzyme level is an increasing function of D. At high dilution rates, dilution dominates, and the peripheral enzyme level is a decreasing function of D.

   (c) The ribosome levels approach a nonzero level at small dilution rates. According to the model, this is the result of the futile cycling of proteins.

   (d) The nonzero level of ATP was also maintained by the futile cycle as the dilution rate approaches zero.

   (e) At high dilution rate ($D > 0.1$), the constant level of ATP in the cell is a consequence of the balance between *de novo* synthesis of nucleotide and RNA. The homeostasis of energy charge is a simple balance between the net energy generation in glycolysis and respiration and the net energy consumption in biosynthesis.

2. Transients

   (a) The model shows good agreement with a wide variety of transients including continuous-to batch shifts, feed switches, dilution rate shift-ups, dilution rate shift-downs and starvation phase.

   (b) Feed switchs and low dilution rate shift-ups transients are governed by transport enzyme.

   (c) The low level of ribosomes produces the transient observed in continuous to batch shifts and high dilution rate shift ups.

   (d) The distribution of total nucleotide between charged and uncharged nucleotide defines energy charge, which helps in the metabolic division of incoming substrate into respiration and biosynthesis.

   (e) The maintenance of low level of energy charge is the result of the futile cycle during starvation phase in the batch reactor.

   (f) The transients observed in continuous reactor are in fact the combinations of two canonical dynamics, namely, the approach to balanced growth under supersaturating substrate concentrations, and the approach to steady state under subsaturating substrate concentrations.

REFERENCES

[1] M. H. Saier, Jr., "Multiple mechanisms controlling carbon metabolism in bacteria," *Biotechnol. Bioeng.*, vol. 58, pp. 170–174, 1998.

[2] O. Maaloe and N. O. Kjeldgaard, *Control of macromolecular synthesis: A study of DNA, RNA, and protein synthesis*, W. A. Benjamin, New York, 1966.

[3] M. Nomura, "The control of ribosome synthesis," *Scientific American*, vol. 250, pp. 102–114, 1984.

[4] X. Zhang, P. Dennis, M. Ehrenberg, and H. Bremer, "Kinetic properties of *rrn* promoters in *Escherichia coli*," *Biochimie*, vol. 84, pp. 981–996, 2002.

[5] K. F. Jensen and S. Pedersen, "Metabolic growth rate control in *Escherichia coli* may be a consequence of subsaturation of the macromolecular biosynthetic apparatus with substrates and catalytic components," *Microbiol. Rev.*, vol. 54, pp. 89–100, 1990.

[6] E. A. Dawes, "Storage polymers in prokaryotes," in *Prokaryotic structure and function*, S. Mohan, C. Dow, and J. A. Coles, Eds., New York, 1991, Society for General Microbiology, Symposia of the Society for General Microbiology, pp. 81–122, Cambridge University Press.

[7] E. A. Dawes and P. J. Senior, "The role and regulation of energy reserve polymers in microorganisms," *Adv. Microb. Physiol.*, vol. 10, pp. 135–266, 1973.

[8] W. H. Holms, "The central metabolic pathways of *Escherichia coli*: Relationship between flux and control at a branch point, efficiency of conversion to biomass, and excretion of acetate," *Curr. Top. Cell. Regul.*, vol. 28, pp. 69–105, 1986.

[9] D. W. Tempest and O. M. Neijssel, "The physiology of metabolite overproduction," in *Microbial technology: Current state, future prospects*, vol. 29 of *Symposia of the Society for General Microbiology*, pp. 53–82. Cambridge University Press, New York, 1979.

[10] T. Suzuki, "Phosphotransacetylase of *Escherichia coli* B: Activation by pyruvate and inhibition by NADH and certain nucleotides," *Biochem. Biophys. Acta*, vol. 191, pp. 559–569, 1969.

[11] Heinrich Senn, Urs Lendenmann, Mario Snozzi, and Thomas Egli, "The growth of *Escherichia coli* in glucose-limited chemostat cultures: A reexamination of the kinetics," *Biochem. Biophys. Acta*, vol. 1201, pp. 424–436, 1994.

[12] D. W. Tempest, D. Herbert, and P. J. Phipps, "Studies on the growth of *Aerobacter aerogenes* at low dilution rates in a chemostat," in *Microbial Physiology and Continuous Culture*, pp. 240–253. HMSO, London, HMSO, 1967.

[13] D. W. Tempest and J. R. Hunter, "Magnesium-limited growth of *Aerobacter aerogenes* in a chemostat," *J. Gen. Microbiol.*, vol. 39, pp. 355–366, 1965.

[14] R. J. Harvey, "Metabolic regulation in glucose-limited chemostat cultures of *Escherichia coli*," *J. Bacteriol.*, vol. 104, pp. 698–706, 1970.

[15] P. H. Clarke, M. A. Houldsworth, and M. D. Lilly, "Catabolite repression and the induction of amidase synthesis by *Pseudomonas aeruginosa* 8602 in continuous culture," *J. Gen. Microbiol.*, vol. 51, pp. 225, 1968.

[16] R. W. Smith and A. C. R. Dean, "β-galactosidase synthesis in *Klebsiella aerogenes* growing in continuous cultures," *J. Gen. Microbiol.*, vol. 72, pp. 37–47, 1972.

[17] D. E. F. Harrison and P. K. Maitra, "Control of respiration and metabolism in growing *Klebsiella aerogenes*," *Biochem. J.*, vol. 112, pp. 647–656, 1969.

[18] D. Herbert, R. Elsworth, and R. C. Telling, "The continuous culture of bacteria: A theoretical and experimental study," *J. Gen. Microbiol.*, vol. 14, pp. 601–622, 1956.

[19] S. J. Pirt, "Prospects and problems in continuous flow culture of microorganisms," *J. Appl. Chem. Biotechnol.*, vol. 22, pp. 55–64, 1972.

[20] K. L. Schulze and R. S. Lipe, "Relationship between substrate concentration, growth rate, and respiration rate of *Escherichia coli* in continuous culture," *Arch. Microbiol.*, vol. 48, pp. 1–20, 1964.

[21] A. C. R. Dean, "Influence of environment on the control of enzyme synthesis," *J. Appl. Chem. Biotechnol.*, vol. 22, pp. 245–259, 1972.

[22] A. Matin, "Microbial regulatory mechanisms at low nutrient concentrations as studied in a chemostat," in *Strategies of Microbial Life in Extreme Environments*, Moshe Shilo, Ed., pp. 323–339. Verlag Chemie, Weinheim, 1978.

[23] Kiyoshi Toda, "Induction and repression of enzymes in microbial cultures," *J. Chem. Tech. Biotechnol.*, vol. 31, pp. 775–790, 1981.

[24] D. E. Atkinson, "Phosphoenolpyruvate synthetase from *eschericha coli*," *J. Biol. Chem.*, vol. 248, pp. 2712–2715, 1973.

[25] D. W. Tempest, J. L. Meers, and C. M. Brown, "Influence of enviroment on the content and composition of microbial free amino acid pools," *J. Gen. Microbiol.*, vol. 64, pp. 171–185, 1970.

[26] C. M. Brown and S. O. Stanley, "Environment-mediated changes in the cellular content of the "pool" constituents and their associated changes in cell physiology," *J. Appl. Chem. Biotechnol.*, vol. 22, pp. 363–389, 1972.

[27] M. Schaechter, O. Maaloe, and N. O. Kjeldgaard, "Dependency on medium and temperature of cell size and chemical composition during balanced growth of *Salmonella typhimurium*," *J. Gen. Microbiol.*, vol. 19, pp. 592–606, 1958.

[28] D. Herbert, "The chemical composition of microoorganisms as a function of their environment," *Symp. Soc. Gen. Microbiol.*, vol. 28, pp. 391–416, 1961.

[29] C. L. Cooney, D. I. C. Wang, and R. I. Mateles, "Growth of *Enterobacter aerogenes* in a chemostat with double nutrient limitations," *Appl. Environ. Microbiol.*, vol. 31, pp. 91–98, 1976.

[30] E. T. M. El-Mansi and W. H. Holms, "Control of carbon flux to acetate excretion during growth of *Escherichia coli* in batch and continuous cultures," *J. Gen. Microbiol.*, vol. 135, pp. 2875–2833, 1989.

[31] K. Han, H. C. Lim, and J. Hong, "Acetic acid formation in *Escherichia coli* fermentation," *Biotechnol. Bioeng.*, vol. 39, pp. 663–671, 1992.

[32] H. P. Meyer, C. Leist, and A. Fiechter, "Acetate formation in continuous culture of *Escherichia coli* K12 D1 on defined and complex media," *J. Biotechnol.*, vol. 1, pp. 355–358, 1984.

[33] Peter Grindrod, *The theory and applications of reaction-diffusion equations: Patterns and waves*, Clarendon Press, Oxford, second edition, 1996.

[34] R. I. Mateles, D. Y. Ryu, and T. Yasuda, "Measurement of unsteady state growth rates of microorganisms," *Nature*, vol. 208, pp. 263–265, 1965.

[35] S. Aiba, S. Nagai, Y. Nishizawa, and M. Onodera, "Nucleic approach to some response of chemostatic culture of *Azotobacter vinelandii*," *J. Gen. Appl. Microbiol.*, vol. 13, pp. 85–101, 1967.

[36] C. T. Chi and J. A. Howell, "Transient behavior of a continuous stirred tank biological reactor utilizing phenol as an inhibitory substrate," *Biotechnol. Bioeng.*, vol. 18, pp. 63–80, 1976.

[37] C. N. Standing, A. G. Fredrickson, and H. M. Tsuchiya, "Batch- and continuous-culture transients for two substrate systems," *Appl. Microbiol.*, vol. 23, pp. 354–359, 1972.

[38] N. Nyholm, "Kinetics of phosphate limited algal growth," *Biotechnol. Bioeng.*, vol. 19, pp. 467–492, 1977.

[39] N. Nyholm, "Dynamics of phosphate limited algal growth: Simulation of phosphate shocks," *J. Theor. Biol.*, vol. 70, pp. 415–425, 1978.

[40] Matthias Bally and Thomas Egli, "Dynamics of substrate consumption and enzyme synthesis in *Chelatobacter heintzii* during growth in carbon-limited continuous culture with different mixtures of glucose and nitrilotriacetic acid (NTA)," *Appl. Environ. Microbiol.*, vol. 62, pp. 133–140, 1996.

[41] J. Shoemaker, G. T. Reeves, S. Gupta, S. S. Pilyugin, T. Egli, and A. Narang, "The dynamics of single-substrate continuous cultures: Role of transport enzymes," *J. Theor. Biol.*, vol. 222, pp. 307–322, 2003.

[42] S. Baloo and D. Ramkrishna, "Metabolic regulation in bacterial continuous cultures - II," *Biotechnol. Bioeng.*, vol. 29, pp. 940–943, 1990.

[43] Urs Lendenmann and Thomas Egli, "Is *Escherichia coli* growing in glucose-limited chemostat culture able to utilize other sugars without lag?," *Microbiology*, vol. 141, pp. 71–78, 1995.

[44] A. Natarajan and F. Srienc, "Glucose uptake rates of single *E. coli* cells grown in glucose-limited cultures," *J. Microbiol. Meth.*, vol. 42, pp. 87–96, 2000.

[45] R. W. O'Brien, O. M. Neijssel, and D. W. Tempest, "Glucose phosphoenolpyruvate phosphotransferase activity and glucose uptake rate of *Klebsiella aerogenes* growing in a chemostat culture," *J. Gen. Microbiol.*, vol. 116, pp. 305–314, 1980.

[46] O. M. Neijssel, S. Hueting, and D. W. Tempest, "Glucose transport capacity is not the rate-limiting step in the growth of some wild-type strains of *Escherichia coli* and *Klebsiella aerogenes* in chemostat culture," *FEMS Microbiol. Lett.*, vol. 2, pp. 1–3, 1977.

[47] S. Nagai, Y. Nishizawa, I. Endo, and S. Aiba, "Response of a chemostatic culture of *Azotobacter vinelandii* to a delta type pulse of glucose," *J. Gen. Appl. Microbiol.*, vol. 14, pp. 121–134, 1968.

[48] H. S. Yun, J. Hong, and H. C. Lim, "Regulation of ribosome synthesis in *Escherichia coli*: Effects of temperature and dilution rate changes," *Biotechnol. Bioeng.*, vol. 52, pp. 615–624, 1996.

[49] H. Brunschede, T. L. Dove, and H. Bremer, "Establishment of exponential growth after a nutritional shift-up in *Escherichia coli* B/r: Accumulation of deoxyribonucleic acid, ribonucleic acid, and protein," *J. Bacteriol.*, vol. 129, pp. 1020–1033, 1977.

[50] A. G. Chapman and D. E. Atkinson, "Adenine nucleotide concentrations and turnover rates. Their correlation with biological activity in bacteria and yeast," *Adv. Microb. Physiol.*, vol. 15, pp. 253–306, 1977.

[51] Uwe Theobald, Werner Mailinger, Matthias Reuss, and Manfred Rizzi, "In vivo analysis of glucose-induced fast changes in yeast adenine nucleotide pool appling a rapid sampling technique," *Analytical Biochemistry*, vol. 214, pp. 31–37, 1993.

[52] Diana Visser, Gertan A. van Zuylen, Jan C. van Dam, Arthur Oudshoorn, Michael R. Eman, Cor Ras, Walter M. van Gulik, Johannes Frank, Gijs W. K. van Dedem, and Joseph J. Heijnen, "Rapid sampling for analysis of in vivo kinetics using the bioscope: A system for continuous-pulse experiments," *Biotechnol. Bioeng.*, vol. 79, no. 6, pp. 674–681, 2002.

[53] M. M. Domach, S. K. Leung, R. E. Cahn, G. G. Cocks, and M. L. Shuler, "Computer model for glucose-limited growth of a single cell of *escherichia coli* B/r-A," *Biotechnol. Bioeng.*, vol. 26, pp. 203–216, 1984.

[54] S. Baloo and D. Ramkrishna, "Metabolic regulation in bacterial continuous cultures - I," *Biotechnol. Bioeng.*, vol. 29, pp. 940–943, 1990.

[55] G. Yagil and E. Yagil, "On the relation between effector concentration and the rate of induced enzyme synthesis," *Biochem. J.*, vol. 11, pp. 11–17, 1971.

[56] Atul Narang, "The steady states of microbial growth on mixtures of substitutable substrates in a chemostat," *J. Theor. Biol.*, vol. 190, pp. 241–261, 1998.

[57] E. O. Powell, "Transient changes in the growth rate of microorganisms," in *Continuous cultivation of microorganisms*, I. Malek, K. Bevan, Z. Fencl, V. Munk, J. Ricica, and H. Smrckova, Eds. 1969, pp. 275–284, Academic Press, New York.

[58] H. Bremer and P. P. Dennis, "Transition period following a nutritional shift-up in the bacterium *Escherichia coli* B/r: Stable RNA and protein synthesis," *J. Theor. Biol.*, vol. 52, pp. 365–382, 1975.

[59] H. Bremer, "Parameters affecting the rate of synthesis of ribosomes and RNA polymerase in bacteria," *J. Theor. Biol.*, vol. 53, pp. 115–124, 1975.

[60] Koch. A. L., "Overall controls on the biosynthesis of ribosomes in growing bacteria," *J. Theor. Biol.*, vol. 28, pp. 203–231, 1970.

[61] K Gausing, "Regulation of ribosome production in Escherichia coli: synthesis and stability of ribosomal RNA and of ribosomal protein messenger RNA at different growth rates.," *J Mol Biol*, vol. 115, no. 3, pp. 335–54, Sep 1977.

[62] C. P. L. Grady, Jr., L. J. Harlow, and R. R. Riesing, "Effects of growth rate and influent substrate concentrations on effluent quality from chemostats containing bacteria in pure and mixed culture," *Biotechnol. Bioeng.*, vol. 14, pp. 391–410, 1972.

[63] G. T. Daigger and C. P. L. Grady, Jr., "The dynamics of microbial growth on soluble substrates," *Biotechnol. Bioeng.*, vol. 16, pp. 365–382, 1982.

[64] P. Duboc, U. von Stockar, and J. Villadsen, "Simple generic model for dynamic experiments with *Saccharomyces cerevisiae* in continuous culture: Decoupling between anabolism and catabolism," *Biotechnol. Bioeng.*, vol. 60, pp. 180–189, 1998.

[65] Shakti Gupta, SS Pilyugin, and Atul Narang, "The dynamics of single-substrate continuous cultures: the role of ribosomes.," *J Theor Biol*, vol. 232, no. 4, pp. 467–90, Feb 2005.

[66] A. G. Chapman, L. Fall, and D. E. Atkinson, "Adenylate energy charge in *Escherichia coli*," *J. Bacteriol.*, vol. 108, pp. 1072–1086, 1971.

[67] M. Walker-Simmons and D. E. Atkinson, "Functional capacities and the adenylate energy charge in *Escherichia coli* under conditions of nutritional stress," *J. Bacteriol.*, vol. 130, pp. 676–683, 1977.

BIOGRAPHICAL SKETCH

Shakti Gupta was born in India, on June 1, 1976. He received a Bachelor of Science from India Institute of Technology, Kanpur, India. After completing his bachelors degree he joined the Department of Chemical Engineering, University of Florida, in 2000. His research interests are modeling of biological systems.